Structure-function relationship of human melanocortin-4 receptor and characterization of fish neural melanocortin receptors

By

Li-Kun Yang

A dissertation submitted to the Graduate Faculty of
Auburn University
in partial fulfillment of the
requirements for the Degree of
Doctor of Philosophy

Auburn, Alabama
August 3, 2019

Keywords: G protein-coupled receptor, Melanocortin-3 receptor, Melanocortin-4 receptor, Energy homeostasis, Obesity, Fish

Approved by

Ya-Xiong Tao, Chair, Professor of Physiology
Mahmoud Mansour, Professor of Veterinary Anatomy
Robert L. Judd, Professor of Pharmacology
Ramesh B. Jeganathan, Associate Professor of Nutrition
Jianzhong Shen, Associate Professor of Drug Discovery and Development

Abstract

The neural melanocortin receptors, including melanocortin-3 and -4 receptors (MC3R and MC4R), are two important factors in regulation of energy homeostasis. MC3R primarily regulates feed efficiency and nutrient partitioning, whereas MC4R plays an essential role in controlling both food intake and energy expenditure. In several other G protein-coupled receptors, the DRYxxI motif and intracellular loop 2 (ICL2) have been shown to play a significant role in receptor activation. To gain a better understanding of functions of this region in human MC4R (hMC4R), we performed systematic functional study using alanine-scanning mutagenesis in terms of DRYxxI motif and ICL2 of hMC4R. We identified several residues important for receptor cell surface expression (T150), receptor and ligand interaction (D146, Y148, Y153, Q156, Y157, M161, and T162), constitutive cAMP signaling (R147, FI151, L155, Y157), ligand-induced cAMP (R147, I151, and L155) and ERK1/2 signaling pathways (R147, F149, H158, and I160), as well as biased signaling between cAMP and ERK1/2 pathways (Y148, F149, T150, H158, I160, and M161). The investigation of structure-function relationship of hMC4R provides a better understanding towards the role of MC4R in obesity pathogenesis and will be valuable for the structure-based drug design of molecules with the capacity to modulate MC4R activity as potential therapeutics.

Currently, the approaches for improving growth and feed efficiency of fish are limited to the time-consuming selective breeding methods. Therefore, understanding of endocrine regulation of energy metabolism in economically important species can potentially lead to novel approaches to achieve better economic return. In this investigation, we attempted to functionally investigate channel catfish (*Ictalurus punctatus*) MC3R (ipMC3R). Five agonists, including adrenocorticotropin, α-melanocyte stimulating hormone (α-MSH), β-MSH, [Nle^4, D-Phe^7]-α-MSH, and D-Trp^8-γ-MSH, were used in the pharmacological studies. Our results showed that ipMC3R bound β-MSH with a higher affinity and D-Trp^8-γ-MSH with a lower affinity compared with human MC3R. All agonists were demonstrated to stimulate ipMC3R and increase intracellular cAMP production with sub-nanomolar potencies. The ERK1/2 activation was also be triggered by ipMC3R. The ipMC3R exhibited constitutive activities in both cAMP and ERK1/2 pathways, and the Agouti-related protein served as an inverse agonist at ipMC3R, potently inhibiting the high basal cAMP level. Moreover, we showed that melanocortin receptor accessory protein 2 preferentially modulated ipMC3R in cAMP production rather than ERK1/2 activation. Our study leads to further investigation of the physiological roles of the ipMC3R, especially in energy homeostasis, in channel catfish.

We have also cloned swamp eel (*Monopterus albus*) *mc4r* (ma*mc4r*), consisting of a 981 bp open reading frame encoding a protein of 326 amino acids. The sequence of maMC4R was homologous to those of several teleost MC4Rs. Phylogenetic and chromosomal synteny analyses showed that maMC4R was closely related to piscine MC4Rs. qRT-PCR revealed that *mc4r* transcripts were highly expressed in brain and gonads of swamp eel. The maMC4R was further demonstrated to be a functional receptor

by pharmacological studies. Four agonists, α-MSH, β-MSH, [Nle^4, D-Phe^7]-α-MSH, and adrenocorticotropin, could bind to maMC4R and induce intracellular cAMP production dose-dependently. Small molecule agonist THIQ allosterically bound to maMC4R and exerted its effect. Similar to other fish MC4Rs, maMC4R also exhibited significantly increased basal activity compared with that of hMC4R. The high basal activity of maMC4R could be decreased by inverse agonist ML00253764, suggesting that maMC4R was indeed constitutively active. The availability of maMC4R and its pharmacological characteristics will facilitate the investigation of its function in regulating diverse physiological processes in swamp eel.

In summary, we studied DRYxxI motif and ICL2 of hMC4R in a systemic manner, and identified some critical residues for receptor functions. We also investigated functionality of MC3R and MC4R in two economically important fish species, laying a foundation for future physiological studies.

Acknowledgment

I would like to express my sincere appreciation to my graduate committee members, friends, colleagues, and family members, who have all provided strong support for my graduate work. This thesis would not have been possible without their help and support.

My deepest gratitude goes to my mentor, Dr. Ya-Xiong Tao, who has provided me with the opportunity to study abroad as a PhD student in his lab. It is really an honor for both of me and my family. Throughout my four-year study in Auburn, Dr. Tao has provided strong guidance for my research, and kind encouragement and inspirations for my study. Without his guidance, help, encouragement, and support, I would never have been able to finish my dissertation. I'm also indebted to my advisory committee, Drs. Mahmoud Mansour, Robert L. Judd, Ramesh B. Jeganathan, and Jianzhong Shen for sharing their wisdom, advice, and expertise throughout the years. I appreciate Dr. Chengming Wang for working as my outside reader and providing valuable guidance.

I would like to thank my lab colleagues and alumni, Ren-Lei Ji, Ting Liu, Zheng-Rui Zhang, Li-Qin Ji, Zhi-Shuai Hou, Chuanling Xu, Drs. Min Tao, Yinzhu Rao, Wei Wang, and Zhao Yang, for their valuable contributions to my work. I would like to thank all the faculty members and students in the Department of Anatomy, Physiology and Pharmacology for their kind support. Specifically, I would like to acknowledge China

Scholarship Council of the People's Republic of China for the financial support throughout these four years.

Finally, I am grateful to my loved parents, Jun Yang and Xiaoyan Ha, for their unconditional and endless love, encouragement, and tremendous support. I would like to thank my girlfriend, Dr. Yujia Yang, for her love, support, and encouragement all the time.

Table of Contents

List of Tables

List of Figures

List of Abbreviations

AC	Adenylyl cyclase
ACTH	Adrenocorticotropin
AgRP	Agouti-related peptide
AMPK	5'-AMP-activated protein kinase
ARC	Arcuate nucleus
BSA	Bovine serum albumin
cAMP	3′,5′-cyclic adenosine monophosphate
CNS	Central nervous system
DMEM	Dulbecco's Modified Eagle Medium
EC_{50}	Half maximal effective concentration
ECL	Extracellular loop
ERK1/2	Extracellular signal-regulated protein kinases 1 and 2
Gi	Inhibitory G protein
GnRH	Gonadotropin-release hormone
GPCR	G protein-coupled receptor

Gs	Stimulatory G protein
HEK293T	Human embryonic kidney 293T
hMC3R	Human melanocortin-3 receptor
hMC4R	Human melanocortin-4 receptor
IC_{50}	Half maximal inhibitory concentration
ICL	Intracellular loop
ipMC3R	*Ictalurus punctatus* melanocortin-3 receptor
ipMRAP2	*Ictalurus punctatus* melanocortin receptor accessory protein 2
JNK	c-Jun N-terminal kinases
LH	Luteinizing hormone
maMC4R	*Monopterus albus* melanocortin-4 receptor
MAPK	Mitogen-activated protein kinase
MC3R	Melanocortin-3 receptor
MC4R	Melanocortin-4 receptor
MCR	Melanocortin receptor
MRAP	Melanocortin receptor accessory protein
MSH	Melanocyte-stimulating hormone
MTII	Melanotan II

NDP-MSH	[Nle^4, D-Phe^7]-α-melanocyte-stimulating hormone
pERK1/2	Phosphorylated ERK1/2
PI3K	Phosphoinositide 3-kinase
PKA	Protein kinase A
PKC	Protein kinase C
POMC	Proopiomelanocortin
PRL	Prolactin
PTX	Pertussis toxin
PVN	Paraventricular nucleus
RACE	Rapid amplification of cDNA ends
TMD	Transmembrane domain
WT	Wild type

Chapter 1: Literature review

1.1. Introduction

G protein-coupled receptors (GPCRs), with more than 1000 putative members identified in human genome, constitute the largest part of cell surface receptors (Bockaert and Pin, 1999). GPCRs are regarded as devices that transmit a variety of extracellular signals into the interior. These signals comprise chemical and sensory stimuli, such as hormones, neurotransmitters, chemokines, ions, light, and odorants (Bockaert and Pin, 1999), indicating the significant roles of GPCRs in mediating diverse physiological functions. Based on sequence homology and functional similarity, GPCRs are divided into six classes including rhodopsin-like (Class A), secretin-like (Class B), metabotropic glutamate (Class C), pheromone (Class D), cAMP (Class E), and frizzled (Class F) GPCRs. Of these, Classes D and E are not found in vertebrates. Class A rhodopsin-like GPCRs are the largest component of GPCR superfamily, which consist of more than half of all GPCRs including hormones, neurotransmitters and light receptors.

The melanocortin receptors (MCRs), from melanocortin-1 to -5 receptors (MC1R to MC5R), are members of Family A GPCRs, which play significant roles in regulating diverse physiological processes, such as skin and hair pigmentation (MC1R) (Valverde et al., 1995), adrenal steroidogenesis (MC2R) (Mountjoy et al., 1992), energy homeostasis (MC3R and MC4R) (Cone, 2006), and exocrine gland secretion (MC5R)

(Chen et al., 1997) (reviewed in (Cone, 2006; Tao, 2017). MC3R and MC4R, with the high expression in central nervous system (CNS), are also named neural MCRs. These two receptors have non-redundant roles in regulation of energy homeostasis as emphasized by mice lacking both receptors exhibiting more severe obesity phenotype than mice lacking either receptor alone (Chen et al., 2000). In addition to their critical roles in regulation of energy homeostasis, neural MCRs have been shown to regulate various other physiological processes, such as cardiovascular function, reproduction and sexual function, anti-inflammation, and other functions (Getting et al., 2008; Tao, 2009; Tao, 2010a; Begriche et al., 2013).

This chapter provides an overview of the central melanocortin system including receptors and ligands. The importance of central melanocortin system in regulation of energy homeostasis is discussed. The intracellular signaling pathways triggered by neural MCRs are also highlighted.

1.2. The central melanocortin system

1.2.1. Molecular cloning and tissue distribution of neural MCRs

The human MC3R, first cloned by Gantz and colleagues, was predicted to a single exon gene located on chromosome 20q13.2, encoding a 360 amino acid protein (Gantz et al., 1993a; Magenis et al., 1994). Two studies also suggested that the translation of human MC3R starts at the evolutionary conserved second ATG codon instead of the originally assumed non-conserved first ATG, resulting in a 37 amino acid shorter protein

than previously assumed (Tarnow et al., 2012; Park et al., 2014). Park et al., 2014 further indicated that human MC3R has an additional upstream exon that directs the utilization of the second ATG codon as the translational start site (Park et al., 2014). The MC3R is primarily expressed in hypothalamus, especially in the arcuate nucleus of the hypothalamus (ARC), the ventromedial nucleus of the hypothalamus, and the posterior hypothalamic region (Jegou et al., 2000). In addition to its central distribution, MC3R is also shown to be distributed in several peripheral tissues, such as the placenta, gut, heart, kidney, and peritoneal macrophages (Gantz et al., 1993a; Chhajlani, 1996; Getting et al., 2003; Ni et al., 2006). The peripheral expression of MC3R may suggest its other functions in addition to regulation of energy homeostasis. For example, MC3R activation in macrophages has been shown to exert immunomodulatory effects by controlling some pro-inflammatory and anti-inflammatory mediators, and resolution of inflammation (efferocytosis and phagocytosis) (Patel et al., 2011).

The human MC4R, first cloned in 1990s, is a protein of 332 amino acids encoded by an intronless gene located at chromosome 18q21.3 (Gantz et al., 1993b; Mountjoy et al., 1994). Among five MCRs, the MC4R share the highest homology with the MC3R, with 58% overall amino acid identity and 76% similarity. MC4R is primarily expressed in brain. By *in situ* hybridization in mouse brain sections, Gantz et al. showed that MC4R mRNA is localized in regions of the thalamus, hypothalamus, and hippocampus (Gantz et al., 1993b). Mountjoy et al. also found MC4R to be extensively expressed in the CNS of rat, including the cortex, thalamus, hippocampus, hypothalamus, brain stem, and spinal cord (Mountjoy et al., 1994). In human hypothalamus, highly consistent with that observed in mice and rats, MC4R is primarily expressed in the paraventricular nucleus (PVN), the

supraoptic nucleus, and the nucleus basalis of Meynert (Siljee et al., 2013). In addition to its central expression, the transcripts of MC4R have also been detected in several peripheral tissues, such as heart, lung, muscle, kidney, and testis during the fetal period (Mountjoy et al., 2003). In non-mammalian species, such as fish, MC4R is also abundantly expressed in brain. In spiny dogfish, MC4R expression is exclusive to brain (Ringholm et al., 2003), however in several other fish, MC4R expression can be detected in peripheral tissues, such as gonads, liver, intestine, heart, and kidney (Klovins et al., 2004a; Wei et al., 2013; Li et al., 2016a; Li et al., 2017).

1.2.2. Endogenous ligands of neural MCRs

The neural MCRs have endogenous agonists and antagonists. There are four endogenous agonists, including α-, β-, and γ-melanocyte stimulating hormone (MSH), and adrenocorticotropin (ACTH). They are post-translational processing products of the precursor polypeptide pro-opiomelanocortin (POMC) which is primarily produced by ARC in CNS and the anterior pituitary as well as the skin (Smith and Funder, 1988). The post-translational processing of POMC is tissue specific and only MSHs are produced in the CNS (Pritchard et al., 2002). As the major endogenous agonist in CNS, α-MSH activates neural MCRs to induce a negative energy balance, consisting the catabolic arm of melanocortin system (Krashes et al., 2016). Among numerous GPCRs, of which MCRs belong to, MCRs are quite unique to have endogenous antagonists Agouti and Agouti-related peptide (AgRP). Agouti binds to MC1R with high affinity, whereas AgRP selectively binds to neural MCRs (Fong et al., 1997; Ollmann et al., 1997). AgRP principally antagonizes α-MSH binding to neural MCRs and stimulates a long-lasting

increase in food intake to result in a positive energy balance, representing the anabolic arm of melanocortin system (Hagan et al., 2000; Krashes et al., 2016). However, recent studies found that in mice lacking neuronal MSH, the delayed and long-lasting effects of AgRP on appetite control are independent of melanocortin signaling (Tolle and Low, 2008; Wu et al., 2008). Also, the basal intracellular cAMP levels in cells with MC3R or MC4R expression are decreased by AgRP (Haskell-Luevano and Monck, 2001; Nijenhuis et al., 2001; Chai et al., 2003; Tolle and Low, 2008; Tao et al., 2010). These studies indicate AgRP to be an inverse agonist independent of antagonizing α-MSH.

1.3. The role of central melanocortin system in regulation of energy homeostasis

The central melanocortin system is defined as a collection of central nervous system circuits including different types of neurons in CNS that express either the ligands or the receptors (Fig. 1.1). There are two subsets of neurons within the ARC that express endogenous ligands POMC and AgRP for neural MCRs, respectively (Cone, 2005). These two subsets of neurons are described as “first order” neurons since they are able to sense and integrate the external stimuli (humoral and nutrient cues) including leptin, insulin, ghrelin, serotonin, orexin, and glucose (Cheung et al., 1997; Cowley, 2003; van den Top et al., 2004; Konner et al., 2007; Parton et al., 2007; Xu et al., 2008; Krashes et al., 2016). Among these external stimuli, leptin is the most significant ligand, circulating at levels proportional to the body fat mass to act on the full-length leptin receptor (LepRb) highly expressed in first order neurons (Cheung et al., 1997; Hill et al., 2008), thus stimulating the POMC neurons to increase α-MSH production and suppressing AgRP

neurons to inhibit the release of AgRP. Neurons expressing MC3R and MC4R within multiple areas of brain are the target of α-MSH and AgRP, which are defined as “second order” neurons (Krashes et al., 2016). MC3R and MC4R in these neurons can be activated by α-MSH or inactivated by AgRP to exhibit negative or positive energy balance, respectively (Krashes et al., 2016).

The MC4R is the most intensively studied target in central melanocortin system. In *Mc4r* knockout mouse model, it was demonstrated that MC4R is required for inhibitory effect of leptin on food intake (Marsh et al., 1999) and involved in regulation of metabolism (Ste Marie et al., 2000). Notably, control of food intake and energy expenditure is exerted by different neurons, as demonstrated using loxTB *Mc4r* mice (transcription of *Mc4r* gene was blocked by loxTB sequence), with MC4R in PVN and amygdala regulating food intake while MC4R on neurons outside of PVN and amygdala controlling energy expenditure (Balthasar et al., 2005). Restoration of MC4R expression in PVN/amygdala using Cre-lox technique attenuates 60% of weight gain in loxTB *Mc4r* mice (Balthasar et al., 2005). The increased food intake is completely rescued since 100% of the hyperphagia is prevented in those mice, while reduced energy expenditure is not altered, thus indicating the divergence of melanocortin pathways in controlling food intake and energy expenditure (Balthasar et al., 2005). Subsequent studies showed that MC4R regulates energy expenditure via neurons located in the intermediolateral nucleus of the spinal cord (IML) (Rossi et al., 2011) and dorsomedial nucleus of the hypothalamus (DMH) (Chen et al., 2017). Moreover, cardiovascular functions, linear growth, and cholesterol metabolism are mediated by MC4R within the PVN, whereas glucose metabolism and thermogenesis are mediated by MC4R outside of the PVN (Li et al., 2016b; Chen et al., 2017). Another recent

study demonstrated that MC4R in POMC neurons may act as an auto-excitatory and/or an auto-potentiation mechanism enhancing POMC neuron activation to regulate energy homeostasis (do Carmo et al., 2013). Although studies on functional roles of MC3R in energy homeostasis are less extensive compared with that of the MC4R, MC3R is also important in regulation of energy homeostasis (Butler et al., 2000; Chen et al., 2000). Different from *Mc4r* deletion causing hyperphagia in mice, *Mc3r* deleted mice exhibit increased fat mass and reduced lean mass despite normal food intake or hypophagia (Butler et al., 2000; Chen et al., 2000), suggesting that MC3R is primarily involved in regulation of feed efficiency. Another important role of MC3R in maintaining energy homeostasis is regulation of circadian rhythm: *Mc3r* deleted mice display abnormal rhythmic expression of clock genes (Girardet and Butler, 2014), impaired behavioral adaption (Begriche et al., 2012), and anomalous metabolic adaption to restricted feeding (Sutton et al., 2010). Also, MC3R expressed by POMC neurons was identified and proposed to serve an auto-inhibitory role inhibiting POMC neuron activation to regulate energy homeostasis (Bagnol et al., 1999; Cowley et al., 2001).

In addition to studies using animal models, human genetic studies provided further evidence for the function of these two receptors in regulating energy homeostasis. So far, a substantial number of human *MC3R* and *MC4R* naturally occurring mutation have been identified to be associated with obesity, with 33 *MC3R* mutations and more than 170 *MC4R* mutations identified in different cohorts from Asia, Europe and North America (reviewed in (Tao, 2010a; Demidowich et al., 2017)).

Collectively, the central melanocortin system serves as the intersection point which connects the neural pathways controlling satiety and metabolism to maintain energy homeostasis by sensing and integrating the signals of external stimuli (Fig. 1.1).

1.4. Multiple signaling pathways of neural MCRs

On the cell membrane, upon agonist binding, neural MCRs are activated and undergo conformational change, thereby generating intracellular signaling, including both G protein-dependent and -independent signaling.

Like other Gαs-coupled GPCR family members, once neural MCRs are activated, the α-subunit of Gs protein will disassociate from the βγ heterodimer and then activate adenylyl cyclase (AC) to increase the intracellular cAMP levels and subsequently activate protein kinase A (PKA). This Gαs-protein mediated signaling is the conventional intracellular signaling and also the most commonly investigated in MCR intracellular signaling studies.

In addition to Gαs, the MC4R can couple to other G proteins, such as Gαi protein which inhibits AC activity to decrease cAMP level (Büch et al., 2009) and Gαq protein which activates phospholipase C (PLC) and downstream kinase protein kinase C (PKC) (Newman et al., 2006). Büch et al. observed that in hypothalamic cell line GT1–7 cells , α-MSH-induced incorporation of GTPγS35 (a measure of G protein activation) can be partially (~50%) blocked by pertussis toxin (PTX) and α-MSH-induced cAMP accumulation is increased due to the PTX treatment by 53% (PTX is a Gi inhibitor),

suggesting that both Gαs and Gαi proteins are activated through MC4R upon α-MSH stimulation (Büch et al., 2009). Newman et al. confirmed that MC4R mediates increase of intracellular Ca^{2+} level through Gαq-PLC dependent signaling in another hypothalamic cell line, GT1–1 cell (Newman et al., 2006). Other signaling pathways are also identified in cells expressing MC4Rs, including extracellular signal–regulated kinases 1/2 (ERK1/2), c-Jun N-terminal kinases (JNK), 5'-AMP-activated protein kinase (AMPK), and protein kinase B (PKB or AKT) (Minokoshi et al., 2004; Vongs et al., 2004; Sutton et al., 2005; Chai et al., 2007; Chai et al., 2009; Damm et al., 2012; Yang and Tao, 2016a).

ERK1/2 pathway is one of three mitogen-activated protein kinases (MAPK) pathways, and the other two pathways are JNK and p38 (Johnson and Lapadat, 2002). ERK1/2 activation through MC4R varies based on cell types and ligands used. In GT1-7 cells, ERK1/2 activation through MC4R induced by α-MSH is only PKA-dependent (Damm et al., 2012). In rat solitary nucleus neurons, the PKA-dependent ERK1/2 activation through MC4R is increased after central administration of MCR agonist, Melanotan II (MTII) (Sutton et al., 2005). [Nle^4, D-Phe^7]-α-MSH (NDP-MSH) induces ERK1/2 activation via Gi protein in HEK293 cells expressing MC4Rs, but through Ca^{2+}/PKC pathway in GT1-1 cells (Chai et al., 2006). In CHO-KI cells, ERK1/2 activation through MC4R is mediated by phosphoinositide 3-kinase (PI3K) rather than PKA (Vongs et al., 2004). The diversity of ERK1/2 activation through MC4R makes this signaling pathway complicated. Although β-arrestin mediated ERK1/2 activation was observed in MC5R (Rodrigues et al., 2012) and other GPCRs such as β_2-adrenergic receptor, V2 vasopressin receptor, parathyroid hormone receptor subtype 1, and angiotensin II receptor type 1A (DeWire et al., 2007), and even β-arrestin mediated MC4R endocytosis

was demonstrated (Shinyama et al., 2003; Breit et al., 2006), there is still no evidence of β-arrestin-mediated ERK1/2 activation in MC4R.

For the JNK pathway, NDP-MSH does-dependently inhibits JNK in HEK293 cells stably expressing MC4R (Chai et al., 2009). AMPK phosphorylation level was demonstrated to be decreased by MC4R activation with MTII in PVN neurons and NDP-MSH stimulation in MC4R-transfected HEK293T cells (Minokoshi et al., 2004; Yang and Tao, 2016a). AKT activation is induced by NDP-MSH in GT1-7 cells (Yang and Tao, 2016a). Ion channels on the cell membrane are thought to be effectors in a variety of signaling pathways initiated by GPCRs. Regulation of ion channels by G protein can be indirect (via second messengers and activation of downstream kinase) or direct (via G protein βγ subunits) (Dascal, 2001). One recent study showed that MC4R in PVN neurons can couple to potassium channel Kir7.1 independent of G protein (Ghamari-Langroudi et al., 2015), further expanding the intracellular signaling effectors of MC4R.

Intracellular signaling of MC3R, compared to that of MC4R, is less extensively studied. In addition to the Gαs signaling pathway, MC3R can couple to Gαi protein and activate ERK1/2 signaling via a Gαi protein-PI3K signaling system in HEK293 cells upon NDP-MSH stimulation, which is independent of PKA, PKC and Ca^{2+} (Chai et al., 2007). However, data obtained from our lab showed that AgRP induces ERK1/2 activation through MC3R in HEK293T cells independent of PKA and PI3K (Yang and Tao, 2016a), suggesting the mechanism of ERK1/2 activation through MC3R is also different based on cell types and ligands. As with MC4R, it is still unclear on the role of β-arrestin in ERK1/2 activation, although MC3R endocytosis and desensitization are mediated by β-arrestin

(Breit et al., 2006; Nyan et al., 2008). MC3R activation was also demonstrated to activate AKT (Nyan et al., 2008; Yang and Tao, 2016a), to increase intracellular Ca^{2+} levels dependent or independent of inositol 1,4,5 triphosphate (IP3) (Konda et al., 1994; Mountjoy et al., 2001), to induce PKC pathway (Wachira et al., 2003), and to induce sustained inhibition of AMPK activity (Yang and Tao, 2016a).

So far, several studies have identified the physiological functions of multiple intracellular signaling pathways initiated by neural MCRs. The conventional Gαs signaling of MC4R has been shown to be crucial in inducing anorexigenic signaling in hypothalamus to result in a negative energy balance. However, paradoxical evidences that some constitutively active mutant MC4Rs with increased cAMP generation were identified from obese individuals (Tao, 2010a) suggest that Gαs signaling pathway through MC4R is not the only pathway involved in regulation of energy homeostasis, and other pathways through MC4R independent of Gαs protein may also be involved. Further studies confirmed that only energy expenditure mediated by MC4R is through Gαs signaling pathway since CNS-specific Gαs deficiency results in a specific defect in energy expenditure without effect on food intake (Chen et al., 2009; Chen et al., 2012). Food intake, as another aspect of maintaining energy homeostasis through MC4R, is shown to be controlled by several signaling pathways. Regulation of food intake mediated by MC4R is controlled by Gαq signaling pathway with the evidence that PVN-specific Gαq deletion causes hyperphagic obesity without affecting energy expenditure (Li et al., 2016b).

MC4R modulation of the AMPK pathway in PVN neurons is also involved in regulating food take. MC4R activation decreases AMPK phosphorylation thereby

inhibiting food intake (Minokoshi et al., 2004). ERK1/2 signaling through MC4R is thought to be involved in regulating energy homeostasis by mediating inhibition of food intake (Sutton et al., 2005; Damm et al., 2012) in addition to its function on mediating cell proliferation and inhibiting apoptosis (Chai et al., 2006). A recent study showed that food intake inhibition caused by MC4R activation is dependent on coupling to closure of potassium channel Kir7.1 to cause PVN neuron depolarization (Ghamari-Langroudi et al., 2015). Although MC3R primarily regulates energy homeostasis by controlling feed efficiency and maintaining circadian rhythm, the relationship between its G protein-mediated intracellular signaling pathways and the physiological effects has not been widely investigated. Additionally, MC3R-mediated ERK1/2 signaling cascade is involved in regulation of feeding behaviors (Begriche et al., 2012) other than its function on mediating cell proliferation (Chai et al., 2007) and anti-inflammation (Montero-Melendez et al., 2015).

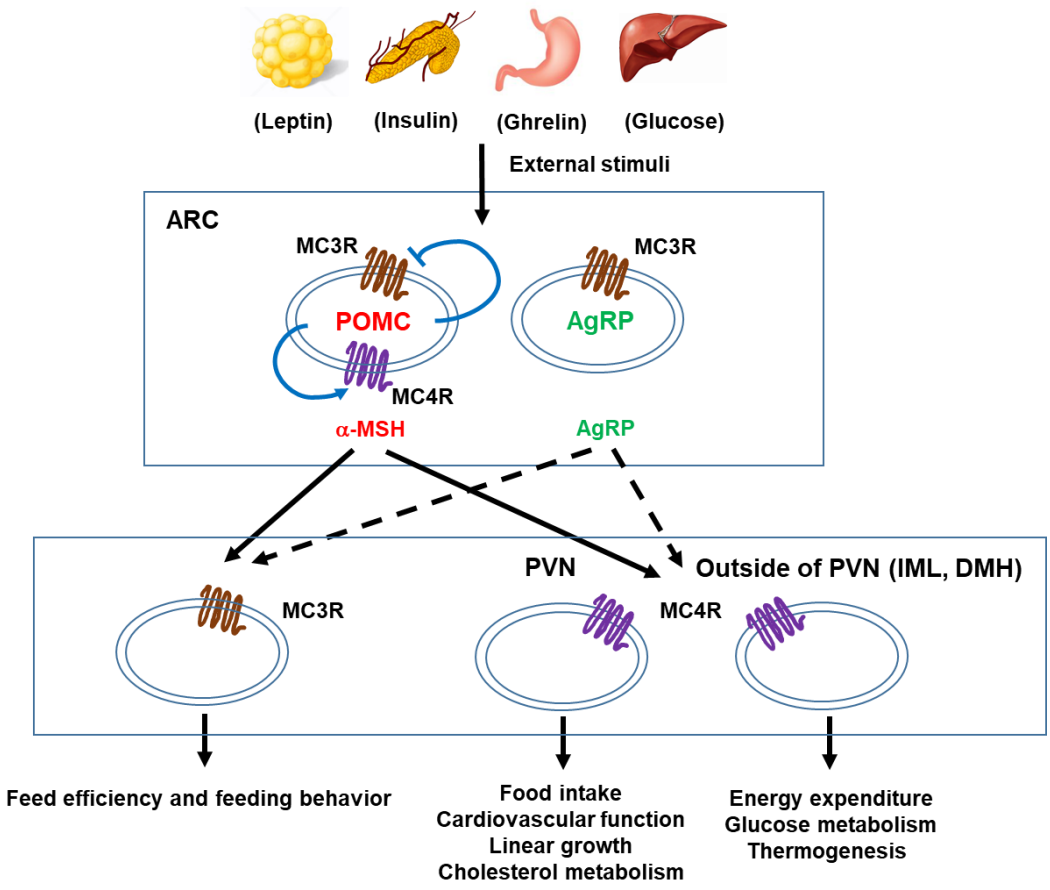

Fig. 1.1 The central melanocortin system. POMC and AgRP neurons in the ARC are defined as “first order” neurons which integrate external stimuli and project to “second order” neurons with neural MCR expression. Neurons in PVN, intermediolateral nucleus of the spinal cord (IML), and dorsomedial nucleus of the hypothalamus (DMH), mediate different physiological functions in energy homeostasis. MC3R and MC4R in POMC neurons can also serve auto-inhibitory and auto-excitatory roles to regulate energy homeostasis.

Chapter 2: Functions of DRYxxI motif and intracellular loop 2 of human melanocortin-4 receptor

2.1. Introduction

Obesity, usually associated with several adverse health conditions, such as type 2 diabetes mellitus, hypertension, cardiovascular disease, and certain types of cancer (Guh et al., 2009), has become a critical healthy issue over the world. It is commonly caused by imbalanced energy intake and expenditure. Many genetic factors are involved in the development of obesity (O'rahilly et al., 2003). The melanocortin-4 receptor (MC4R), highly expressed in central nervous system (CNS), is one of the major factors in obesity pathogenesis. MC4R is crucial in regulation of both food intake and energy expenditure (Huszar et al., 1997). Targeted deletion of *Mc4r* in mice causes maturity onset obesity associated with hyperphagia, hyperinsulinemia, and hyperglycemia (Huszar et al., 1997). Human genetic studies also revealed that 5.8% of subjects with severe obesity commencing childhood have mutations in MC4R, demonstrating dysfunction of MC4R to be the most common cause of monogenetic obesity (Farooqi et al., 2003).

As a member of Family A G protein-coupled receptors (GPCRs), MC4R has seven hydrophobic transmembrane domains (TMDs) connected by several intracellular and

extracellular loops (ICLs and ECLs). Activation of MC4R results in GDP/GTP exchange in the α-subunit of stimulatory G (Gs) protein. The α-subunit dissociates from $\beta\gamma$ heterodimer and activates adenylyl cyclase (AC) to increase intracellular cyclic AMP (cAMP) level and subsequently enhance protein kinase A (PKA) activity. This conventional Gs-cAMP signaling pathway is crucial in inducing anorexigenic effect to result a negative energy balance. In addition, MC4R also activates ERK1/2 (Daniels et al., 2003; Vongs et al., 2004), one of three mitogen-activated protein kinases (MAPK) pathways. The ERK1/2 activation through MC4R has been shown to regulate energy homeostasis by inhibiting food intake (Sutton et al., 2005; Damm et al., 2012). Therefore, both Gs-cAMP and ERK1/2 signaling pathways are related to the MC4R function of energy homeostasis.

Constitutive activation of GPCRs is characterized by signaling in the absence of agonist stimulation. The constitutive activity of MC4R is essential for maintaining normal energy homeostasis in humans. It has been suggested that defect in constitutive activity of MC4R in the cAMP pathway attenuates the tonic satiety signal resulting in dysfunctional energy balance and obesity (Srinivasan et al., 2004; Tao, 2014). Recent study suggested that constitutive and agonist-induced MC4R activations differentially modulate signal to impact on distinct subtypes of voltage-gated calcium channels (Agosti et al., 2017). The constitutive activity of MC4R can affect the specific channels controlling transcriptional activity coupled to depolarization and neurotransmitter release (Agosti et al., 2017). Moreover, MC4R can also be constitutively active in the ERK1/2 pathway (Mo et al., 2012), suggesting that the constitutive activation of ERK1/2 pathway may be involved in maintaining normal energy homeostasis.

The interactions involving highly conserved residues at the cytoplasmic surface are crucial for signaling properties in GPCRs. Crystal structural studies in several Family A GPCRs reveal that DRYxxI motif in the end of TMD3 is of importance for receptor function. Conversed amino acids in DRYxxI motif and TMD6 form polar interactions (commonly termed as 'ionic lock'), bridging two transmembrane domains to stabilize receptor in an inactive conformation (Vogel et al., 2008; Rosenbaum et al., 2009). Once receptor binds to ligands, this 'ionic lock' is broken and the new interaction forms between DRYxxI motif and TMD5, triggering receptor into an active conformation (Yao et al., 2006; Rosenbaum et al., 2009). Therefore, DRYxxI motif is critical in constraining receptor in inactive conformation. The ICL2, linking TMD3 and TMD4, serves as a platform for hydrogen-bonding interaction between a conserved tyrosine on ICL2 and DRYxxI motif (Rosenbaum et al., 2009). ICL2 participates in G protein coupling and β-arrestin binding, indicating the significance of this loop in receptor activation and desensitization (Raman et al., 1999).

One of our previous studies based on alanine-scanning mutagenesis has proven that DRYxxI motif and ICL2 are critical for human MC3R (hMC3R) function (Huang and Tao, 2014). However, systematic study of this domain in human MC4R (hMC4R) is still lacking. In order to enhance the understanding of structure-functional relationship of hMC4R, we generated seventeen mutants in total using alanine-scanning mutagenesis to investigate the functional roles of residues in this domain. Cell surface expression, ligand binding properties, and signaling properties of Gs-cAMP and ERK1/2 pathways of these seventeen mutants were investigated in the present study.

2.2. Materials and methods

2.2.1. Materials

Human embryonic kidney 293T (HEK293T) cells were purchased from American Type Culture Collection (Manassas, VA, USA). [Nle^4, D-Phe^7]-α-melanocyte-stimulating hormone (NDP-MSH) and Agouti-related peptide (AgRP) (8-132) were purchased from Peptides International (Louisville, KY, USA). Ipsen 5i and ML00253764 were synthesized by Enzo Life Sciences, Inc. (Plymouth Meeting, PA, USA). [^{125}I]-NDP-MSH and [^{125}I]-cAMP were iodinated using the chloramine-T method as described previously (Steiner et al., 1969; Mo et al., 2012). The N-terminal c-myc-tagged WT hMC4R subcloned into pcDNA3.1 vector was generated as previous described (Tao and Segaloff, 2003).

2.2.2. Site-directed mutagenesis

Mutant hMC4Rs were generated from the WT receptor by QuikChange site-directed mutagenesis kit (Stratagene, La Jolla, CA, USA) using the primers listed in Table 1.1. The sequences were verified by direct nucleotide sequencing by the DNA Sequencing Facility of University of Chicago Cancer Research Center (Chicago, IL., USA).

2.2.3. Cell culture and transfection

HEK293T cells were cultured in Dulbecco's Modified Eagle's Medium (DMEM) (Invitrogen, Carlsbad, CA, USA) containing 10% newborn calf serum (PAA Laboratories Inc., Etobicoke, ON, Canada), 10 mM HEPES, 100 units/ml penicillin, 100 μg/mL streptomycin, 50 μg/mL of gentamicin, and 0.25 μg/mL amphotericin B, at 37 °C and 5% CO_2 humidified atmosphere. For flow cytometry, ligand binding, and cAMP signaling

studies, cells were seeded into gelatin-coated six-well plates (Corning, NY, USA) and were transfected with WT or mutant hMC4Rs at approximately 70% confluence using the calcium phosphate precipitation method as described previously (Chen and Okayama, 1987). For western blot, cells were plated into gelatin-coated 100 mm dishes (Corning) and transfected using same method.

2.2.4. Quantification of receptor cell surface expression by flow cytometry

HEK293T cells were transfected as described above. Approximately 48 h after transfection, six-well plates were placed on ice, and cells were washed once with cold PBS for immunohistochemistry (PBS-IH) (Tao and Segaloff, 2003), detached with PBS-IH, and centrifuged at 1,500 rpm for 5 min. Then, cells were fixed with 4% paraformaldehyde in PBS-IH for 15 min. After blocking with PBS-IH containing 5% bovine serum albumin (BSA, EMD Millipore Corporation, USA) for 1 h, cells were incubated for another 1 h, with the primary antibody 9E10 monoclonal anti-myc antibody (Developmental Studies Hybridoma Bank at the University of Iowa, Iowa City, IA, USA) 1:40 diluted in PBS-IH containing 0.5% BSA (PBS-IH/BSA). After incubation, cells were washed once with PBS-IH/BSA, and incubated for 1 h, with the secondary antibody Alexa Fluor 488-conjugated goat anti-mouse IgG (Invitrogen) 1:1500 diluted in PBS-IH/BSA. After incubation, cells were washed once with PBS-IH/BSA, filtered to obtain single cell suspension, and assayed using a C6 Accuri Cytometer (Accuri Cytometers, Ann Arbor, MI, USA). Cells transfected with pcDNA3.1 were used as control for background staining. The expression levels of mutant hMC4Rs were calculated by the following formula: (mutant-pcDNA3.1)/(WT-pcDNA3.1) × 100% (Wang et al., 2008).

2.2.5. Ligand binding assay

HEK293T cells were transfected as described above. Approximately 48 h after transfection, cells were washed with warm DMEM containing 1 mg/mL BSA. Then, cells were incubated with DMEM/BSA, ~80,000 cpm of [^{125}I]-NDP-MSH, and without or with different concentrations of unlabeled NDP-MSH at 37 °C (final concentrations ranged from 10^{-11} to 10^{-6} M). One hour later, cells were washed with cold Hank's balanced salt solution containing 1 mg/mL BSA, lysed by 100 μL 0.5 N NaOH, and collected by cotton swabs. The radioactivity of cells lysates was measured in a gamma counter (Cobra II Auto-Gamma, Packard Bioscience Co., Germany).

2.2.6. cAMP assay

HEK293T cells were transfected as described above. Approximately 48 h after transfection, cells were washed with warm DMEM/BSA and incubated with fresh DMEM/BSA containing 0.5 mM isobutylmethylxanthine at 37 °C for 30 min. Cells were then treated without or with NDP-MSH (final concentrations ranged from 10^{-12} to 10^{-6} M) for investigation of ligand-induced cAMP signaling. Cells were also treated without or with Ipsen 5i (10^{-6} M), ML00253764 (10^{-5} M), or AgRP (8-132) (10^{-8} M) for investigation of constitutive activities of some mutant hMC4Rs in cAMP signaling. After one hour incubation, cells were lysed by 0.5 M perchloric acid containing 180 μg/mL theophylline and neutralized by 0.72 M KOH/0.6 M $KHCO_3$. The cAMP levels were determined by radioimmunoassay (RIA) as described previously (Steiner et al., 1969). The diluted samples (500 μl) were acetylated by adding 20 μl 5 N KOH and 5 μl acetic anhydride followed by immediate vortex and incubation on ice for 30 min. Then, the acetylated

samples were transferred into plastic test tubes (50 μl for each), and mixed with 10 μl 250 mM NaOAc, 50 μl cAMP anti-body solution, and 50 μl [^{125}I]-cAMP solution (~ 15,000 cpm). Then, the mixtures were incubated at 4 °C overnight. Nest day, 12% polyethylene glycol was added into each tube to separate the anti-body-bound cAMP from the free cAMP. The samples were centrifuged at 3,200 rpm at 4 °C for 30 min. The supernatant was aspirated, and the radioactivity of precipitate was counted by a gamma counter (Packard Bioscience).

2.2.7. Protein preparation and western blot

For protein preparation, HEK293T cells were transfected as described above. Approximately 24 h after transfection, cells were starved in DMEM/BSA at 37 °C for 24 h. On the day of experiment, cells were treated without or with 10^{-6} M NDP-MSH at 37 °C for 5 min. After treatment, cells were then solubilized in lysis buffer containing phosphatase and protease inhibitors. Total protein concentrations of cell lysates were determined using the Bradford protein assay.

For western blot, 35 μg protein samples were separated on 10% SDS-PAGE gel and transferred onto PVDF membrane for immunoblotting. The PVDF membranes were blocked in 10% nonfat dry milk (containing 0.2% Tween-20) for 4 h at room temperature, and immunoblotted with rabbit anti-phosphorylated ERK1/2 (pERK1/2) antibody (Cell signaling, Beverly, MA, USA) 1:5000 and mouse anti-β-tubulin antibody (Development Studies Hybridoma Bank, University of Iowa, Iowa City, IA, USA) 1:5000 diluted in Tris-buffered saline containing Tween-20 (TBST) with 5% BSA overnight at 4 °C. On the next day, PVDF membranes were washed with TBST for 1 h and then probed with horseradish

peroxidase-conjugated secondary antibodies, donkey anti-rabbit IgG (Jackson ImmunoResearch Laboratories, West Grove, PA, USA) 1:5000 and donkey anti-mouse IgG (Jackson ImmunoResearch Laboratories, West Grove, PA, USA) IgG 1:5000 diluted in 10% nonfat dry milk for 1~2 h at room temperature. Membranes were washed with TBST for 1 h and specific bands were detected with ECL reagent (Thermo Scientific, Rockford, IL, USA) and were analyzed and quantified by Image J Software (NIH, Bethesda, MD, USA).

2.2.8. Statistical analysis

GraphPad Prism 4.0 Software (San Diego, CA, USA) was used to calculate the ligand binding parameters including IC_{50} and maximal binding, and cAMP signaling parameters including EC_{50} and maximal response. To determine the significance of differences in cell surface expression, ligand binding and cAMP signaling parameters, and pERK1/2 levels between WT and mutant hMC4Rs, Two-tailed Student's *t*-test was performed.

2.3. Results

To investigate the function of each residue of DRYxxI motif and ICL2 of hMC4R (Fig. 2.1), alanine-scanning mutagenesis was performed to mutate each residue to alanine or alanine to glycine. A total of seventeen mutant hMC4Rs were generated. NDP-MSH, a super-potent analog of endogenous agonist α-MSH (Sawyer et al., 1980), was used in the present study.

2.3.1. Cell surface expression of the mutant hMC4Rs

It is known that mutations may impact receptor on cell surface expression with defective protein synthesis or failure of passing through the quality control and retention in endoplasmic reticulum. To quantitate the cell surface expression of mutant hMC4Rs, flow cytometry technique was performed in the present study. As shown in Fig. 2.2, T150A, had significantly lower cell surface expression (57.98 ± 10.03% of WT), suggesting that this mutant was defective in synthesis or partially retained. Four mutants (A154G, Q156A, Y157A, and M161A) had slightly increased cell surface expression with statistical significance. All the other mutants were expressed normally on the cell surface as WT hMC4R.

2.3.2. Ligand-binding properties of the mutant hMC4Rs

To study ligand binding of the mutant hMC4Rs, unlabeled NDP-MSH and radiolabeled NDP-MSH ([^{125}I]-NDP-MSH) were used in the competitive ligand binding assay. Fig. 2.3 showed the results from ligand binding experiments of WT and mutant hMC4Rs to [^{125}I]-NDP-MSH, displaced by unlabeled NDP-MSH with the increase of ligand concentration. As shown in Table 2.2, [^{125}I]-NDP-MSH bound to WT hMC4R was displaced by unlabeled NDP-MSH with an IC_{50} of 19.43 ± 2.10 nM similar as the previous values. Of these mutant hMC4Rs, D146A, Y148A, M160A, and M161A had significantly decreased IC_{50}s compared with the WT hMC4R, indicating that these four mutants exhibited increased affinities with the ligand. However, T150A had significantly increased IC_{50} (40.25 ± 6.11 nM) relative to the WT hMC4R therefore decreased affinities with the ligand. In addition, seven mutants (D146A, Y148A, Y153A, Q156A, Y157A, M161A, and

T162A) had significantly decreased maximal binding compared to the WT hMC4R whereas two mutants (F149A and N159A) exhibited increased maximal binding with statistically significance (Table 2.2 and Fig. 2.3).

2.3.3. Signaling properties of the mutant hMC4Rs in cAMP pathway

To investigate both constitutive activities and ligand-induced signaling properties of hMC4R variants in cAMP pathway, HEK293T cells with WT or mutant hMC4Rs expression were stimulated without or with different concentrations of NDP-MSH. Consistent with previous studies, the WT hMC4R, in the present study, was constitutively active (basal cAMP level: 41.45 ± 4.38 pmol/10^6 cells). Five mutants (R147A, T150A, I151A, L155A, and Y157A) had significantly decreased basal cAMP levels compared to WT receptor (Table 2.2 and Fig. 2.4A). The basal cAMP production of T150A, which had reduced cell surface expression, was only 19.34 ± 4.05% of WT basal. However, six mutants (D146A, Y148A, F149A, F152A, Y153A, and H158A) displayed the elevation of basal cAMP levels compared with WT basal (Table 2.2 and Fig. 2.4A).

To further confirm whether these six mutants are indeed constitutively active mutants. Three inverse agonists, including two MC4R small molecule ligands, Ipsen 5i and ML00253764, and one MC4R endogenous ligand AgRP (8-132), were used to treat the cells with expression of these six mutants. As shown in Fig. 2.4B, the basal cAMP levels of five mutants (Y148A, F149A, F152A, Y153A, and H158A) could be reduced by treatment of Ipsen 5i (10^{-6} M) and ML00253764 (10^{-5} M). Of the WT and five mutants, the inhibition ranged from 60 to 86%. In contrast, D146A showed activation rather than inhibition after treatment of these two small molecules. Moreover, AgRP (8-132) (10^{-8} M)

could decrease the basal cAMP levels of WT and all six mutants with the inhibition ranging from 36 to 63%.

NDP-MSH-stimulated cAMP levels were also measured in WT MC4R and mutants. As shown in Table 2.2 and Fig. 2.5, we found that NDP-MSH dose-dependently increased intracellular cAMP accumulation in cells transfected with WT hMC4R with an EC_{50} of 0.38 ± 0.07 nM. Seven mutants (D146A, R147A, T150A, I151A, L155A, Q156A, and Y157A) were less capable of producing cAMP reflected by their significantly increased EC_{50}s. Two mutants (F152A and H158A) showed the decreased EC_{50}s, suggesting that they could response to NDP-MSH stimulation more potently. When maximal responses were analyzed, only one mutant, T150A, was demonstrated to have remarkably decreased maximal response (17.62 ± 3.60% of WT) despite normal maximal binding. Two mutants, M161A and T162A, which had very low maximal binding, showed significantly, although very slightly, increased maximal response.

2.3.4. Signaling properties of the mutant hMC4Rs in ERK1/2 pathway

To investigate the signaling properties of mutant hMC4Rs in ERK1/2 pathway, pERK1/2 levels were measured by western blot. Our data showed that all mutants did not exhibit statistically significant alternations on the basal pERK1/2 levels relative to WT basal (Fig. 2.6A and C). WT hMC4R could respond to NDP-MSH stimulation in ERK1/2 pathway with more than two-fold increased pERK1/2 level. The mutants also had significantly increased pERK1/2 levels in presence of NDP-MSH stimulation except for five mutants (D146A, F149A, Y153A, Y157A, and M161A) (Fig. 2.6A and B). Although the pERK1/2 levels of four mutants (R147A, Y148A, H158A, and I160A) were increased

significantly upon NDP-MSH stimulation, the fold-changes were significantly lower than that of WT receptor (Fig. 2.6B).

2.4. Discussion

In the present study, we performed a systematic investigation on the seventeen residues of DRYxxI motif and ICL2 of hMC4R based on the alanine-scanning site-directed mutagenesis. NDP-MSH, a super-potent analog of α-MSH (Sawyer et al., 1980), was used in this study to assess ligand binding, Gs-cAMP signaling, and ERK1/2 signaling properties of hMC4R mutants.

The flow cytometry experiment was performed to quantitate the mutant receptors expression on cell membrane. All the mutant hMC4Rs had normal or higher cell surface expression compared with WT hMC4R except for one mutant T150A with ~60% cell surface expression level of WT receptor, suggesting its defective synthesis or intracellular retention (Fig. 2.2). One naturally occurring mutant, T150I, also showed the defective cell surface expression (Xiang et al., 2006). We speculated that the corresponding residue might be a critical site for cell surface expression of MC4R.

Competitive binding assay revealed that alanine mutations of eight residues (D146, Y148, T150, Y153, Q156, Y157, M161, and T162) impaired ligand binding with either increased IC_{50}s or decreased maximal binding (Table 2.2 and Fig. 2.3). D146A, M161A, and T162A caused severely reduced maximal binding (Table 2.2 and Fig. 2.3), which was similar as our previous finding that alanine mutants of corresponding residues in hMC3R

(D178, M193, and T194) exhibited undetectable binding properties (Huang and Tao, 2014), suggesting that these three residues were important for ligand binding in both melanocortin receptors. Residues in the DRYxxI motif and ICL2 are located at the transmembrane and cytoplasmic region (Fig. 2.1). Although these residues are remote from the binding pocket which is formed by residues located in extracellular side, and not directly involved in receptor-ligand interaction, these residues are still indispensable in receptor-ligand binding by influencing receptor conformational change and indirectly modulating the receptor-ligand interaction. This observation was similar with previous results reported in MC3R and MC4R, as well as other GPCRs (Erlenbach et al., 2001; Lu et al., 2005; Huang and Tao, 2014; Yang et al., 2015b).

Constitutive activities of the hMC4R have been suggested to play a significant role in physiology and pathophysiology. Loss of constitutive activity in the mutant hMC4Rs is known as one cause of obesity (Srinivasan et al., 2004). Some naturally occurring *MC4R* mutations were indeed found to decrease the constitutive activity (Tao and Segaloff, 2005). Paradoxically, some could increase the constitutive activity (Vaisse et al., 2000; Hinney et al., 2003; Valli-Jaakola et al., 2004). It remains unknown whether mutations resulting in the enhanced constitutive activation of receptor are the cause of obesity.

In cAMP assay, we found that eleven alanine mutants exhibited altered basal cAMP levels on Gs-cAMP pathway (Table 2.2 and Fig. 2.4A). Mutations on the corresponding sites might break and shift the equilibrium between receptor inactive and active states, resulting in either enhanced or reduced constitutive activation. Five mutant hMC4Rs (R147A, T150A, I151A, L155A, and Y157A) exhibited decreased basal cAMP levels, implicating that these residues were important for signal transduction in the

absence of agonist. Six mutants (D146A, Y148A, F149A, F152A, Y153A, and H158A) displayed enhanced basal cAMP levels which could be partially inhibited by Ipsen 5i, ML00253764, and AgRP (8-132) with the exception that two small molecule ligands (Ipsen 5i and ML00253764) failed to decrease the basal cAMP level of D146A (Fig. 2.4B). Our results indicated that these six mutants were indeed constitutively active mutants.

It has been suggested that the highly conserved DRYxxI motif can interact with residues on TMD6 to regulate the receptor conformational switch between inactive and active states in Family A GPCRs (Ballesteros et al., 2001; Angelova et al., 2002; Greasley et al., 2002; Zhang et al., 2005a). The crystal structure of the inactive state of rhodopsin indicates that the basic arginine ($R^{3.50}$) forms double salt bridges with neighboring aspartic acid ($D^{3.49}$) and glutamic acid ($E^{6.30}$) on TMD6 (Ballesteros & Weinstein numbering scheme (Ballesteros and Weinstein, 1995)) to constrain receptor in the ground state (Palczewski et al., 2000). Mutations on $D^{3.49}$ in several GPCRs, such as rhodopsin, α_{1B}-adrenergic receptor, vasopressin type II receptor, β_2-adrenergic receptor, and μ-opioid receptor, could frequently induce constitutive activation (reviewed in (Rovati et al., 2007)). Our results demonstrated that alanine substitution on $D146^{3.49}$ of hMC4R resulted in approximately three-fold increase of basal cAMP level (Table 2.2 and Fig. 2.4), indicating the crucial role of $D146^{3.49}$ in constraining receptor in its ground state. One hMC4R naturally occurring mutant, $D146N^{3.49}$, has also been shown to exhibit increased constitutive activity (Wang and Tao, 2011). However, alanine mutation on $R147^{3.50}$ of hMC4R caused decreased basal cAMP level (Table 2.2 and Fig. 2.4A), implicating that $R147^{3.50}$ might be important in involved in contacting Gα to stabilize the active status of the receptor-G protein complex as supported by previous well know findings (Scheerer et

al., 2008; Rasmussen et al., 2011), but might not form salt bridge with the residue on TMD6 (N240A$^{6.30}$) to constrain receptor in the ground state (Huang and Tao, 2012).

T150$^{3.53}$ is also highly conserved throughout the rhodopsin-like GPCRs. Our data showed that alanine mutations on this residue could dramatically decrease the constitutive activity (Table 2.2 and Fig. 2.4A). The reduced constitutive activity of T150A should be considered with its low cell surface expression. Among the residues important for MC4R constitutive activation in ICL2, alanine mutation on H158 caused almost eight-fold increase in constitutive activity. Given that one naturally occurring mutant H158R exhibited more than six-fold increase on constitutive activity compared with WT hMC4R (Hinney et al., 2006), we consider that H158 might also be a significant residue for constraining receptor in inactive conformation.

Seven mutants, D146A, R147A, T150A, I151A, L155A, Q156A, and Y157A, had impaired Gs-cAMP signaling upon NDP-MSH stimulation. Alanine mutations on these residues were shown to result in the defect of NDP-MSH-stimulated Gs-cAMP pathway with reduced signaling potencies (Table 2.2 and Fig. 2.5). The signaling deficiencies of three mutants (D146A, Q156A, and Y157A) were likely due to their impaired ligand binding properties. Among other signaling defective mutants, we found that T150A had severely reduced maximal response apart from increased EC_{50} (Table 2.2 and Fig. 2.5). The defective signaling properties of T150A might be primarily caused by low cell surface expression (Fig. 2.2). Moreover, low affinity to NDP-MSH might also be a cause (Table 2.2). Alanine mutations on the corresponding position 3.53 in MC3R (Huang and Tao, 2014), follicle-stimulating hormone receptor (Timossi et al., 2002), and angiotensin II type 1 receptor (Miura et al., 2000) were also reported to affect receptor signaling.

Alanine mutation on I151$^{3.54}$, which is distal to the DRYxxI motif, impaired Gs-cAMP signaling (reduced constitutive activity and increased EC_{50}) without changing ligand binding properties, suggesting that this residue was also critical in signaling transduction. Some previous studies have demonstrated that the corresponding residue 3.54 is involved in receptor-G protein coupling. Several mutations on this residue of MC3R, including I183A$^{3.54}$, I183N$^{3.54}$, and I183R$^{3.54}$, caused profound loss of agonist-stimulated cAMP production (Tao and Segaloff, 2004; Huang and Tao, 2014). One hMC4R mutant, I151N$^{3.54}$, also displayed no-detectable agonist-stimulated cAMP production despite normal ligand binding (Tao and Segaloff, 2004). L155$^{3.58}$ is a highly conserved residue in rhodopsin-like GPCRs and was reported to be critical for G protein coupling. Impaired receptor activation caused by mutations on corresponding position has been shown in other GPCRs, such as MC3R (Huang and Tao, 2014), β_2-adrenergic receptor (Rasmussen et al., 2011), and G-protein coupled receptor 54 (Wacker et al., 2008). Consistently, the defective signaling properties of L155A$^{3.58}$ of hMC4R also suggested that the corresponding residue was important in MC4R activation.

It should be noted that although 4 mutants, D146A, Y157A, M161A, and T162A, had severely impaired maximal binding with ligands (less than 20% of WT MC4R maximal binding), they exhibited the comparable cAMP production as WT hMC4R upon NDP-MSH stimulation (Table 2.2, Figs. 2.3 and 2.5). Presence of spare receptors in heterologous expression system might be an explanation (Strickland and Loeb, 1981; Tao, 2005). Similar results were also observed in some naturally occurring hMC4R mutants such as S58C and I102T (Tao and Segaloff, 2003), as well as some artificial alanine mutants (Mo et al., 2012).

The activation of ERK1/2 is a significant signaling cascade triggered by MC4R, which is thought to be involved in regulation of energy homeostasis by mediating inhibition of food intake (Sutton et al., 2005; Damm et al., 2012). Five alanine mutants, including D146A, R149A, Y153A, Y157A, and M161A, could not respond to NDP-MSH stimulation in ERK1/2 pathway (Fig. 2.6A and B). In our previous study of the DRYxxI motif and ICL2 of hMC3R, two mutants, Y185A and M193A (corresponding to Y153 and M161 in hMC4R), were also unable to induce ERK1/2 signaling with NDP-MSH stimulation (Huang and Tao, 2014). This indicated that the two residues were important for ERK1/2 signaling in both melanocortin receptors. Four alanine mutants, including R147A, Y148A, H158A, and I160A, also exhibited defective ERK1/2 activation since the efficacies of NDP-MSH at these mutants were lower compared to WT receptor, although they could respond to stimulation significantly (Fig. 2.6B).

Biased agonism, including biased mutants and ligands, has been proposed in MC4R by several research groups (Nickolls et al., 2005; Büch et al., 2009; Mo and Tao, 2013; He and Tao, 2014; Ghamari-Langroudi et al., 2015; Yang and Tao, 2016a) (reviewed in (Yang and Tao, 2017)). Previous studies in our lab have identified many biased hMC4R mutants which trigger biased signaling between Gs-cAMP and ERK1/2 pathways (Huang and Tao, 2012; Mo and Tao, 2013; He and Tao, 2014). Our present study also investigated biased signaling of mutant hMC4Rs. With the stimulation of NDP-MSH, one mutant T150A could induce biased ERK1/2 activation, whereas five mutants (Y148A, F149A, H158A, I160A, and M161A) exhibited biased Gs-cAMP signaling (Table 2.2, Figs. 2.5 and 2.6), suggesting the importance of corresponding residues in selectivity of receptor signaling. Previous studies also showed that the certain alanine mutations on

TMD3 of gonadotropin-releasing hormone receptor and ICL2 of V2 vasopressin receptor potentially cause receptor conformational selection and therefore different ligand-induced selective signaling (Erlenbach et al., 2001; Lu et al., 2005).

In summary, based on systematic study of the DRYxxI motif and ICL2 of hMC4R, we have identified the residues that were crucial for ligand binding, signaling in Gs-cAMP pathway, and signaling in ERK1/2 pathway (Fig. 2.7). Biased signaling was also investigated in our present study, which expands our understanding of the MC4R intracellular signaling. The structure-functional relationship of MC4R established in the present study will be valuable for investigating MC4R physiological role in regulation of energy homeostasis and rationally designing agonists and antagonists for treatment of MC4R-related diseases.

Table 2.1 Forward primer sequences used for site-directed mutagenesis studies of hMC4R. The mutated codons are underlined.

Constructs	Forward primer sequences
D146A	CAATTGCAGTG**GC**CAGGTACTTTAC
R147A	CAATTGCAGTGGAC**GC**GTACTTTACT
Y148A	GCAGTGGACAGG**GC**CTTTACTATCTT
F149A	CAGTGGACAGGTAC**GC**TACTATCTTC
T150A	GACAGGTACTTT**GC**TATCTTCTATG
I151A	CAGGTACTTTACT**GC**CTTCTATGCTCT
F152A	GTACTTTACTATC**GC**CTATGCTCTCCA
Y153A	CTTTACTATCTTC**GC**TGCTCTCCAGTA
A154G	CTATCTTCTATG**G**TCTCCAGTACC
L155A	CTATCTTCTATGCT**GC**CCAGTACCATA
Q156A	CTATGCTCTC**GC**GTACCATAAC
Y157A	CTATGCTCTCCAG**GC**CCATAACATTAT
H158A	GCTCTCCAGTAC**GC**TAACATTATGAC
N159A	CTCCAGTACCAT**GC**CATTATGACAG
I160A	CCAGTACCATAAC**GC**TATGACAGTTA
M161A	GTACCATAACATT**GC**GACAGTTAAGC
T162A	CATAACATTATG**G**CAGTTAAGCGGG

Table 2.2 The ligand binding and signaling properties of WT and mutant hMC4Rs.

hMC4R construct	NDP-MSH binding		Basal activities (% WT)	NDP-MSH-stimulated cAMP		NDP-MSH-stimulated ERK1/2
	IC_{50} (nM)	B_{max} (% WT)		EC_{50} (nM)	R_{max} (% WT)	
WT	19.43 ± 2.10	100 ± 0	100 ± 0	0.38 ± 0.07	100 ± 0	+
D146A	3.24 ± 0.70[a]	6.47 ± 0.97[b]	292.67 ± 35.94[b]	1.07 ± 0.18[a]	108.52 ± 12.25	-
R147A	11.86 ± 0.25	176.71 ± 38.93	23.62 ± 4.31[b]	1.73 ± 0.44[a]	121.75 ± 14.65	-
Y148A	4.31 ± 1.78[b]	60.38 ± 10.62[a]	126.90 ± 9.86[a]	0.21 ± 0.09	136.92 ± 8.17[a]	-
F149A	6.30 ± 0.83	156.37 ± 13.73[a]	233.51 ± 26.15[a]	0.24 ± 0.08	154.21 ± 31.84	-
T150A	40.25 ± 6.11[a]	95.30 ± 3.43	19.34 ± 4.05[b]	11.55 ± 2.38[b]	17.62 ± 3.60[b]	+
I151A	10.87 ± 1.08	124.47 ± 28.35	38.42 ± 15.77[a]	3.29 ± 0.27[b]	93.52 ± 24.82	+
F152A	17.29 ± 5.63	76.21 ± 14.64	228.74 ± 56.31[b]	0.06 ± 0.02[a]	115.47 ± 14.57	+
Y153A	13.02 ± 5.03	56.84 ± 4.52[b]	194.08 ± 31.05[b]	0.26 ± 0.10	152.24 ± 28.47	-
A154G	28.72 ± 9.72	84.83 ± 6.18	80.70 ± 21.17	0.87 ± 0.10	110.06 ± 10.78	+
L155A	50.80 ± 14.05	79.61 ± 8.63	21.77 ± 5.64[b]	6.03 ± 1.42[b]	100.44 ± 5.25	+
Q156A	15.41 ± 5.45	61.26 ± 6.10[b]	133.59 ± 27.19	1.76 ± 0.43[a]	129.25 ± 23.87	+
Y157A	7.43 ± 2.02	14.88 ± 2.18[b]	24.72 ± 2.89[b]	2.85 ± 0.61[b]	131.64 ± 18.30	-
H158A	10.36 ± 3.15	138.97 ± 25.34	761.86 ± 111.54[b]	0.03 ± 0.02[a]	109.75 ± 26.84	-
N159A	15.19 ± 5.31	119.92 ± 6.62[a]	79.16 ± 16.55	0.30 ± 0.07	92.29 ± 16.32	+
I160A	6.77 ± 2.07[a]	95.24 ± 16.43	88.84 ± 15.64	0.20 ± 0.18	109.91 ± 28.73	-
M161A	3.47 ± 1.19[b]	13.18 ± 2.67[b]	72.38 ± 9.95	0.41 ± 0.16	137.22 ± 11.70[a]	-
T162A	5.79 ± 2.35	13.73 ± 1.17[b]	60.37 ± 13.41	0.46 ± 0.10	145.81 ± 13.95[a]	+

Values are expressed as the mean ± S.E.M. of at least three independent experiments. The R_{max} of WT hMC4R was 1662.19 ± 136.63 pmol cAMP/10^6 cells with NDP-MSH stimulation.

[a] significantly different from WT, $P < 0.05$; [b] significantly different from WT, $P < 0.01$.

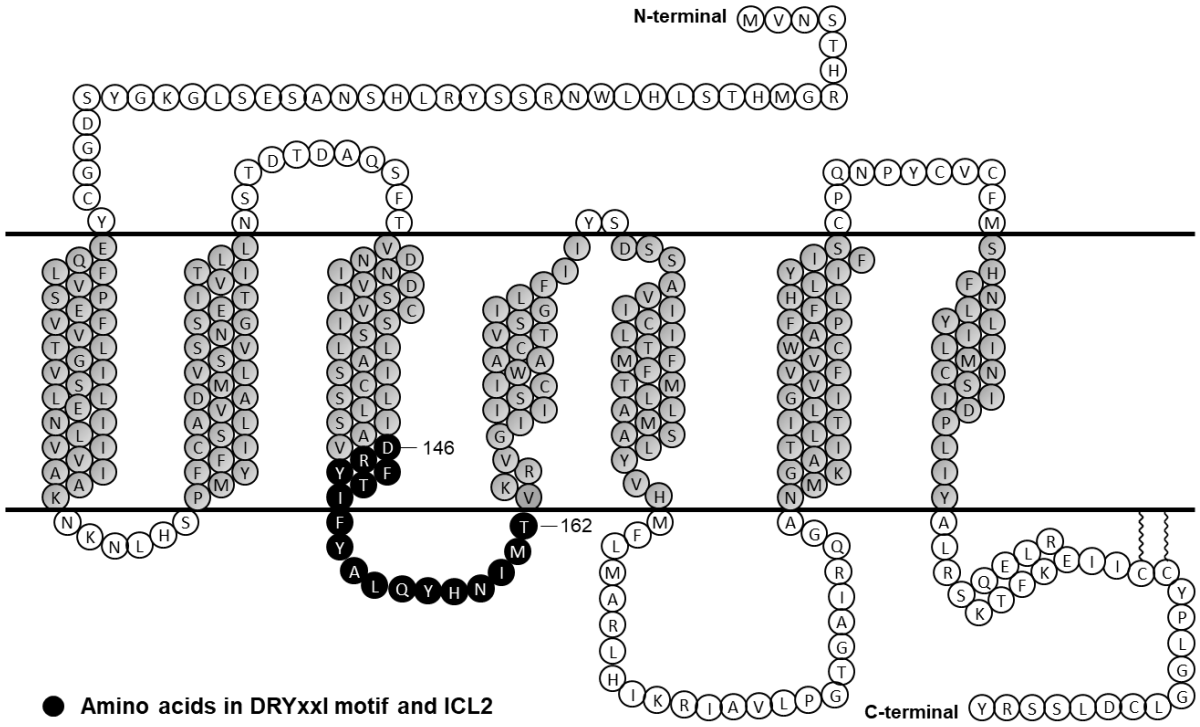

Fig. 2.1 Schematic model of hMC4R. Amino acids residues in DRYxxI motif and ICL2 are indicated in black circles.

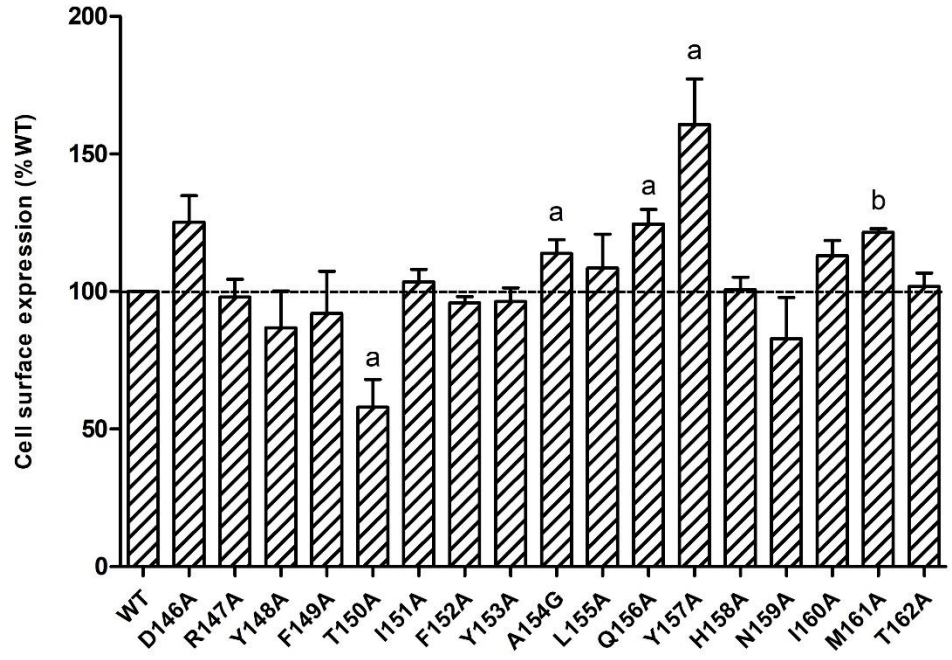

Fig. 2.2 Cell surface expression of WT and mutant hMC4Rs by flow cytometry. HEK293T cells were transiently transfected with WT and mutant hMC4Rs. Results are expressed as % cell surface expression level of WT hMC4R. Values are mean ± S.E.M of at least three independent experiments. The significant difference between WT and mutant: a, $P < 0.05$; b, $P < 0.001$.

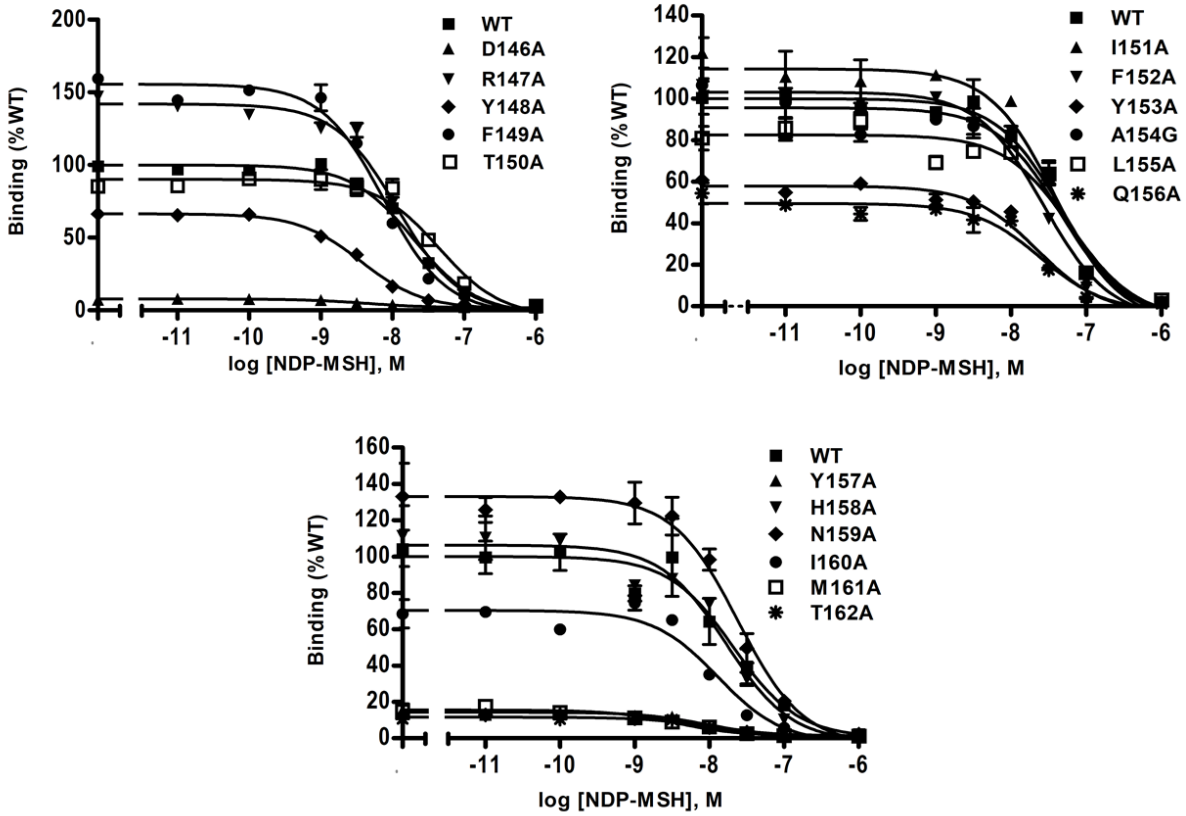

Fig. 2.3 NDP-MSH binding properties of WT and mutant hMC4Rs. HEK293T cells were transiently transfected with WT and mutant hMC4Rs. Intact cell surface binding was measured by competitive inhibition of [^{125}I]-NDP–MSH with different concentrations of unlabeled NDP–MSH. Results are expressed as % of WT maximal binding ± S.E.M. of duplicate measurements within one experiment. Curves are representative of at least three independent experiments.

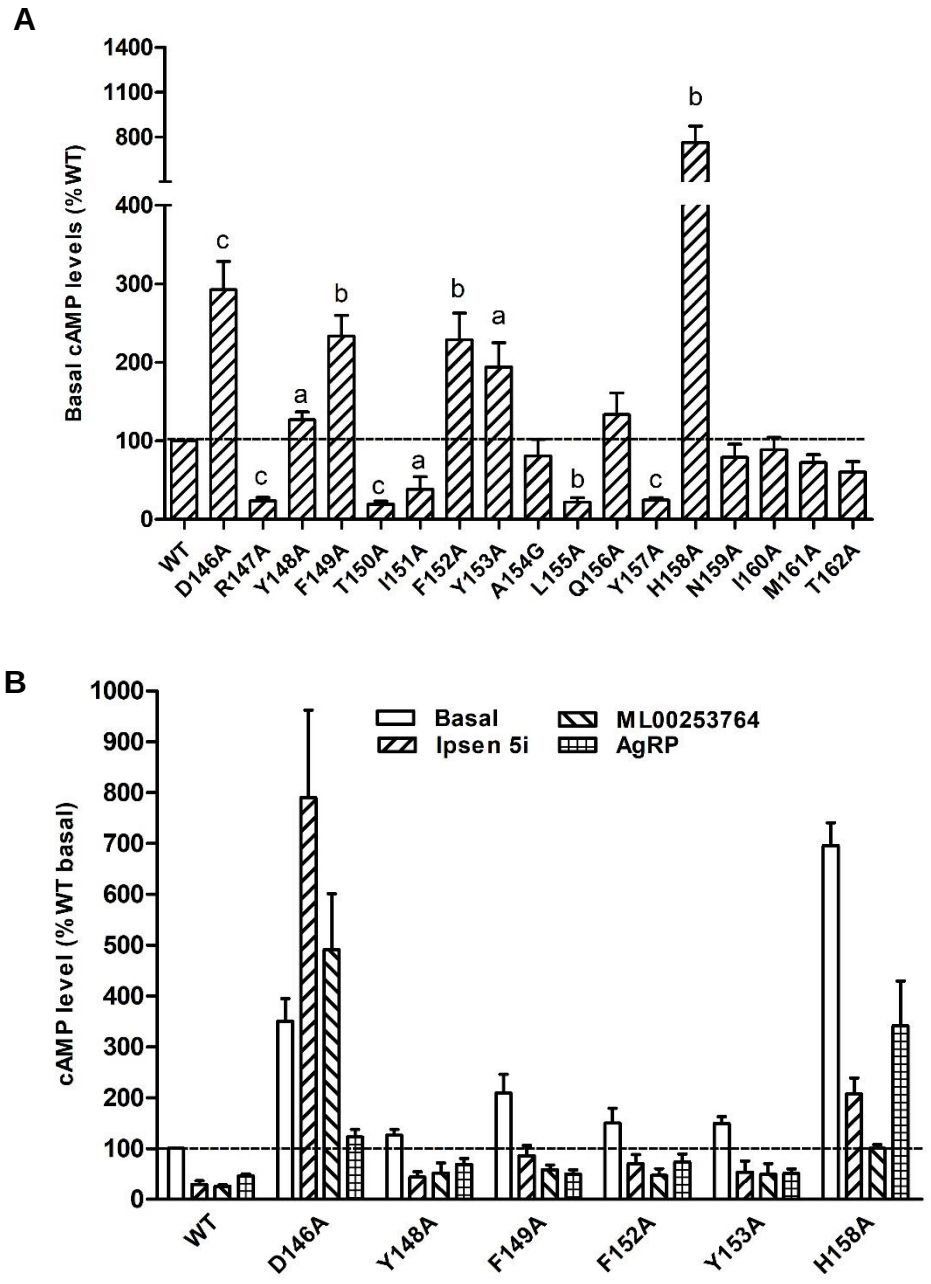

Fig. 2.4 Constitutive activity of WT and mutant hMC4Rs in cAMP pathway. (A) HEK293T cells were transiently transfected with WT and mutant hMC4Rs, and intracellular cAMP levels were measured by RIA without NDP-MSH stimulation. Results are expressed as % of basal WT cAMP level ± S.E.M. of at least three independent

experiments. The basal cAMP level of WT hMC4R was 41.45 ± 4.38 pmol/10^6 cells. The significant difference between WT and mutant: a, $P < 0.05$; b, $P < 0.01$; c, $P < 0.001$. (B) Partial inverse agonism of Ipsen 5i, ML00253764, and AgRP (8-132) on WT and six mutants with high basal activities. HEK293T cells were transiently transfected with WT and six mutant hMC4Rs. Cells were treated with 10^{-6} M Ipsen 5i, 10^{-5} M ML00253764, or 10^{-8} M AgRP (8-132), and intracellular cAMP levels were measured by RIA. Significant differences are observed between all control and treatment groups ($P < 0.05$).

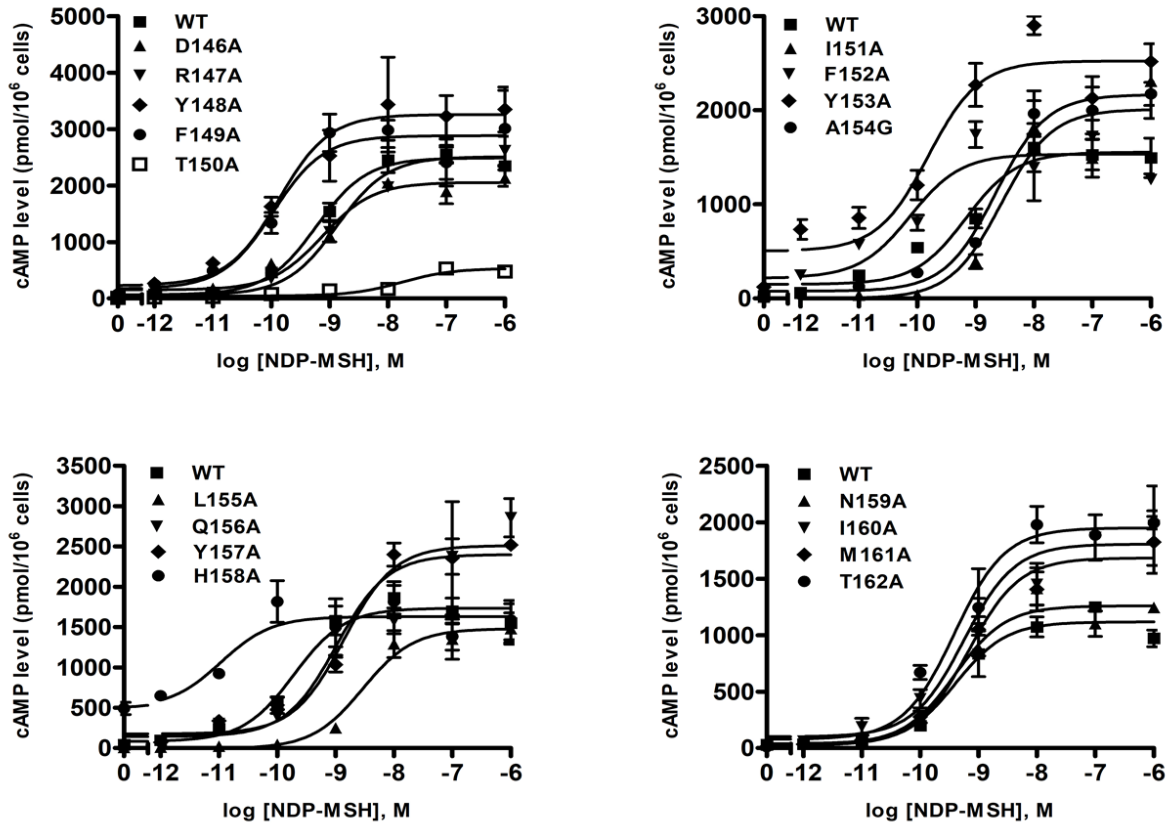

Fig. 2.5 NDP-MSH-stimulated cAMP signaling properties of WT and mutant hMC4Rs. HEK293T cells were transiently transfected with WT and mutant hMC4Rs, and intracellular cAMP levels were measured by RIA after stimulation with different concentrations of NDP-MSH. Results are mean ± S.E.M. from triplicate measurements within one experiment. Curves are representative of at least three independent experiments.

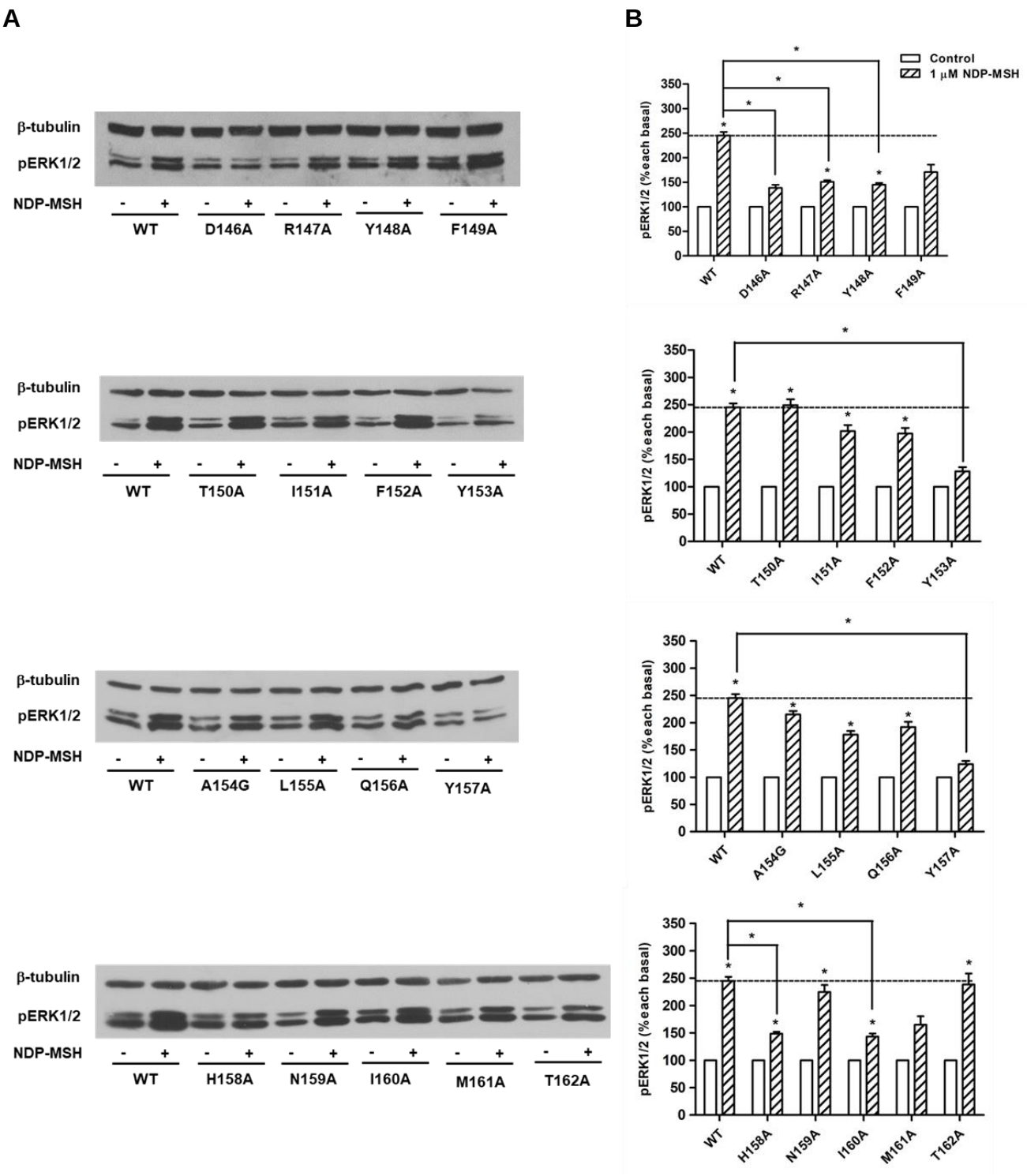
A
B
β-tubulin
pERK1/2
NDP-MSH
WT
D146A
R147A
Y148A
F149A
T150A
I151A
F152A
Y153A
A154G
L155A
Q156A
Y157A
H158A
N159A
I160A
M161A
T162A
Control
1 μM NDP-MSH
pERK1/2 (% each basal)

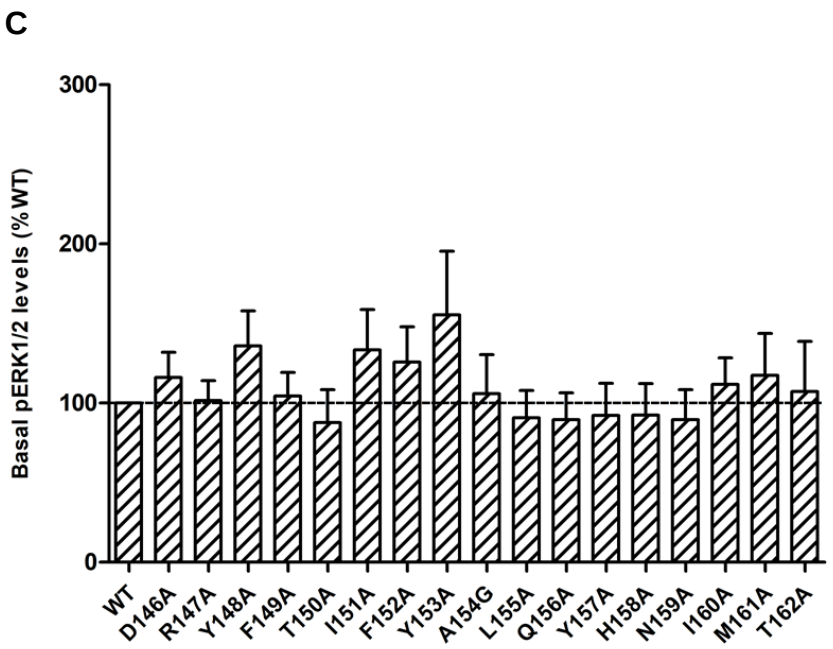

Fig. 2.6 The ERK1/2 signaling properties of WT and mutant hMC4Rs. HEK293T cells were transiently transfected with WT and mutant hMC4Rs, and pERK1/2 levels were measured by western blot without or with stimulation of 10^{-6} M NDP-MSH for 5 min. (A) Western blot analysis was performed using antibody against pERK1/2 and β-tubulin as control. (B) Data of the pERK1/2 levels of WT and mutant hMC4Rs after NDP-MSH stimulation are expressed as % of each basal from at least six independent experiments. * indicates significant difference from basal pERK1/2 level or from the stimulation of the WT MC4R ($P < 0.05$). (C) Data of the basal pERK1/2 levels are mean ± S.E.M. of at least six independent experiments.

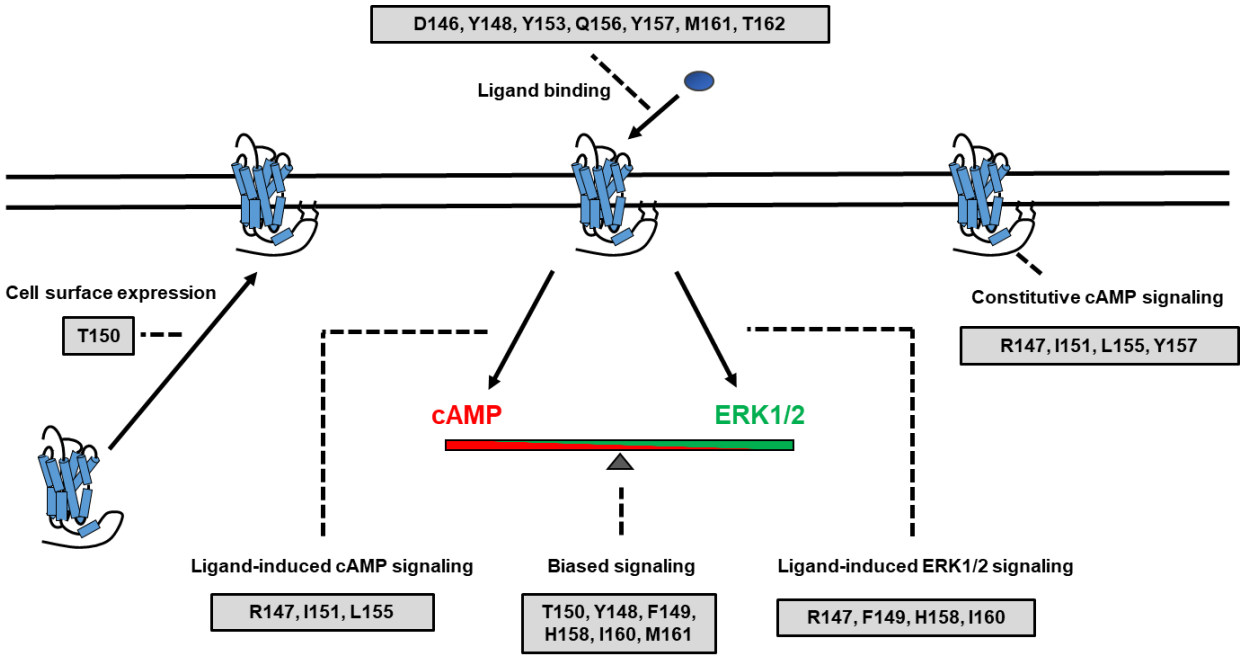

Fig. 2.7 Summary of the functions of DRYxxI motif and ICL2. Residues critical for receptor cell surface expression, ligand binding, and/or signaling pathways were shown in grey boxes.

Chapter 3: Characterization of channel catfish (*Ictalurus punctatus*) melanocortin-3 receptor reveals a potential network in regulation of energy homeostasis

3.1. Introduction

Melanocortin-3 and -4 receptor (MC3R and MC4R), with high expression in central nervous system, are also known as neural melanocortin receptors (MCRs) (Gantz et al., 1993a; Gantz et al., 1993b; Roselli-Rehfuss et al., 1993; Mountjoy et al., 1994). These two MCRs have been extensively studied in obesity pathogenesis due to their important functions in regulating energy homeostasis. Targeted deletion of either *Mc3r* or *Mc4r* in mice results in the obesity phenotype (Huszar et al., 1997; Butler et al., 2000; Chen et al., 2000). Human genetic studies also showed that mutations in *MC3R* or *MC4R* are associated with obesity (reviewed in (Tao, 2009; Tao, 2010b; Hinney et al., 2013; Yang and Tao, 2016b; Demidowich et al., 2017)). Although both MC3R and MC4R are important regulators of energy homeostasis, the mechanisms involved are distinct. MC4R primarily regulates food intake and energy expenditure (Balthasar et al., 2005; Tao, 2010a), whereas MC3R regulates feed efficiency (the ratio of weight gain to food intake) and nutrient partitioning (Butler et al., 2000; Chen et al., 2000; Zhang et al., 2005b), maintaining circadian rhythm, and adapting to fasting (Sutton et al., 2010; Begriche et al., 2012; Girardet and Butler, 2014). *Mc3r* knockout mice display a moderate obesity

phenotype with altered nutrient partitioning (increased fat mass and reduced lean mass) despite normal food intake or even hypophagia, which may be explained by subtle imbalance between fat intake and oxidation (Sutton et al., 2006). Recent studies also showed that *Mc3r* knockout mice exhibit reduced wakefulness before food presentation and abnormal rhythmic expression of clock genes (Girardet and Butler, 2014), as well as anomalous metabolic adaption to restricted feeding (Begriche et al., 2012). Cone and colleagues suggested that MC3R sets the upper and lower boundaries of energy homeostasis (Ghamari-Langroudi et al., 2018).

In addition to the central expression, MC3R has also been shown to be expressed in several peripheral tissues, indicating other potential physiological functions in the periphery. For example, the expression of MC3R can be detected in immune cells, such as macrophages, including both human and rodent macrophage cell lines and primary macrophages from different tissues (reviewed in (Patel et al., 2011)). MC3R is an important modulator in immune response with effective anti-inflammatory and pro-resolving actions (Patel et al., 2011).

MC3R primarily couples to the heterotrimeric stimulatory G protein (Gs) to activate adenylyl cyclase, thereby increasing intracellular cAMP production and subsequent protein kinase A (PKA) activation. MC3R activation also triggers extracellular signal-regulated kinases 1 and 2 (ERK1/2) phosphorylation (Chai et al., 2007; Huang and Tao, 2014; Yang et al., 2015a; Yang et al., 2015b; Yang and Tao, 2016a). The endogenous ligands for MC3R include four agonists (α-, β-, and γ-melanocyte-stimulating hormones (MSHs), and adrenocorticotropin (ACTH)) produced from post-translational processing of

the precursor protein, proopiomelanocortin (POMC), and one antagonist, Agouti-related peptide (AgRP).

Recently, two small single transmembrane proteins, melanocortin receptor accessory proteins (MRAPs), including MRAP1 and MRAP2, have been shown to interact with and modulate MCR functions (Rouault et al., 2017). MRAP2, with its highly central expression, is more involved in regulation of energy homeostasis. Mice with *Mrap2* deletion display severe obesity (Asai et al., 2013; Novoselova et al., 2016). Potential pathogenic *MRAP2* mutations have also been identified in humans with early-onset obesity (Asai et al., 2013; Schonnop et al., 2016). MRAP2 modulation of MC4R signaling is an important pathway for regulating energy homeostasis in mammals and other species such as zebrafish and chicken (Sebag et al., 2013; Zhang et al., 2017). In addition, the role of MRAP2 on modulation of energy homeostasis through MC3R has also been suggested (Chan et al., 2009; Zhang et al., 2017). Therefore, MC3R and MC4R, together with α-MSH, AgRP, and MRAP2, form a complex system within the hypothalamus which connects the neural pathways governing satiety and metabolism with external signals of metabolic status to maintain energy homeostasis.

Although MC3R is well studied in humans and rodents, the functional studies of teleost MC3Rs are still very limited, potentially due to the absence of *mc3r* genes in some teleosts, such as fugu, medaka, and stickleback (Logan et al., 2003; Klovins et al., 2004a; Selz et al., 2007). Channel catfish (*Ictalurus punctatus*), belonging to the family of Ictaluridae, is the most extensively cultured species in North America. The genome and transcriptome data of this species have shown that channel catfish has a single intronless *mc3r* gene located on chromosome 5 (Liu et al., 2016). Currently, the approaches for

improving the growth and feed efficiency are limited to the use of traditional selective breeding methods that are time consuming. Therefore, understanding of endocrine regulation of energy metabolism in this economically important species can potentially lead to novel approaches to achieve better economic return.

Previous studies have reported the effects of several gut neuropeptides on feeding behavior, glycemia, and hypothalamic *neuropeptide Y* and *pomc* expression in channel catfish (Kobayashi et al., 2008; Peterson et al., 2012; Schroeter et al., 2015), suggesting potential roles of central melanocortin system in the growth and feeding in this fish. In the present study, we investigated the pharmacological properties of channel catfish MC3R (ipMC3R). In addition, the modulatory role of channel catfish MRAP2 (ipMRAP2) on ipMC3R signaling was also studied. These experiments, as the first step towards elucidating the roles of MC3R in energy homeostasis of channel catfish, laid a solid foundation for future physiological studies.

3.2. Materials and methods

3.2.1. Ligands and plasmids

[Nle^4, D-Phe^7]-α-MSH (NDP-MSH) and D-Trp^8-γ-MSH were purchased from Peptides International (Louisville, KY, USA). α-MSH and human β-MSH were purchased from Pi Proteomics (Huntsville, AL, USA). Human ACTH (1–24) and AgRP were purchased from Phoenix Pharmaceuticals (Burlingame, CA, USA). [^{125}I]-NDP-MSH and [^{125}I]-cAMP were iodinated using chloramine T method as described in previous

publications (Steiner et al., 1969; Mo et al., 2012). The human MC3R (hMC3R) subcloned into pcDNA3.1 vector was generated as previously described (Tao and Segaloff, 2004). The coding sequences of ipMC3R and ipMRAP2 were commercially synthesized and subcloned into pcDNA3.1 vector by GenScript (Piscataway, NJ, USA) to generate the plasmids used for transfection.

3.2.2. Homology, phylogenetic, and chromosome synteny analyses

Multiple alignments of amino acid sequences of MC3Rs, POMCs, and MRAP2s from different species were performed with BioEdit software using ClustalW multiple alignment. The putative transmembrane domains (TMDs) of ipMC3R were predicted based on the crystal structure of rhodopsin (Palczewski et al., 2000). A phylogenetic tree based on the amino acid sequences was constructed by MEGA X software with 1000 bootstrap replications using the neighbor-joining (NJ) method (Saitou and Nei, 1987; Kumar et al., 2018). Chromosome synteny analysis was performed between several fish and mammalian species with National Center for Biotechnology Information (NCBI) genome browser (https://www.ncbi.nlm.nih.gov) and Genomicus (http://www.genomicus.biologie.ens.fr/genomicus).

3.2.3. Cell culture and transfection

Human Embryonic Kidney (HEK) 293T cells (ATCC, Manassas, VA, USA) were cultured in Dulbecco's Modified Eagle's medium (DMEM) (Invitrogen, Carlsbad, CA, USA) containing 10% newborn calf serum (PAA Laboratories, Etobicoke, ON, Canada), 10 mM HEPES, 0.25 μg/mL of amphotericin B, 50 μg/mL of gentamicin, 100 IU/mL of penicillin, and 100 μg/mL of streptomycin at an incubator (37 °C and 5% CO_2-humidified

atmosphere). The cells were plated into plates pre-coated with 0.1% gelatin and cultured for about 24 hours prior to transfection (24-wells plates for cAMP assays and 6-well plates for ligand binding assay and western blot). At approximately 70% confluency, the cells were transfected or co-transfected with plasmids using calcium phosphate precipitation method (Chen and Okayama, 1987). For ligand binding and signaling assays, ipMC3R and hMC3R plasmids (1 μg in 2 mL media) were transfected into cells, respectively. To study the constitutive activity, ipMC3R plasmids at different concentrations were transfected into cells. To investigate the potential modulation of ipMC3R signaling by ipMRAP2, cells were co-transfected with ipMC3R (1 μg in 2 mL media) and ipMRAP2 plasmids at different ratios (1:0, 1:1, 1:3, and 1:5). Total plasmid was kept identical for all groups by the addition of empty vector pcDNA3.1.

3.2.4. Ligand binding assay

Forty-eight hours after transfection, HEK293T cells were washed twice with warm DMEM containing 1 mg/mL bovine serum albumin (BSA, EMD Millipore Corporation, Billerica, MA, USA) (DMEM/BSA) and then incubated at 37 °C with DMEM/BSA containing ~80,000 cpm of [^{125}I]-NDP-MSH without or with different concentrations of unlabeled ligands for 1 h (Tao and Segaloff, 2003). The ligands and their final concentrations used in this study were NDP-MSH (10^{-11} to 10^{-6} M), α-MSH (10^{-10} to 10^{-5} M), β-MSH (10^{-10} to 10^{-5} M), ACTH (1-24) (10^{-11} to 10^{-6} M), and D-Trp^{8}-γ-MSH (10^{-11} to 10^{-6} M). After incubation, the plates were placed on ice, and then the cells were washed twice with cold Hank's balanced salt solution containing 1 mg/mL BSA to terminate the reaction. The cells were lysed with 100 μL 0.5 M NaOH and collected using cotton swabs.

The radioactivity was counted by a gamma counter (Cobra II Auto-Gamma, Packard Bioscience, Frankfurt, Germany).

3.2.5. cAMP assay

Forty-eight hours after transfection, HEK293T cells were washed twice with warm DMEM/BSA and then incubated with DMEM/BSA containing 0.5 mM isobutylmethylxanthine (Sigma–Aldrich, St. Louis, MO, USA) at 37 °C for 30 min. To investigate agonist-stimulated cAMP production, the cells were treated without or with different concentrations of agonists. After one hour incubation at 37 °C, the plates were placed on ice to terminate the reaction, and the cells were lysed with 0.5 M perchloric acid containing 180 μg/mL theophylline (Sigma-Aldrich) and neutralized by 0.72 M KOH/0.6 M $KHCO_3$. The cAMP levels were determined by radioimmunoassay (RIA) as described previously (Steiner et al., 1969).

3.2.6. ERK1/2 phosphorylation assay

The phosphorylated ERK1/2 (pERK1/2) activity was measured as described previously (Mo et al., 2012; He and Tao, 2014). Briefly, at 24 hours after transfection, cells were washed with warm DMEM/BSA once and starved in DMEM/BSA at 37 °C for 24 hours. On the day of experiment, cells were treated with buffer alone or agonists (10^{-6} M α-MSH and 10^{-7} M ACTH (1-24)) for 5 min at 37 °C. Cells were then solubilized in lysis buffer and total protein concentrations of cell lysates were determined using the Bradford protein assay. Samples containing 30 μg of proteins were separated on 10% SDS-PAGE gel and transferred onto PVDF membranes for immunoblotting. Membranes were incubated with 10% non-fat dry milk (containing 0.2% Tween-20) for 4 hours at room

temperature, and then immunoblotted with rabbit anti-pERK1/2 antibody (Cell Signaling, Beverly, MA) at a dilution of 1:5000, and mouse anti-β-tubulin antibody (Developmental Studies Hybridoma Bank, University of Iowa, Iowa City, IA) at a dilution of 1:5000, in Tris-buffered saline (TBST) containing 0.1% Tween 20 and 5% BSA overnight at 4 °C. Membranes were then incubated with horseradish peroxidase-conjugated secondary antibodies, donkey anti-rabbit IgG (Jackson ImmunoResearch Laboratories, West Grove, PA) at a dilution of 1:8000 and donkey anti-mouse IgG (Jackson ImmunoResearch Laboratories) at a dilution of 1:10000 in 10% non-fat dry milk (containing 0.2% Tween-20) for one hour at room temperature. Specific bands were visualized using enhanced chemiluminescence reagent (Thermo Scientific, Rockford, IL) and staining intensity was quantified using ImageJ Software (National Institute of Health, Bethesda, MD). The pERK1/2 levels were normalized according to the loading of proteins by expressing the data as a ratio of pERK1/2 over β-tubulin.

3.2.7. Statistical analysis

All data were presented as mean ± SEM. GraphPad Prism 4.0 software (San Diego, CA, USA) was used to calculate parameters in ligand binding and cAMP signaling assays. Two-tailed Student's *t*-test was performed to determine the significant differences in ligand binding and signaling parameters between hMC3R and ipMC3R, basal cAMP levels between AgRP-treated and non-treated groups, and pERK1/2 levels between agonist-treated and non-treated groups. One-way analysis of variance (one-way ANOVA) and two-way analysis of variance (two-way ANOVA) were performed in the investigation

of ipMRAP2 effects on ipMC3R signaling. Statistical significance was established when $P < 0.05$.

3.3. Results

3.3.1. Sequence analyses of ipMC3R, ipPOMC, and ipMRAP2

The catfish *mc3r* gene contained an open reading frame of 1104 bp (NCBI, XM_017467315.1) encoding a putative protein of 367 amino acids (NCBI, XP_017322804.1) and 41.05 kDa molecular mass (Fig. 3.1). Multiple alignment of MC3Rs revealed that the predicated ipMC3R had the classical feature of Family A GPCRs, with seven hydrophobic TMDs and several conserved motifs (PMY, DRYxxI, and DPIIY) at homologous positions with MC3Rs of other species. The deduced amino acid sequence of ipMC3R was significantly conserved to other species in the TMDs, intracellular loops, and extracellular loops, but the amino and carboxyl termini displayed the lowest identities to other species (Fig. 3.2A). The identities between ipMC3R and other piscine MC3R orthologs were 95% (iridescent shark, *Pangasianodon hypophthalmus*), 84% (red piranha, *Pygocentrus nattereri*), 81% (Wuchang bream, *Megalobrama amblycephala*), 81% (common carp, *Cyprinus carpio*), 81% (goldfish, *Carassius auratus*), and 80% (zebrafish, *Danio rerio*). However, ipMC3R had lower identities with mammalian MC3Rs (70% to mouse, 69% to rat, and 67% to human).

POMC is the precursor of several melanocortins including α-, β-, γ-MSH and ACTH. In humans and rodents, all melanocortins share the pharmacophore (HFWR) that is necessary to bind to MCRs. Consistent with one previous study identifying *pomc* gene in

channel catfish (Karsi et al., 2004), multiple alignment of amino acid sequences of POMCs in this study also suggested that α-MSHs, β-MSHs, and ACTHs might exist in channel catfish and other fishes with potential absence of γ-MSHs (the pharmacophore sequence was not found in the region that is supposed to produce γ-MSH) (Fig. 3.2B). Although there were differences in the sequences of ACTH and β-MSH, it is interesting to note that α-MSH of channel catfish was identical to those of other fish and mammals, indicating that α-MSH is highly conserved in structure during evolution and potentially functions similarly in both mammals and fish (Fig. 3.2B).

The ipMRAP2 was also highly conserved with an identical TMD in the species analyzed (Fig. 3.2C). We did not find MRAP1 sequence in channel catfish based on the genome data, suggesting the absence of this gene in channel catfish.

3.3.2. Phylogenetic and chromosome synteny analyses of ipMC3R

Phylogenetic analysis was conducted with full-length amino acid sequences of ipMC3R and other MC3Rs to evaluate the evolutionary relationships between the predicted ipMC3R and other vertebrate MC3Rs. We showed that ipMC3R was nested within a clade of iridescent shark, red piranha and Mexican tetra (Fig. 3.3). Chromosome synteny analysis also revealed that ipMC3R was orthologous to those of other fishes. The *mc3r* gene neighbors exhibited a conserved synteny to those of red piranha, coho salmon, and zebrafish, but not to those of human, mouse, and rat (Fig. 3.4).

3.3.3. Ligand binding properties of ipMC3R

Competitive ligand binding assay was performed to investigate the binding properties of ipMC3R to different MC3R ligands, including three endogenous agonists (α-MSH, β-MSH, and ACTH (1-24)), one super-potent agonist (NDP-MSH), and one MC3R-selective agonist (D-Trp^{8}-γ-MSH) (Grieco et al., 2000). Different concentrations of unlabeled ligands were used to compete for radiolabeled ligand ([^{125}I]-NDP-MSH) binding. In the same experiments, we included hMC3R for comparison to see whether ipMC3R has any unique pharmacological characteristics. As shown in Fig. 3.5 and Table 3.1, the maximal binding value (B_{max}) of ipMC3R was 334 ± 28% of that of the hMC3R ($P < 0.01$). The two MC3Rs had similar IC_{50}s when NDP-MSH, α-MSH, and ACTH (1-24) were used to compete for [^{125}I]-NDP-MSH binding. However, ipMC3R had significantly higher and lower affinities to β-MSH and D-Trp^{8}-γ-MSH, respectively.

3.3.4. Signaling properties of ipMC3R

RIA was performed to determine whether ipMC3R could respond to these agonists in cAMP pathway. All agonists were shown to dose-dependently stimulate ipMC3R and increase intracellular cAMP generation. Cells transfected with empty vector pcDNA3.1 alone did not respond to agonist stimulation. As shown in Fig. 3.6 and Table 3.2, the maximal responses of ipMC3R to the five agonists were significantly lower (~50% to 70% of hMC3R). The EC_{50} of NDP-MSH for ipMC3R was comparable to that of the hMC3R (Fig. 3.6A and Table 3.2), whereas the EC_{50}s of α-MSH, β-MSH, ACTH (1-24), and D-Trp^{8}-γ-MSH for ipMC3R were significantly lower than those of hMC3R (Fig. 3.6B-E, and Table 3.2).

3.3.5. Constitutive activity of ipMC3R

In this experiment, we also found the basal cAMP level of ipMC3R was seven-fold higher than that of hMC3R (109.52 ± 13.17 vs. 15.74 ± 1.63 pmol/10^6 cells, n = 20), suggesting that ipMC3R might be constitutively active. To further study the constitutive activity of ipMC3R, we transfected cells with increasing concentrations of plasmid. Empty vector pcDNA3.1 was used to normalize the amount of DNA added to each well. Our data showed that even very low amount of ipMC3R plasmid transfected resulted in high basal cAMP levels (Fig. 3.7A). The high basal cAMP level at plasmid concentration of 0.5 μg/mL could be reduced by AgRP by 63.83% (Fig. 3.7B), suggesting that AgRP was a potent inverse agonist at ipMC3R.

In addition to cAMP pathway, ERK1/2 signaling was also evaluated. ERK1/2 phosphorylation increased with increasing concentrations of plasmid transfected (Fig. 3.7C and D), suggesting that ipMC3R was also constitutively active in the ERK1/2 pathway.

3.3.6. Modulation of ipMC3R signaling by ipMRAP2

In the present study, we investigated the actions of ipMRAP2 on ipMC3R signaling. Cells were co-transfected with ipMC3R and ipMRAP2 at different ratios (1:0, 1:1, 1:3, and 1:5). Our results showed that ipMRAP2 could dose-dependently reduce the basal cAMP levels with maximal inhibition observed at the 1:5 ratio (56.66% of 1:0 group) (Fig. 3.8A). Significant reduction in agonist-induced cAMP generation was also observed (Fig. 3.8B and C). To further explore the mechanism, cells co-transfected with ipMC3R and ipMRAP2 at the ratios of 1:0 and 1:5 were stimulated with different concentrations of α-

MSH. We showed that ipMRAP2 significantly reduced the maximal response by ~25%, whereas it did not affect the EC_{50} significantly (Fig. 3.8D).

In addition to cAMP production, both α-MSH and ACTH (1-24) could activate ERK1/2 pathway through ipMC3R (Fig. 3.9A and B). Cells transfected with empty vector pcDNA3.1 or ipMRAP2 alone did not respond to α-MSH and ACTH (1-24) stimulation (Fig. 3.9A and B). When ipMRAP2 were co-expressed with ipMC3R, ipMRAP2 had no effect on basal and α-MSH- and ACTH (1-24)-stimulated pERK1/2 levels (Fig. 3.9C and D), different from its actions on cAMP pathway (Fig. 3.8).

3.4. Discussion

The MC3Rs have been extensively studied in human and rodents regarding their roles in regulating energy balance (such as regulation of feed efficiency and nutrient partitioning, maintaining circadian rhythm, and adaptation to fasting and overfeeding) as well as modulation of immune response. Several groups also functionally studied MC3Rs in some other mammals and non-mammalian vertebrates (Fan et al., 2008; Zhang et al., 2017; Zhang et al., 2019). Given the critical functions of MC3Rs in regulation of energy homeostasis, it is also important to understand the roles of MC3Rs in economically important aquaculture fishes. However, to our knowledge, only a few studies investigated MC3Rs in fishes, such as spiny dogfish (Klovins et al., 2004b) and red stingray (Takahashi et al., 2016). In the present study, we characterized ipMC3R by performing several pharmacological and functional studies, aiming to lay a foundation for future

physiological studies that could provide new strategies for enhancing channel catfish culture.

We found that ipMC3R had a typical structure of Family A GPCR, similar as MC3Rs of other species (Fig. 3.1 and Fig. 3.2A). The ipMC3R showed a remarkable conservation with several other teleost MC3Rs at the amino acid level (more than 80% identities). Seven TMDs were present in ipMC3R, which were highly conserved among MC3Rs from different species. Several highly conserved motifs that are known to be important for receptor structure and function, such as PMY in TMD2, DRYxxI in TMD3, and DPIIY in TMD7, were also identified in ipMC3R. It is interesting to note that ipMC3R had a long C-terminal domain similar as in iridescent shark and red piranha but different from those in other fish and mammalian MC3Rs (Fig. 3.2A), which might account for its unique properties. The ipMC3R was also evolutionarily conserved since phylogenetic tree revealed that ipMC3R was clustered with teleost MC3Rs and chromosomal synteny analysis showed that the surrounding genes of catfish *mc3r* were similar to those in red piranha, coho salmon, and zebrafish (Figs. 3.3 and 3.4).

To investigate the pharmacology of ipMC3R, we first performed competitive ligand binding assays in HEK293T cells transfected with ipMC3R plasmid. As shown in Fig. 3.5 and Table 3.1, the super-potent agonist NDP-MSH bound to ipMC3R with the highest affinity, comparable to that of hMC3R. The binding affinities of ipMC3R to α-MSH and ACTH (1-24) were also comparable to those of hMC3R. Significant fifteen-fold difference is observed between IC_{50}s of hMC3R and ipMC3R when D-Trp^8-γ-MSH, an analogue of γ-MSH, was used (Fig. 3.5E and Table 3.1). In mammals, among the five subtypes of

MCRs, MC3R has the highest affinity to γ-MSH and is the only MCR that is fully activated by γ-MSH (Cone, 2006). However, potential γ-MSH region was not found in channel catfish POMC (Karsi et al., 2004) (Fig. 3.2B). Therefore, the low affinity of D-Trp^{8}-γ-MSH to ipMC3R might be explained by the absence of γ-MSH in this species.

The MC3R couples to both Gs-cAMP and ERK1/2 pathways. We next investigated the signaling properties of ipMC3R on both cAMP production and ERK1/2 activation. In cAMP assays, our data showed that the maximal responses of ipMC3R to five agonists were about 50 to 70% of those of hMC3R (Fig. 3.6 and Table 3.2). In addition, all five agonists could stimulate ipMC3R with sub-nanomolar potencies. In particular, the sub-nanomolar potency of ACTH (1-24) at ipMC3R, significantly different from its nanomolar potency at hMC3R (Fig. 3.6D, and Table 3.2), indicated that ACTH might be an important endogenous ligand for ipMC3R. ACTH was proposed as the “original” ligand for the early MCRs during vertebrate evolution, since ACTH could bind to and/or stimulate MC4R with high affinity and/or potency in several fishes (Haitina et al., 2004; Klovins et al., 2004a; Li et al., 2016a; Li et al., 2017; Yi et al., 2018). Only one study reported the results on the MC3R (Klovins et al., 2004b). Our results showing the high affinity and potency of ACTH (1-24) to ipMC3R provide further support for the importance of ACTH as an endogenous ligand for fish MC3R.

As another pathway triggered by MC3R, ERK1/2 activation was shown to be involved in the regulation of energy homeostasis in terms of food intake, feeding behaviors and long-lasting effects of melanocortins (Daniels et al., 2003; Sutton et al., 2005; Begriche et al., 2012). In this study, ERK1/2 activation was also observed when

cells were stimulated by α-MSH and ACTH (1-24) (Fig. 3.9A and B), suggesting that ipMC3R might trigger ERK1/2 pathway similar to hMC3R, thus contributing to the regulation of energy homeostasis.

Previous studies showed that several fish MC4Rs are constitutively active in cAMP pathway (Sanchez et al., 2009; Sebag et al., 2013; Li et al., 2016a; Li et al., 2017). In cavefish, mutations of *mc4r* leading to decreased constitutive activity was considered as one cause of elevated appetite, growth, and starvation resistance, suggesting the physiological relevance of constitutive activity (Aspiras et al., 2015). Only zebrafish MC3R was shown to be constitutively active in the cAMP pathway before (Renquist et al., 2013). We revealed that ipMC3R displayed constitutive activity in cAMP pathway (Fig. 3.7A and Table 3.2) in contrast to hMC3R which has little or no constitutive activity in this pathway (Tao, 2007; Tao et al., 2010). AgRP is orexigenic in fishes (reviewed in (Volkoff, 2016)). The high basal cAMP level of ipMC3R could be potently reduced by AgRP (Fig. 3.7B) in accordance with the findings in chicken and zebrafish MC3Rs (Renquist et al., 2013; Zhang et al., 2017), indicating that AgRP was also a potent inverse agonist for ipMC3R. Therefore, AgRP could potentially regulate energy balance through MC3R in channel catfish. Furthermore, we showed that ipMC3R was also constitutively active in ERK1/2 pathway (Fig. 3.7C and D).

In mammals, MRAP1 is highly expressed in the adrenal gland with the indispensable function in trafficking MC2R to the plasma membrane. Mutations in *MRAP1* accounts for ~20% of cases of familial glucocorticoid deficiency type 2 and causes earlier disease onset compared with familial glucocorticoid deficiency type 1 resulting from mutations in *MC2R* (Metherell et al., 2005; Chung et al., 2010). Different from MRAP1,

MRAP2 is primarily expressed in the hypothalamus and has impact on regulation of energy homeostasis through interaction with MC4R (Asai et al., 2013; Sebag et al., 2013), as well as prokineticin receptors (Chaly et al., 2016) and ghrelin receptor (Srisai et al., 2017). Mice with *Mrap2* deletion display severe obesity (Asai et al., 2013). Potentially pathogenic *MRAP2* mutations have also been identified in humans with obesity (Asai et al., 2013), which impair the function of MC4R and thus lead to obesity. In zebrafish, MC4R signaling can be differentially modulated by two isoforms of MRAP2, MRAP2a and MRAP2b, leading to distinct regulation on energy homeostasis (Sebag et al., 2013). MRAP2a stimulates growth of zebrafish by strongly inhibiting MC4R signaling, whereas MRAP2b increases ligand sensitivity and potentiates MC4R signaling (Sebag et al., 2013).

As for the MC3R, there are only three previous studies reporting the modulation of signaling by MRAPs (Chan et al., 2009; Kay et al., 2013; Zhang et al., 2017). The first study showed that in CHO cells expressing hMC3R, human MRAP2 significantly reduces NDP-MSH-induced cAMP production (Chan et al., 2009). Kay et al. showed that hMRAPa increases agonist-induced signaling (Kay et al., 2013). Zhang et al. demonstrated that in chicken MC3R, MRAP2 decreases constitutive activity but potentiates agonist-induced signaling in the cAMP pathway (Zhang et al., 2017). In the present study, we investigated the role of ipMRAP2 in modulating ipMC3R signaling in both cAMP and ERK1/2 pathways. As shown in Fig. 3.8, ipMRAP2 inhibited both constitutive and agonist-induced signaling in cAMP pathway. However, the constitutive activity and agonist-induced signaling in ERK1/2 pathway were not affected (Fig. 3.9C and D). We suggest that ipMRAP2 preferentially stabilized ipMC3R in an inactive conformation for cAMP production but not ERK1/2 activation.

In the present study, we used a mammalian cell line cultured at 37 °C to perform the pharmacological studies. Although this is a widely used strategy, partly due to the lack of well-established piscine cell expression system, we caution that the activities of fish receptors may potentially be affected by the properties of the mammalian cells and culture temperature, such as different viscosities of cell membrane at different temperatures. Viscosity is known to affect receptor conformational changes and downstream adenylyl cyclase activity (Hirata et al., 1979).

In summary, we showed that ipMC3R was evolutionarily conserved in piscine MC3Rs. The cloned ipMC3R was a functional receptor with unique pharmacological properties compared to hMC3R, such as high constitutive activities and high sensitivities to α-MSH and ACTH (1-24). We also showed that ipMRAP2 could preferentially modulate the cAMP signaling rather than ERK1/2 pathway. Therefore, we propose that MC3R, melanocortins (α-MSH and ACTH), and MRAP2, as well as inverse agonist AgRP, are important components in a complex network that contribute to the central regulation of energy homeostasis in channel catfish. Novel strategies might be developed targeting each of these components to improve the growth and quality of this cultured fish.

Table 3.1 The ligand binding properties of hMC3R and ipMC3R.

MC3R	B_{max} (%)	NDP-MSH	α-MSH	β-MSH	ACTH (1-24)	D-Trp^8-γ-MSH
		IC_{50} (nM)	IC_{50} (nM)	IC_{50} (nM)	IC_{50} (nM)	IC_{50} (nM)
hMC3R	100	3.17 ± 1.13	110.91 ± 24.93	309.00 ± 60.51	33.22 ± 5.30	7.91 ± 0.75
ipMC3R	334.01 ± 28.07[b]	5.23 ± 1.27	106.15 ± 17.57	110.33 ± 44.03[a]	53.84 ± 20.37	118.91 ± 29.58[a]

Values are expressed as the mean ± SEM of at least three independent experiments.

[a] Significantly different from the corresponding parameter of hMC3R, $P < 0.05$.

[b] Significantly different from the corresponding parameter of hMC3R, $P < 0.001$.

Table 3.2 The cAMP signaling properties of hMC3R and ipMC3R.

MC3R	Basal (%)	NDP-MSH		α-MSH		β-MSH		ACTH (1-24)		D-Trp^8-γ-MSH	
		EC_{50} (nM)	R_{max} (%)	EC_{50} (nM)	R_{max} (%)	EC_{50} (nM)	R_{max} (%)	EC_{50} (nM)	R_{max} (%)	EC_{50} (nM)	R_{max} (%)
hMC3R	100	0.29 ± 0.15	100	8.82 ± 1.99	100	7.52 ± 0.99	100	4.89 ± 0.87	100	1.47 ± 0.31	100
ipMC3R	695.81 ± 83.67[c]	0.48 ± 0.20	61.44 ± 6.00[c]	0.24 ± 0.11[a]	69.41 ± 10.50[a]	0.10 ± 0.02[c]	65.64 ± 3.42[c]	0.15 ± 0.07[b]	68.45 ± 13.14[a]	0.32 ± 0.14[a]	53.18 ± 9.40[b]

Values are expressed as the mean ± SEM of at least three independent experiments. The basal cAMP level of hMC3R was 15.74 ± 1.63 pmol/10^6 cells. The maximal response (R_{max}) values of hMC3R were 2514.80 ± 541.54, 2882.33 ± 329.29, 2267.50 ± 470.49, 2873.80 ± 547.63, and 2514.67 ± 357.79 pmol/10^6 cells upon NDP-MSH, α-MSH, β-MSH, ACTH (1-24), and D-Trp^8-γ-MSH stimulation, respectively.

[a] Significantly different from the corresponding parameter of hMC3R, $P < 0.05$.

[b] Significantly different from the corresponding parameter of hMC3R, $P < 0.01$.

[c] Significantly different from the corresponding parameter of hMC3R, $P < 0.001$.

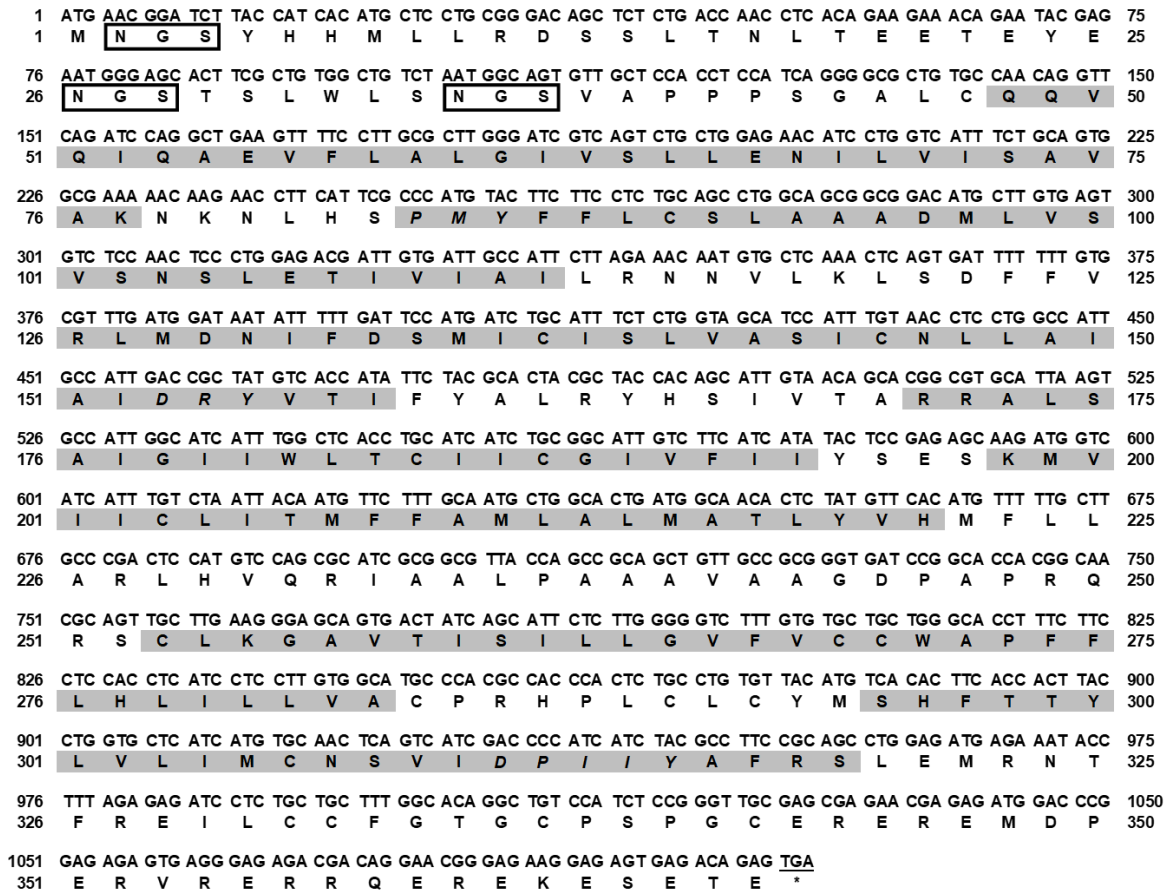

Fig. 3.1 Nucleotide and deduced amino acid sequence of ipMC3R. Positions of nucleotide and amino acid sequences are indicated on both sides. The seven TMDs are shaded in grey. The conserved motifs (PMY, DRYxxI, and DPIIY) are highlighted in italic. Open boxes frame tripeptide sequences with the consensus sequence for *N*-linked glycosylation sites. Asterisk (*) denotes stop codon.

A

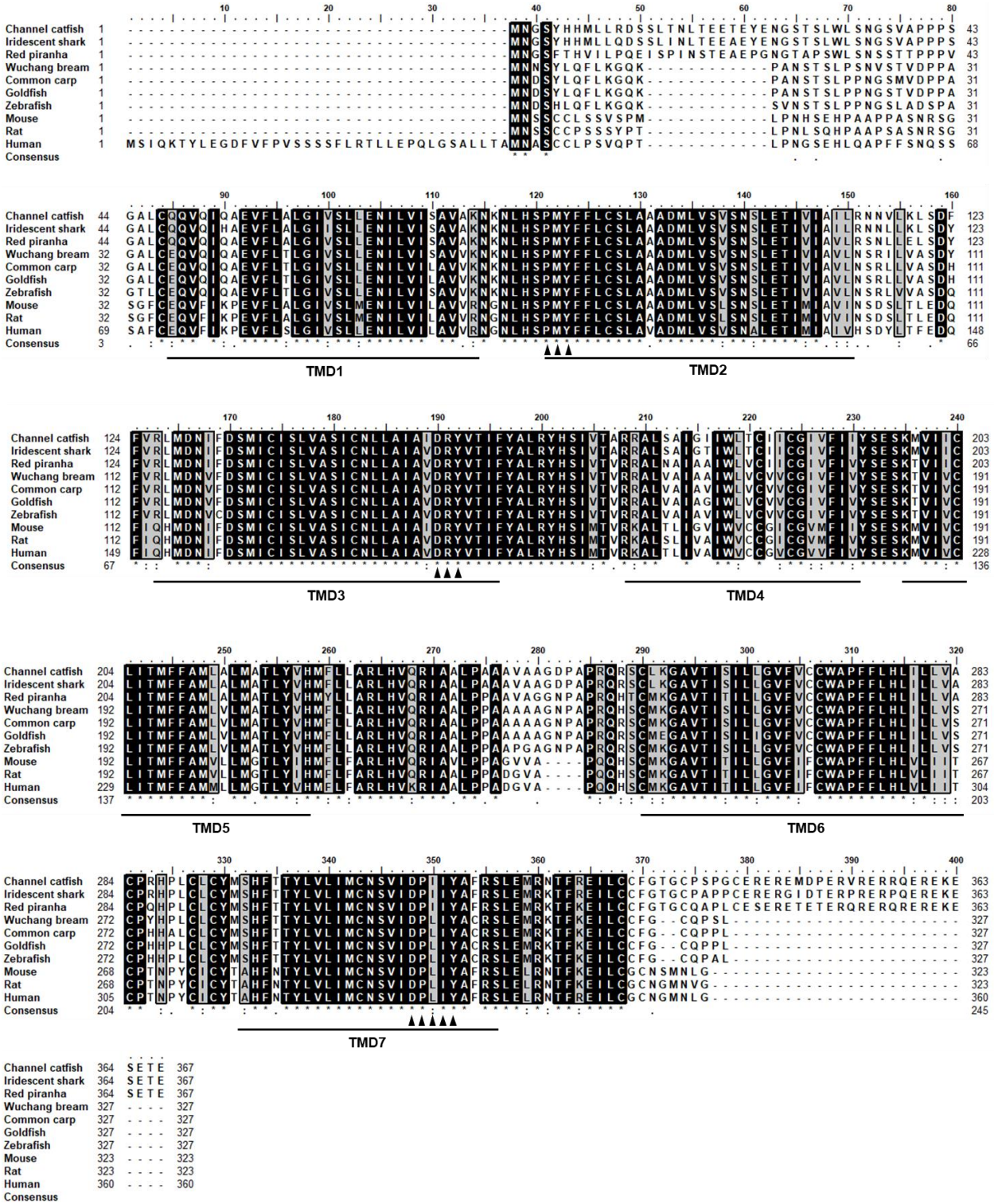
Channel catfish
Iridescent shark
Red piranha
Wuchang bream
Common carp
Goldfish
Zebrafish
Mouse
Rat
Human
Consensus
TMD1
TMD2
TMD3
TMD4
TMD5
TMD6
TMD7

B

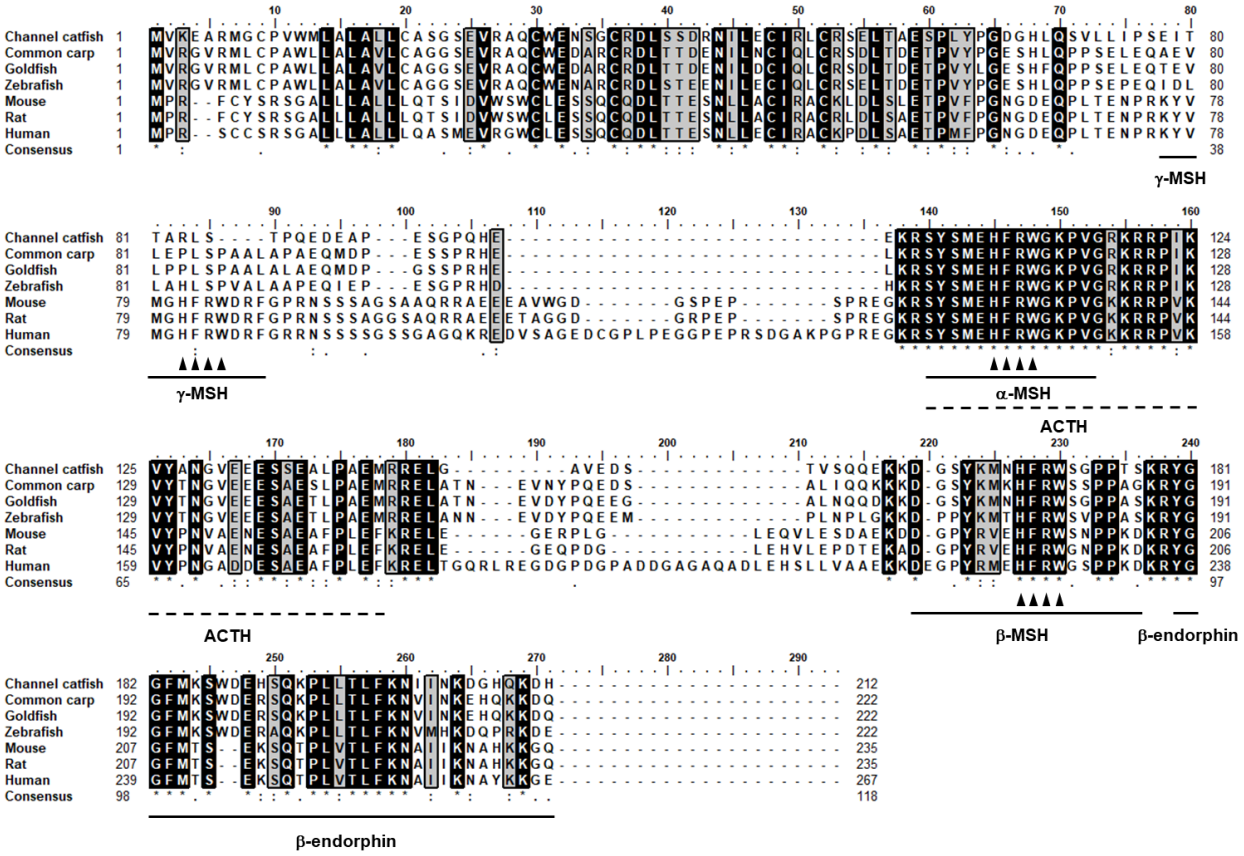
γ-MSH
α-MSH
ACTH
β-MSH
β-endorphin
ACTH
β-endorphin

C

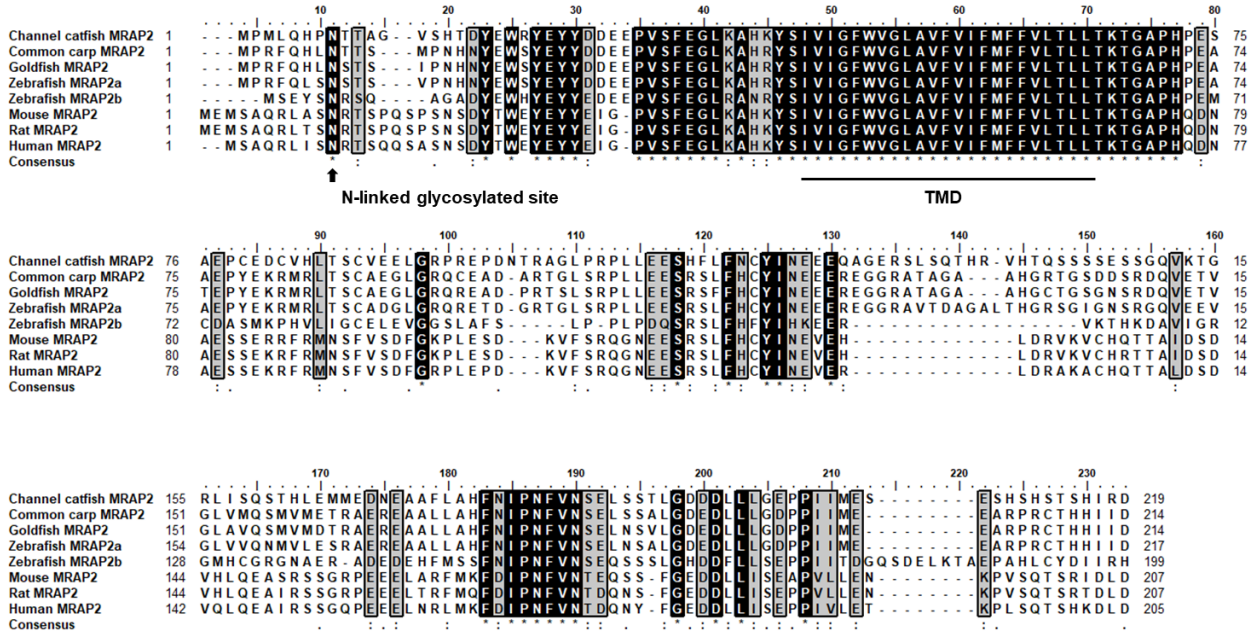
N-linked glycosylated site
TMD

Fig. 3.2 Comparison of amino acid sequences of MC3R, MRAP2, and POMC between channel catfish and other species. (A) Amino acid sequence alignment of MC3Rs. The putative TMDs are marked with lines. PMY, DRYxxI, and DPIIY motifs are indicated by black triangles. (B) Amino acid sequence alignment of POMCs. The putative sequences of peptide hormones derived from POMC are marked with lines. The core sequences of melanocortins (HFRW) are indicated by black triangles. (C) Amino acid sequence alignment of MRAP2s. The single putative TMD is underlined. Asterisk (*) denotes the identical amino acid positions. Dot (**.**) denotes the similar amino acid positions.

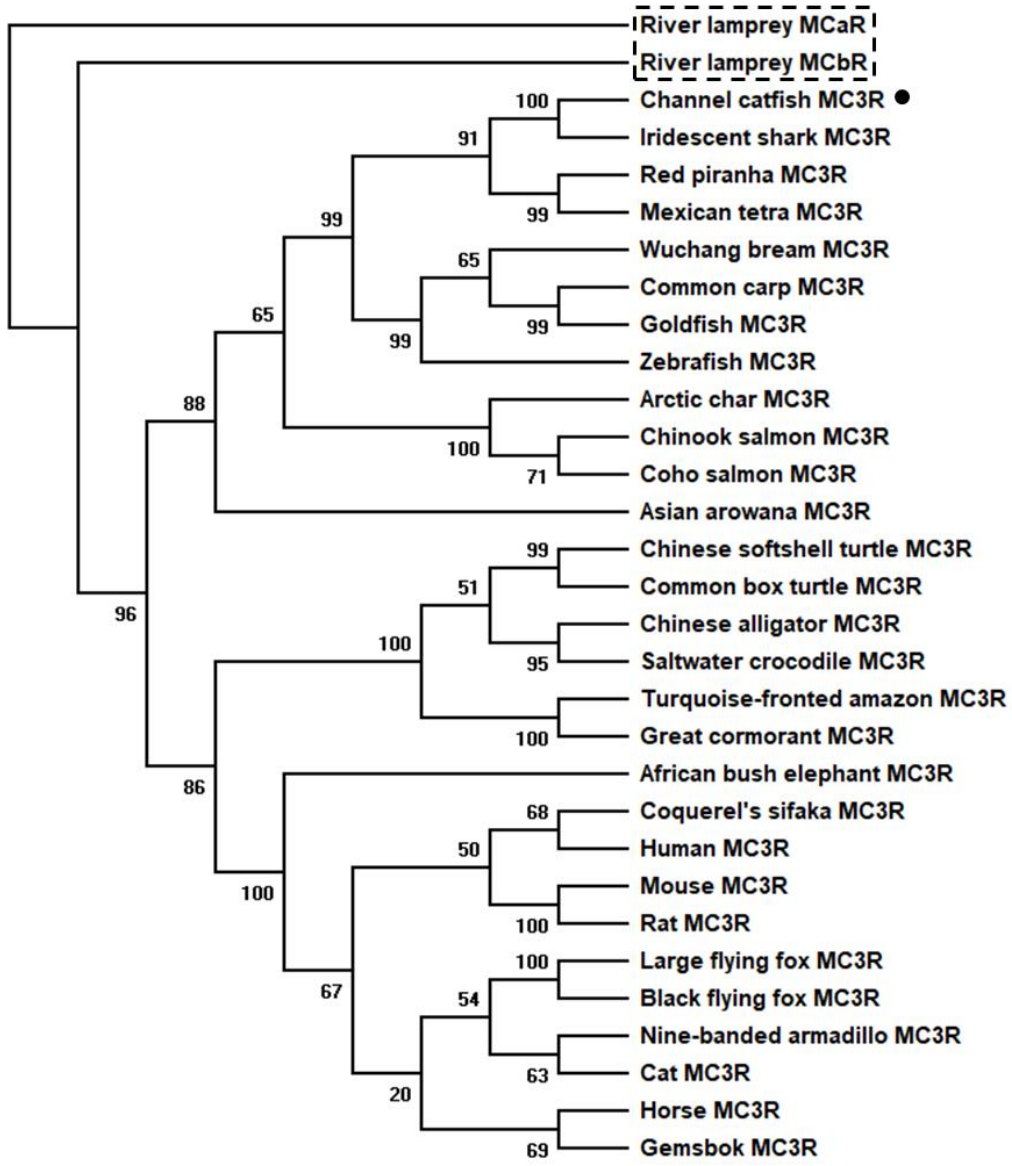

Fig. 3.3 Phylogenetic tree of MC3Rs. The tree was constructed using the neighbor-joining (NJ) method. Numbers at nodes indicate the bootstrap value, as percentages, obtained for 1000 replicates. Dot indicates ipMC3R. Two river lamprey MCRs (MCaR (ABB36647.1) and MCbR (ABB36648.1)) were used as the outgroups. MC3Rs: channel catfish (XP_017322804.1), iridescent shark (XP_026770221.1), red piranha (XP_017548887.1), Mexican tetra (XP_007231215.1), Wuchang bream (AWA81517.1),

common carp (XP_018922723.1), goldfish (BAJ83473.1), zebrafish (NP 851303.2), Chinook salmon (XP 024229914.1), coho salmon (XP_020360426.1), Arctic char (XP_023994975.1), Asian arowana (XP_018615783.1), Chinese softshell turtle (XP_006129463.1), common box turtle (XP_024059166.1), Chinese alligator (XP_006018246.1), saltwater crocodile (XP_019403708.1), turquoise-fronted amazon (KQL61336.1), great cormorant (XP_009512236.1), African bush elephant (XP_003419952.1), sifaka (XP_012501302.1), human (NP_063941.3), mouse (AAI03670.1), rat (NP_001020441.3), large flying fox (XP_011368476.1), black flying fox (XP_006921991.1), nine-banded armadillo (XP_004447768.1), cat (XP_023106851.1), horse (NP_001243901.1), gemsbok (AFH58734.1).

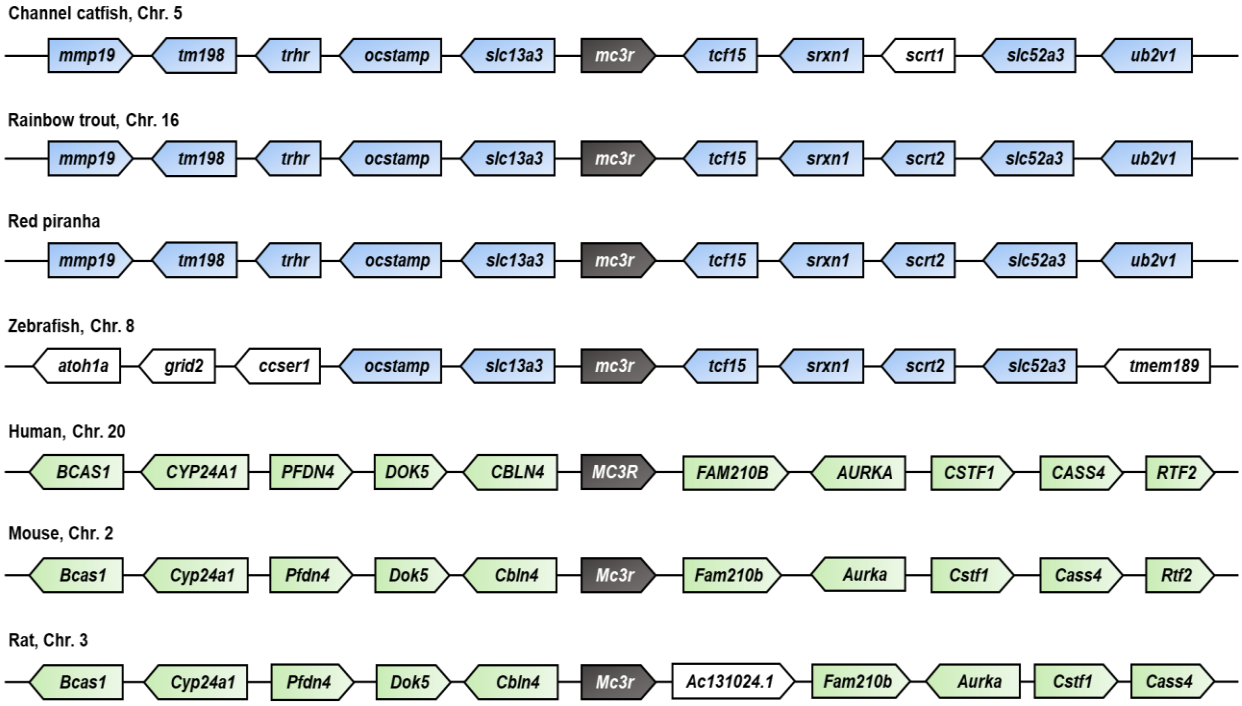

Fig. 3.4 Chromosomal synteny analyses of *MC3R* genes in different species. The syntenic genes are displayed as boxes with the directions and linked by lines. *MC3R* genes are shown in grey boxes. The genes showing conserved synteny in fishes are indicated in blue boxes and those in mammals are shown in green boxes.

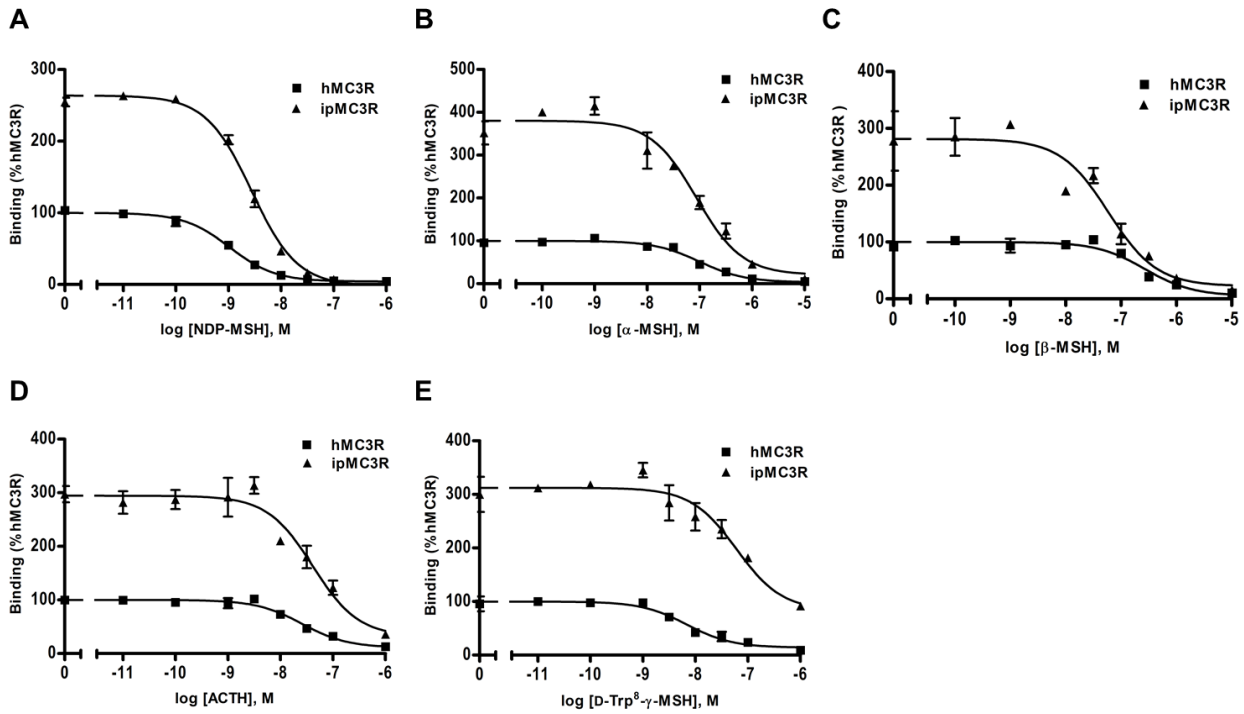

Fig. 3.5 Ligand binding properties of ipMC3R. Different concentrations of unlabeled agonists including (A) NDP-MSH, (B) α-MSH, (C) β-MSH, (D) ACTH (1-24), and (E) D-Trp^8-γ-MSH, were used to displace the binding of [^{125}I]-NDP-MSH to MC3Rs in intact cells. Data are expressed as % of hMC3R binding ± range from duplicate measurements within one experiment. The curves are representative of at least three independent experiments.

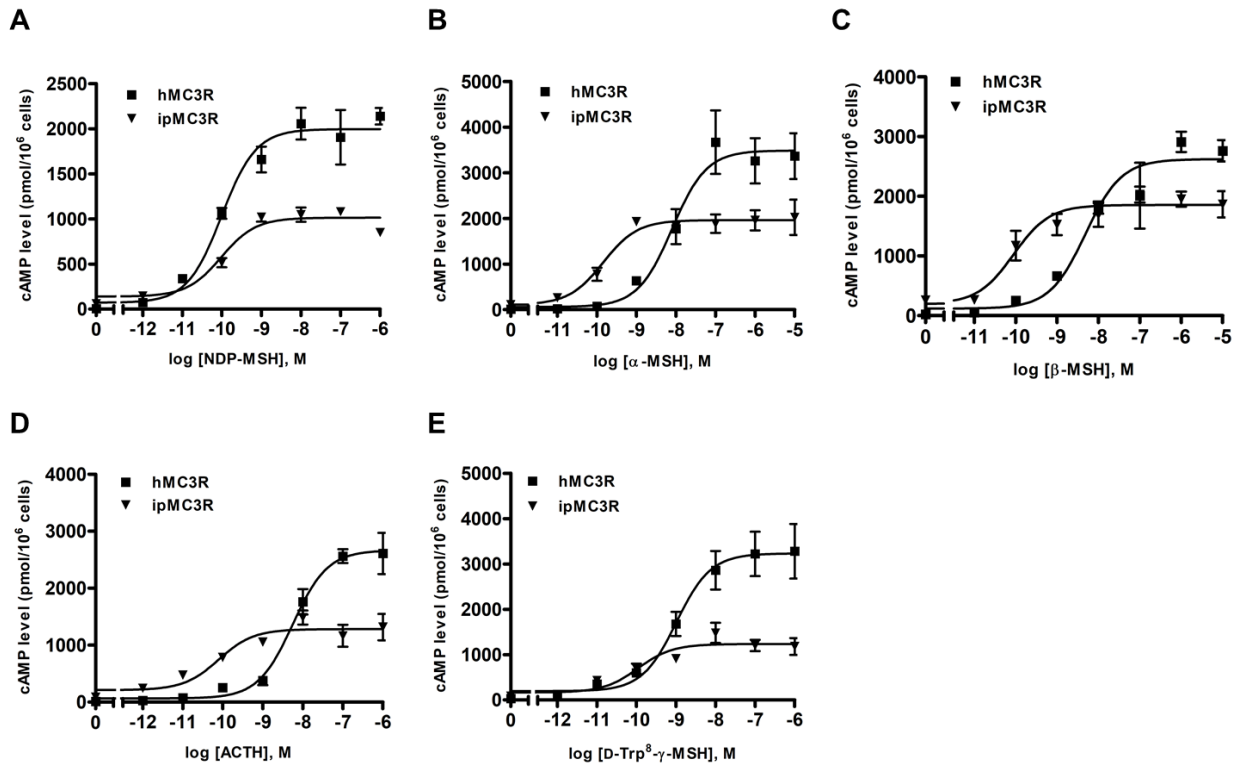

Fig. 3.6 cAMP signaling properties of ipMC3R. Different concentrations of agonists including (A) NDP-MSH, (B) α-MSH, (C) β-MSH, (D) ACTH (1-24), and (E) D-Trp^8-γ-MSH, were used to stimulate cells expressing MC3Rs. The intracellular cAMP levels were measured by RIA. Data are expressed as mean ± SEM from triplicate measurements within one experiment. The curves are representative of at least three independent experiments.

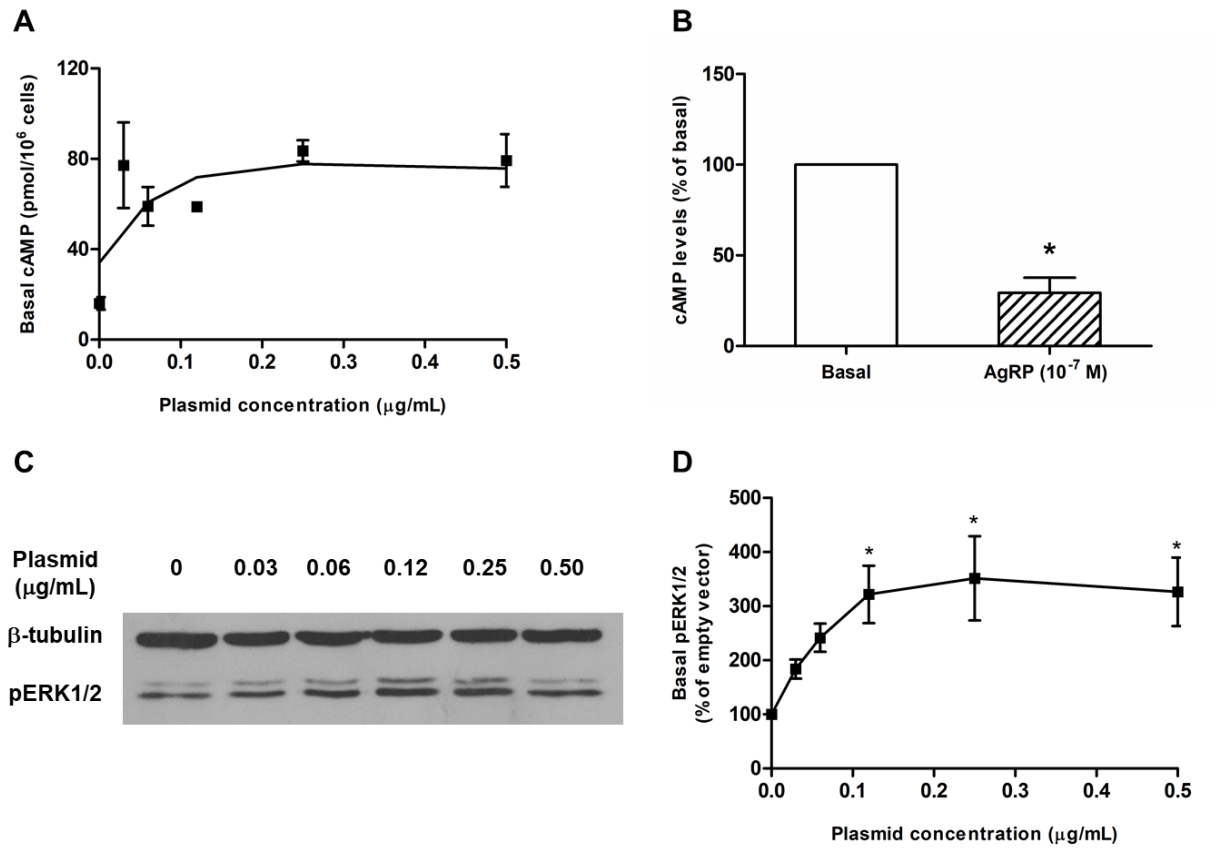

Fig. 3.7 Constitutive activities of ipMC3R in both cAMP and ERK1/2 pathways. (A) The cAMP levels of HEK293T cells transfected with increasing concentrations of ipMC3R plasmids were measured by RIA. The curve is representative of three independent experiments. (B) HEK293T cells transfected with ipMC3R (plasmid final concentration: 0.5 μg/mL) were treated without or with 10^{-7} M AgRP. The intracellular cAMP levels were measured by RIA. The data are expressed as mean ± SEM from three independent experiments. Asterisk (*) indicates significant difference between control and ligand treatment (two-tailed Student's *t*-test). (C) The ERK1/2 phosphorylation levels of HEK293T cells transfected with increasing concentrations of ipMC3R plasmids were measured by western blot. (D) Values are expressed as mean ± SEM of five independent

experiments. Asterisk (*) indicates significant difference from the basal ERK1/2 phosphorylation level of cells transfected with empty pcDNA3.1 vector (One-way ANOVA followed by Dunnett test). In (A), (C), and (D), different concentrations of empty vector pcDNA3.1 were added to maintain the identical total plasmid amount.

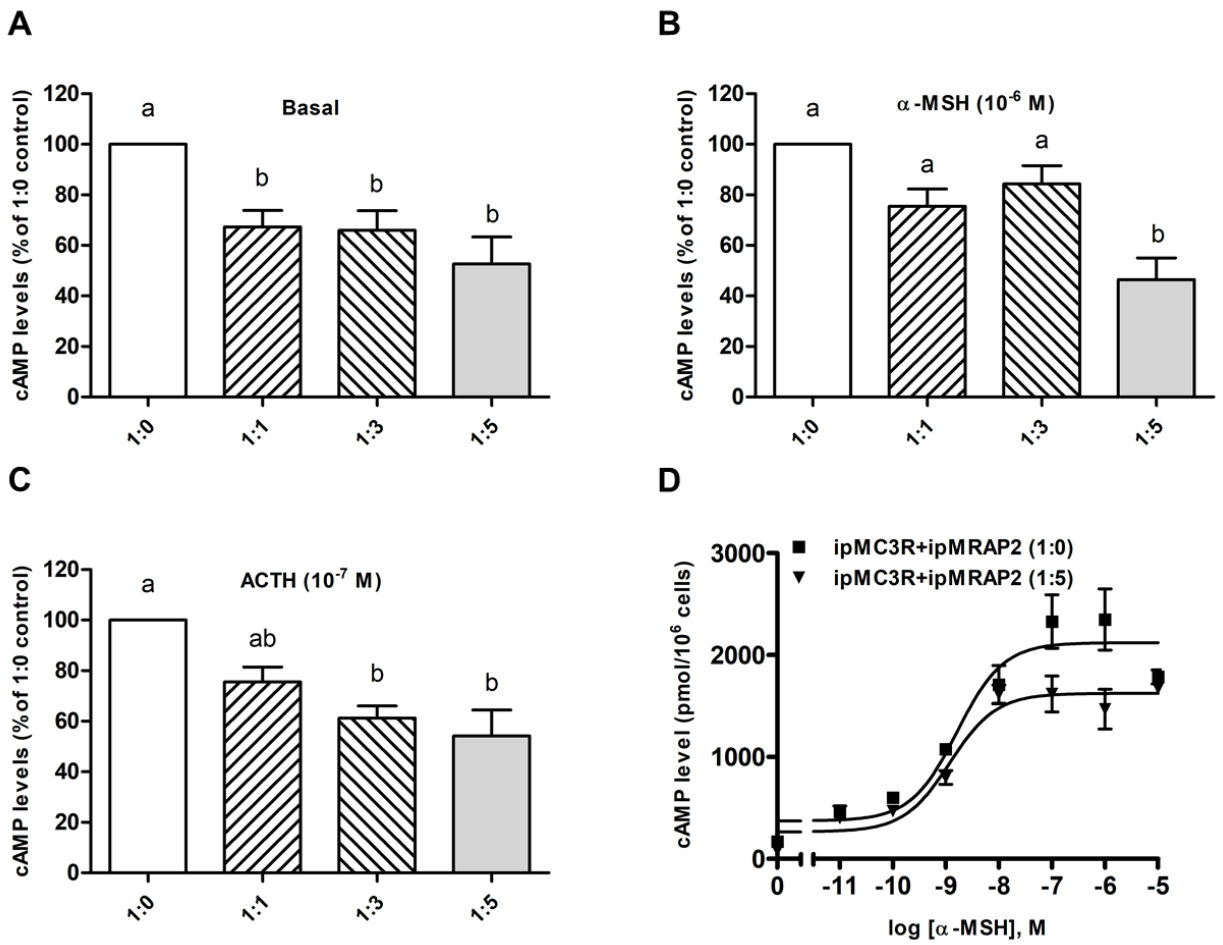

Fig. 3.8 The actions of ipMRAP2 on cAMP signaling of ipMC3R. The cAMP levels of ipMC3R stimulated without (A) or with agonists α-MSH (B) and ACTH (1-24) (C), could be dose-dependently inhibited by ipMRAP2. Values are expressed as mean ± SEM of four independent experiments. Values marked with different lowercase letters are significantly different (One-way ANOVA followed by Tukey test). (D) The curve is representative of five independent experiments in which different concentrations of α-MSH were used to stimulate cells co-transfected with ipMC3R and ipMRAP2 at the ratios of 1:0 and 1:5.

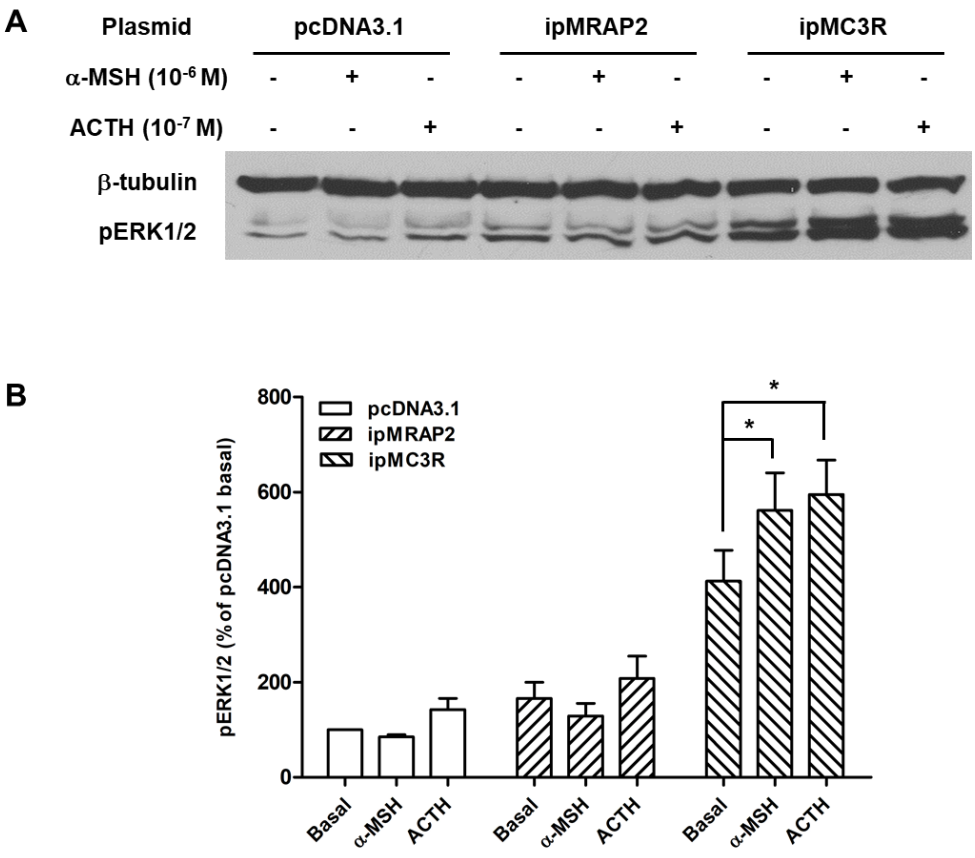
A
Plasmid
pcDNA3.1
ipMRAP2
ipMC3R
α-MSH (10-6 M)
ACTH (10-7 M)
β-tubulin
pERK1/2
B
pERK1/2 (% of pcDNA3.1 basal)
800
600
400
200
0
pcDNA3.1
ipMRAP2
ipMC3R
*
*
Basal
α-MSH
ACTH
Basal
α-MSH
ACTH
Basal
α-MSH
ACTH

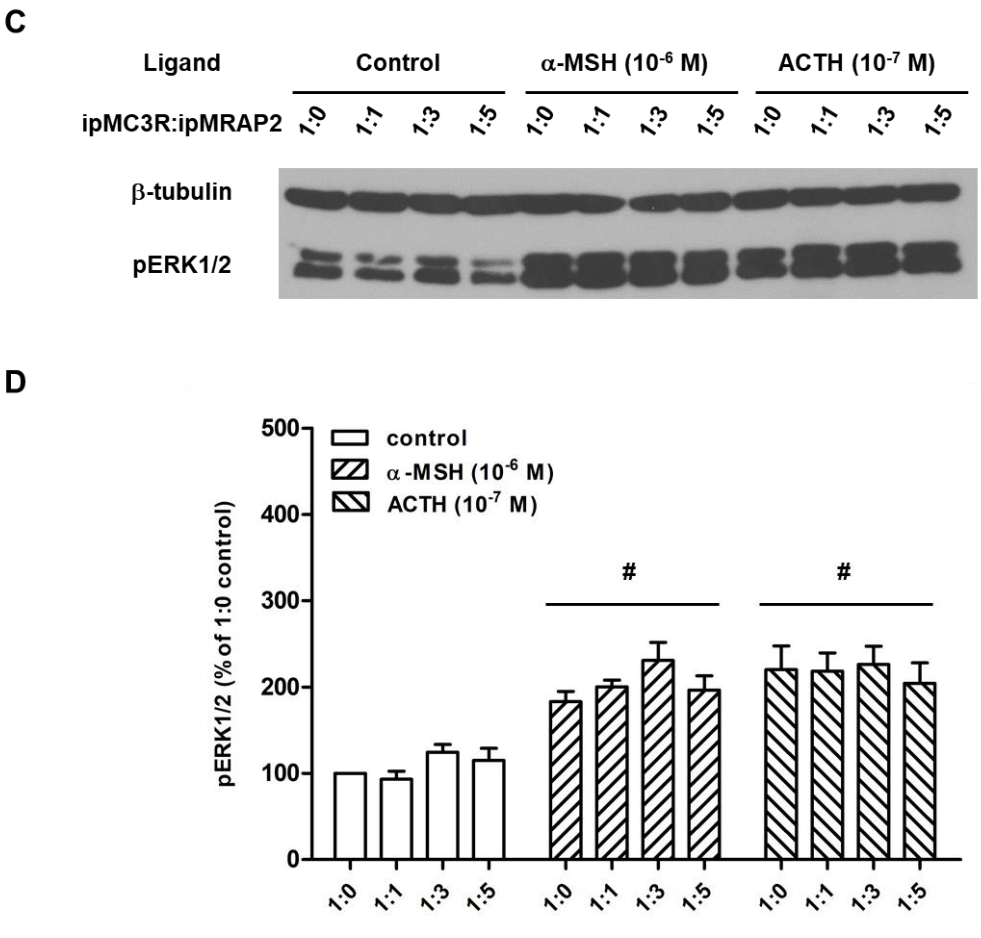

Fig. 3.9 The actions of ipMRAP2 on ERK1/2 signaling of ipMC3R. (A and B) Cells transfected with empty vector pcDNA3.1, ipMRAP2, and ipMC3R were stimulated without or with α-MSH and ACTH (1-24). The ERK1/2 phosphorylation levels were measured by western blot. Asterisk (*) indicates significant difference from the each basal ERK1/2 phosphorylation level (Two-tailed Student's *t*-test). (C and D) Cells co-transfected with ipMC3R and ipMRAP2 at different ratios were stimulated without or with α-MSH and ACTH (1-24). The ERK1/2 phosphorylation levels were measured by western blot. Hash symbol (#) indicates that the ERK1/2 phosphorylation of all ligand-treated groups are significantly different from those of the corresponding control groups (two-way ANOVA

followed by Bonferroni test). All values are expressed as mean ± SEM of at least five independent experiments.

Chapter 4: Melanocortin-4 receptor in swamp eel (*Monopterus albus*): Cloning, tissue distribution, and pharmacology

4.1. Introduction

Melanocortin-4 receptor (MC4R) is a member of Family A G protein-coupled receptors (GPCRs) consisting of seven transmembrane domains (TMDs) linked by several extracellular loops (ECLs) and intracellular loops (ICLs). The human MC4R (hMC4R), consisting of 332 amino acids, is encoded by an intronless gene located at chromosome 18q21.3 (Gantz et al., 1993a; Magenis et al., 1994; Mountjoy et al., 1994). MC4R has been shown to mediate diverse physiological processes, such as energy homeostasis, cardiovascular function, reproductive and sexual functions, and other functions in mammals (Tao, 2009; Tao, 2010a). MC4R plays an essential role in the regulation of energy homeostasis by controlling both food intake and energy expenditure (Balthasar et al., 2005; Tao, 2010a). Targeted deletion of *Mc4r* in mice results in obesity associated with hyperphagia, hyperinsulinemia, and hyperglycemia (Huszar et al., 1997). Mutations on *MC4R* have been shown to be involved in human obesity pathogenesis (Vaisse et al., 1998; Yeo et al., 1998; Hinney et al., 1999) (reviewed in (Tao, 2009; Hinney et al., 2013)). Recent studies suggested that MC4R is also involved in modulating reproductive functions by affecting secretion of several reproductive hormones, such as

gonadotropin-release hormone (GnRH), luteinizing hormone (LH), and prolactin (PRL) (Watanobe et al., 1999; Khong et al., 2001; Roa and Herbison, 2012). Therefore, understanding the important roles of MC4R in regulation of energy homeostasis and reproductive functions provides us implications for artificial feeding and breeding of economically important species.

The MC4R primarily couples to the heterotrimeric stimulatory G (Gs) protein. Activated MC4R leads to dissociation of α subunit (Gαs) from $\beta\gamma$ subunits, resulting in stimulation of adenylyl cyclase activity and increased generation of the intracellular second messenger cAMP to trigger downstream signaling pathways. The endogenous ligands for MC4R mainly comprise four agonists (α-, β-, and γ-melanocyte-stimulating hormones (MSHs), and adrenocorticotropin (ACTH)) and two antagonists (Agouti and Agouti-related peptide (AgRP)). The endogenous agonists are post-translational processing products of the precursor pro-opiomelanocortin (POMC), which is expressed in arcuate nucleus of hypothalamus in the CNS (Smith and Funder, 1988; Dores and Lecaude, 2005). The endogenous antagonist, AgRP, antagonizes agonists binding to MC4R (Fong et al., 1997; Ollmann et al., 1997). Recent studies also clarified that AgRP is also an inverse agonist which can decrease basal intracellular cAMP levels (Haskell-Luevano and Monck, 2001; Nijenhuis et al., 2001) (reviewed in (Tao et al., 2010)).

MC4R has also been characterized in lower vertebrates such as fish. MC4R is expressed in the CNS as well as many peripheral tissues such as gill, liver, intestine, and gonads in fish (reviewed in (Tao, 2010a)). Several functional studies have revealed the important roles of fish MC4Rs in the regulation of energy homeostasis. Overexpression

of AgRP in zebrafish resulted in obesity phenotype with increased linear growth and adipocyte hypertrophy (Song and Cone, 2007). Melanocortin receptor accessory protein 2a (MRAP2a) stimulated growth of zebrafish by reducing the ability of MC4R binding to α-MSH and specifically blocking the MC4R activation (Sebag et al., 2013). Intracerebroventricular injection of MC4R agonists, [Nle^4, D-Phe^7]- α-MSH (NDP-MSH) or melanotan II (MTII), inhibits food intake, whereas MC4R antagonist HS024 increases food intake in both goldfish and rainbow trout (Cerda-Reverter et al., 2003b; Schjolden et al., 2009). Moreover, nonsynonymous *mc4r* mutations in cavefish have been shown to contribute to elevated appetite, growth, and starvation resistance (Aspiras et al., 2015). In addition to regulation of energy homeostasis, fish MC4Rs are suggested to be involved in modulation of onset of sexual maturity and reproductive tactics. The *mc4r* copies are located on the X and Y chromosomes in both platyfish and swordtails. Sequence polymorphisms of *mc4r* genes comprising both functional and non-functional receptors may modulate onset of puberty (Lampert et al., 2010; Volff et al., 2013). The copy number variation of *mc4r* in swordtails is associated with variation in male body size, affecting the mating behavior (Lampert et al., 2010; Smith et al., 2015).

Swamp eel, *Monopterus albus*, belongs to the family of Synbranchidae of the order Synbranchiformes, which is a protogynic, diandric, freshwater fish (Lo Nostro et al., 2003). This fish is an important economic species distributed in the tropics and subtropics with great value for food production. In addition, swamp eel is also an ideal model for genomic and physiological studies owing to its unique evolutionary status and natural sex reversal from female into male via a special stage of intersex with ovotestis (Liu, 1944; Liem, 1963; Tao et al., 1993; Zhou et al., 2002; Cheng et al., 2003). To explore the potential roles of

MC4R in the growth and reproduction of swamp eel, we cloned swamp eel (*Monopterus albus) mc4r* (ma*mc4r*) and investigated tissue distribution of its mRNA. We also performed pharmacological characterization of swamp eel MC4R (maMC4R) in order to lay a foundation for future physiological studies.

4.2. Materials and methods

4.2.1. Ligands and plasmids

NDP-MSH was purchased from Peptides International (Louisville, KY, USA), α- and β-MSH from Pi Proteomics (Huntsville, AL, USA), ACTH (1-24) from Phoenix Pharmaceuticals (Burlingame, CA, USA), THIQ (Sebhat et al., 2002) from Tocris Bioscience (Ellisville, MO, USA). Ipsen 5i (Poitout et al., 2007) and ML00253764 (Vos et al., 2004) were custom synthesized by Enzo Life Science, Inc. (Plymouth Meeting, PA, USA) and used in our previous studies (Fan and Tao, 2009; Tao and Huang, 2014). [^{125}I]-NDP-MSH and [^{125}I]-cAMP were iodinated in our lab using chloramine T method (Steiner et al., 1969; Mo et al., 2012). The N-terminal c-myc-tagged hMC4R subcloned into pcDNA3.1 vector (pcDNA3.1-hMC4R) was generated as previously described (Tao and Segaloff, 2003).

4.2.2. Molecular cloning of maMC4R

Total RNA used for obtaining ma*mc4r* cDNA was extracted from brain using total RNA extraction reagent, RNAiso^{TM}plus (Takara, Dalian, China) and reverse transcribed using reverse transcriptase M-MLV (RNase H$^-$) (Takara). The PCR reaction was

performed using degenerate primers (Table 1) to obtain the partial fragment of ma*mc4r* cDNA based on the conversed regions of the known *mc4r* sequences. The remaining regions of cDNA were obtained by 5' and 3' Rapid amplification of cDNA ends (RACE) reactions with 5'- and 3'-Full RACE Kit (Takara) using specific RACE primers designed according to the DNA sequences of the 5'- and 3' end of ma*mc4r* (Table 4.1). The full-length ma*mc4r* cDNA was then obtained using primers flanking the open reading frame (Table 4.1). All the amplified PCR products were separated by 1.8% agarose gel electrophoresis, purified by Gel Extraction kit (Omega Bio-tek, Norcross, GA, USA), ligated into pMD18-T (Takara), and transformed into Escherichia coli for sequencing. The verified coding sequence of ma*mc4r* was then synthesized by PCR and subcloned into pcDNA3.1 vector by GenScript (Piscataway, NJ, USA) to generate the plasmid for expressing maMC4R.

4.2.3. Homology, phylogenetic, and chromosome synteny analyses of maMC4R

Multiple alignments of amino acid sequences of MC4Rs from different species were performed with Clustal X 2.1. The putative TMDs of maMC4R were predicted based on the crystal structure of rhodopsin (Palczewski et al., 2000) and that reported for hMC4R (Tao, 2010a). A phylogenetic tree based on the amino acid sequences (sequence numbers are listed in Fig. 2 legend) was constructed with 1000 bootstrap replications using the neighbor-joining (NJ) method (Saitou and Nei, 1987) and MEGA 7.0 (Kumar et al., 2016). Chromosome synteny analysis was performed between swamp eel, fugu, medaka, zebrafish, human, mouse, and rat with National Center for Biotechnology Information (NCBI) genome browser (https://www.ncbi.nlm.nih.gov).

4.2.4. Quantitative real-time PCR (qRT-PCR) for tissue distribution

The following tissues (liver, muscle, brain, spleen, kidney, intestine, heart, and gonad) were taken from six male, intersex, and female adults, respectively (the average body length and body weight: 32.50 ± 2.17cm and 103.00 ± 1.41g for male, 27.33 ± 1.21cm and 85.00 ± 2.24g for intersex, and 16.83 ± 1.47cm and 43.67 ± 3.14g for female). Total RNA was extracted from fresh tissues using total RNA extraction reagent, RNAiso^{TM}plus (Takara) and treated with RNase-free DNase I (Takara). Reverse Transcriptase M-MLV (Takara) was used for cDNA synthesis. The synthesized cDNA was subjected to amplification using specific primers designed based on sequence of ma*mc4r*. The expression of swamp eel *β-actin* was used as a reference gene, which was used as an internal control for normalization because of its similar expression levels in all tissues studied. All the primers used in qRT-PCR were designed as shown in Table 4.1. Amplifications were performed with a CFX Connect™ Real-Time PCR Detection System (Bio-Rad, Hercules, CA, USA) in 25 μL reaction volume containing 12.5 μL Power SYBR® Green PCR Master Mix (Applied Biosystems, Foster City, CA, USA), 1 μL each of specific forward and reverse primer (10 μM), 5.0 μL dilute cDNA (1 ng/μL), and 5.5 μL H_2O. The following conditions were used for reaction: 95 °C (3 min) for pre-incubation, followed by 40 cycles at 95 °C (10 s), 55 °C (30 s), 72 °C (20 s), and 75 °C (5 s). Melting curves were generated at the end of each run to verify the presence of a single product. The relative expression levels in different tissues were calculated via the $2^{-\Delta\Delta Ct}$ method (Livak and Schmittgen, 2001). The results were presented as the relative expression ratio of each target to reference gene. All data were expressed as the mean ± SEM. All samples were run in triplicate.

4.2.5. Cell culture and transfection

Human Embryonic Kidney (HEK) 293T cells (Manassas, VA, USA) were cultured in Dulbecco's Modified Eagle's medium (DMEM) (Invitrogen, Carlsbad, CA, USA) containing 10% newborn calf serum (PAA Laboratories, Etobicoke, ON, Canada), 10 mM HEPES, 0.25 μg/ml of amphotericin B, 50 μg/ml of gentamicin, 100 IU/ml of penicillin, and 100 μg/ml of streptomycin at 37 °C in a 5% CO_2-humidified atmosphere. The cells were plated into 6-wells plates (Corning, Corning, NY, USA) pre-coated with 0.1 % gelatin. At approximately 70% confluence, the cells were transfected with plasmids hMC4R and maMC4R using calcium phosphate precipitation method (Chen and Okayama, 1987). Ligand binding and cAMP assays were performed 48 h after transfection.

4.2.6. Ligand binding assays

To perform the pharmacological studies on the maMC4R and hMC4R, seven ligands of the MC4R, including five agonists (NDP-MSH, α-MSH, β-MSH, ACTH (1-24), and THIQ) and two antagonists (Ipsen 5i and ML00253764), were used.

Forty-eight hours after transfection with hMC4R and maMC4R, HEK293T cells were washed twice with warm DMEM containing 1 mg/mL bovine serum albumin (BSA, EMD Millipore Corporation, Billerica, MA, USA) (DMEM/BSA) and then incubated at 37 °C with DMEM/BSA containing ~80,000 cpm of [^{125}I]-NDP-MSH without or with different concentrations of unlabeled ligands for one hour. The final concentration ranged from 10^{-11} to 10^{-6} M for NDP-MSH, THIQ, Ipsen 5i, and ML00253764, or from 10^{-10} to 10^{-5} M for α-MSH, β-MSH, and ACTH (1-24). After incubation, the plates were placed on ice,

and then the cells were washed twice with cold Hank's balanced salt solution containing 1 mg/ml BSA to terminate the reaction. The cells were lysed by 100 μL 0.5 M NaOH and collected using cotton swabs. The radioactivity was counted by a gamma counter (Cobra II Auto-Gamma, Packard Bioscience, Frankfurt, Germany).

4.2.7. cAMP assays

Forty-eight hours after transfection with hMC4R and maMC4R, HEK293T cells were washed twice with warm DMEM/BSA and then incubated with DMEM/BSA containing 0.5 mM isobutylmethylxanthine (Sigma–Aldrich, St. Louis, MO, USA) at 37 °C for 30 min. To investigate agonist-stimulated cAMP production, the cells were treated without or with different concentrations of agonists. The final concentration ranged from 10^{-12} to 10^{-6} M for NDP-MSH and THIQ, or from 10^{-11} to 10^{-5} M for α-MSH, β-MSH, and ACTH (1-24). To investigate effects of the antagonists on the basal activities of hMC4R and maMC4R, the cells were treated without or with 10^{-6} M Ipsen 5i or 10^{-5} M ML00253764. After one hour incubation at 37 °C, the plates were placed on ice to terminate the reaction, and the cells were lysed by 0.5 M perchloric acid containing 180 μg/ml theophylline (Sigma-Aldrich) and neutralized by 0.72 M KOH/0.6 M $KHCO_3$. The cAMP levels were determined by radioimmunoassay (RIA) as described previously (Steiner et al., 1969).

4.2.8. Statistical analysis

GraphPad Prism 4.0 software (San Diego, CA, USA) was used to calculate the parameters of ligand binding and cAMP signaling assays. The significance of differences in expression levels between male and female, ligand binding and cAMP signaling

parameters between maMC4R and hMC4R, as well as vehicle and ligand-treated groups, were all determined by Student's *t*-test.

4.3. Results

4.3.1. Nucleotide and deduced amino acid sequences of maMC4R

The cloned ma*mc4r* gene contained an open reading frame of 981 bp encoding a putative protein of 326 amino acids and 36.43 kDa molecular mass (Fig. 4.1). Similar with previously identified MC4R orthologs, the predicted maMC4R consisted of seven putative hydrophobic TMDs connected by alternating ECLs and ICLs with an extracellular N-terminus and an intracellular C-terminus. In addition, the PMY, DRYxxI, and DPIIY motifs were predicted at homologous positions with MC4Rs of other species. As shown in Figs. 4.1 and 4.2, the potential *N*-linked glycosylation site (Asn^{15}) within N-terminus, consensus sequence for protein kinase C phosphorylation ($Thr^{312}Phe^{313}Lys^{314}$) within C-terminus, and 11 highly conserved cysteine residues were also found. Multiple sequence alignment revealed that maMC4R shared high identities with other piscine MC4Rs, with 90.2% to spotted scat, 89.6% to sea bass, 89.0% to flounder, 85.4% to swordtail fish, and 76.8% to zebrafish. However, the identities of maMC4R to mammalian MC4Rs were relatively low, with 66.1% to hMC4R and 65.5% to rat MC4R. Most of the conversed amino acids were localized in the TMDs and ICLs.

4.3.2. Phylogenetic and chromosome synteny analyses of maMC4R

To evaluate the evolutionary relationships between the predicted maMC4R and other vertebrate MC4Rs, phylogenetic analysis was conducted with full-length amino acid sequences of maMC4R and other MC4Rs. Our results indicated that maMC4R is nested within a clade of Burton's mouthbrooder (*Haplochromis burtoni*), turquoise killifish (*Nothobranchius furzeri*), and red-striped killifish (*Aphyosemion striatum*) (Fig. 4.3). To determine whether ma*mc4r* is orthologous to those of other vertebrates (fishes: fugu, medaka, and zebrafish, and mammals: rat, mouse, and human), chromosome syntenic relationships among different species were then analyzed. The results indicated that ma*mc4r* gene neighbors exhibited a highly conserved synteny to fugu and medaka. The neighboring genes of human, mouse and rat were also conserved, especially those of mouse and rat. However, there was no conserved synteny between swamp eel and human, mouse and rat *mc4r* genes since only *RNF152* and *CDH20* of human were found to locate at the same homologous positions compared with swamp eel, and none of neighboring genes of ma*mc4r* was found in the adjacent regions of mouse and rat *Mc4r* genes (Fig. 4.4).

4.3.3. Tissue expression of ma*mc4r*

Expression of ma*mc4r* in male, intersex and female swamp eel was studied by qRT-PCR. Our results showed that ma*mc4r* transcripts were found to be highly expressed in brain and gonad of male, intersex and female swamp eel, but expressed at low levels in other tissues. We also found that both ma*mc4r* transcripts in brain and gonad of female swamp eel exhibited significantly higher expression levels compared to those of male (*P*

< 0.05, n = 6) (Fig. 4.5). There was no significant difference between expression levels of male and intersex in brain and gonad, although we observed higher expression levels in intersex in these two tissues.

4.3.4. Ligand binding properties of maMC4R

Comparative ligand binding assay was performed to investigate the binding properties of maMC4R to different MC4R ligands, including five agonists (NDP-MSH, α-MSH, β-MSH, ACTH (1-24), and THIQ) and two antagonists (Ipsen 5i and ML00253764). The maximal binding value of maMC4R to radiolabeled NDP-MSH was 30.89 ± 1.38% of that of hMC4R (Table 4.2 and Fig. 4.6). Similar as the binding affinity order of hMC4R, maMC4R bound to super-potent agonist NDP-MSH with the highest affinity (IC_{50}, 2.20 ± 0.19 nM), followed by ACTH (1-24) (33.07 ± 4.91 nM), α-MSH (205.23 ± 19.32 nM), and β-MSH (495.47 ± 66.26 nM). When NDP-MSH, α-MSH, or ACTH (1-24) was used as the competitor to displace the radiolabeled NDP-MSH, maMC4R exhibited significantly decreased IC_{50}s compared to hMC4R. No significant difference was observed between the IC_{50}s of these two MC4Rs when β-MSH was used as the competitor (Table 4.2). THIQ, Ipsen 5i, and ML00253764 were not able to displace the radiolabeled NDP-MSH bound with maMC4R, although they could displace radiolabeled NDP-MSH bound with hMC4R in a dose-dependent manner (Fig. 4.6E, Fig. 4.8 and Table 4.2).

4.3.5. Signaling properties of maMC4R

RIA was performed to investigate the signaling properties of maMC4R to determine whether the cloned maMC4R could respond to ligand stimulation. All agonists

were able to dose-dependently stimulate maMC4R and increase intracellular cAMP production (Fig. 4.7). The maximal response of maMC4R in response to NDP-MSH, α-MSH, or β-MSH was similar as that of hMC4R, whereas maMC4R initiated significantly reduced maximal intracellular cAMP production in response to ACTH (1-24) or THIQ compared with hMC4R (Fig. 4.7D and E, and Table 4.3). EC_{50}s of α-MSH, β-MSH, and ACTH (1-24) for maMC4R were significantly lower than those for hMC4R. In contrast, EC_{50} of THIQ for maMC4R was significantly higher compared with that for hMC4R (Table 4.3).

Ipsen 5i and ML00253764 were previously demonstrated as inverse agonists by decreasing the basal activities of both WT and constitutively active mutant hMC4Rs (Mo and Tao, 2013). In the present study, we found basal cAMP levels of hMC4R decreased approximately 60% after treatment of Ipsen 5i or ML00253764 compared with the control (Fig. 4.8). ML00253764 could decrease basal cAMP level of maMC4R by 50%, whereas Ipsen 5i exhibited agonistic activity, significantly increasing the cAMP level of maMC4R compared with the control (Fig. 4.9).

4.4. Discussion

MC4R has been well studied in mammals as an important factor in regulation of energy homeostasis and reproductive function. However, few studies have focused on non-mammalian vertebrates, especially economically important fish. In the present study, we demonstrated that the cloned ma*mc4r* cDNA encoded a protein with similar structural features as MC4Rs of other species, including TMDs, ECLs, and ICLs. The amino acid

sequence was more than 80% identical to several teleost MC4Rs. The conversed motifs including PMY, DRYxxI, and DPIIY (DPxxY) were also conserved in maMC4R. Other structural features, such as consensus potential *N*-linked glycosylation sites, C-terminal phosphorylation sites, and highly conserved cysteine residues, were also identified in maMC4R (Figs. 4.1 and 4.2). These motifs and residues are known to be significant to maintain receptor 3D structure and function. Phylogenetic tree revealed that maMC4R was clustered with teleost MC4Rs (Fig. 4.3). Furthermore, the maMC4R was suggested to be evolutionarily conserved because chromosomal synteny analysis showed that the genes surrounding ma*mc4r* were highly conserved compared with those in fugu and medaka (Fig. 4.4). Together, these results indicated that the cloned maMC4R might exhibit the same functions as MC4Rs in other species.

The expression pattern of the MC4R in lower vertebrates has been shown to be much wider compared to that in mammals. Our results showed that ma*mc4r* mRNA was highly expressed in the gonads in addition to the brain (Fig. 4.5), similar to the results obtained in other fish, such as barfin flounder, goldfish, and spotted scat (Cerda-Reverter et al., 2003a; Li et al., 2016a), suggesting a putative function of maMC4R in gonadal development. It is interesting to note that swamp eel undergoes natural sex reversal from female via intersex into male. Several genes, such as *dmrt* genes, *sox9* genes (*sox9a1* and *sox9a2*), and androgen receptor (*ar*) gene, have been observed to be involved in the process of sex reversal of swamp eel (Cheng et al., 2003; Zhou et al., 2010; Sheng et al., 2014). Ravaglia et al. observed sex reversal in female swamp eel after administration of salmon GnRH analogue (sGnRH-A) and the dopamine receptor antagonist, domperidone (DOM) (Ravaglia et al., 1997). Although the role of maMC4R in this process has not been

reported so far, studies in mammals have shown that MC4R is involved in regulating reproductive function by modulating hormone secretion through GnRH neurons. Watanobe et al. found that MC4R antagonists decrease the magnitude of LH surges in normal fed rats (Watanobe et al., 1999). Roa et al. further demonstrated that GnRH neurons are activated by α-MSH through direct postsynaptic activation of MC4R in mice (Roa and Herbison, 2012). In spotted scat, MC4R activation increases gene expression of hypothalamic GnRH and pituitary gonadotropins (Jiang et al., 2017). In the present study, of particular interest was the result that expression levels of ma*mc4r* in brain and gonad of females were significantly higher than those of males (Fig. 4.5). However, whether or not MC4R plays a role in the process of sex reversal of swamp eel by activating the hypothalamic-pituitary-gonadal axis is still needed to test.

To investigate the pharmacology of cloned maMC4R, ligand binding and cAMP signaling assays were performed. The results showed that the synthetic agonist NDP-MSH could bind to maMC4R with the highest affinity with an IC_{50} of 2.20 nM and stimulate maMC4R with the highest potency with an EC_{50} of 0.02 nM, consistent with its super-potent agonistic activity (Table 4.2). Although THIQ, a small molecule agonist, could not bind to maMC4R orthosterically by displacing the radiolabeled NDP-MSH, it still activated the receptor and initiate cAMP signaling (Figs. 4.6 and 4.7), indicating that the binding site of THIQ might be different from that of NDP-MSH at maMC4R (allosteric agonist). As for hMC4R, the binding sites for THIQ and NDP-MSH were overlapping since THIQ could displace radiolabeled NDP-MSH in a dose-dependent manner. Our results were consistent with our previous study demonstrating THIQ to be an allosteric agonist for spotted scat MC4R (Li et al., 2016a). In artificial propagation of swamp eel, the GnRH

analogue is used to induce the ovulation of brood females (Guan et al., 1996). We suggest that the small molecule THIQ may be used in artificial propagation of swamp eel considering its stimulatory effects on expression of *gnrh*, *lhb* (luteinizing hormone beta subunit), and *fshb* (follicle-stimulating hormone beta subunit) through MC4R signaling in spotted scat (Jiang et al., 2017).

ACTH was proposed as the “original” ligand for the early melanocortin receptors during vertebrate evolution, supported by evidence that ACTH is able to bind to MC4Rs with high affinity compared to other endogenous agonists in many fishes, such as fugu, rainbow trout, spotted scat, and grass carp (Haitina et al., 2004; Klovins et al., 2004a; Li et al., 2016a; Li et al., 2017). Of three endogenous agonists used in the present study, ACTH (1-24), known to be equipotent to the full-length ACTH (1–39), was also shown to have the highest binding affinity with maMC4R (Table 4.2).

The MC4R has been shown to be constitutively active in cAMP signaling (Tao, 2014). Naturally occurring mutations in the *MC4R* resulting in decreased constitutive activity are considered as the possible causes of human obesity (Tao, 2008). MC4Rs in many fishes, such as seabass, zebrafish, spotted scat, and grass carp, were all reported to be constitutively active (Sanchez et al., 2009; Sebag et al., 2013; Li et al., 2016a; Li et al., 2017). In agreement with these previous results, our present study showed that maMC4R had significantly increased basal activity, which was approximately 6 times higher than that of hMC4R (Table 4.3). It has been reported that the N-termini of GPCRs are critical in regulating constitutive activities (Zhang et al., 2000; Nishi et al., 2002; Paavola et al., 2011). As for hMC4R, N-terminus is proposed to act as a tethered ligand to maintain constitutive activity of the receptor (Srinivasan et al., 2004). By comparing the

amino acid sequences of maMC4R, as well as other fish MC4Rs, with that of hMC4R, we found that in contrast to high identities in TMDs and ICLs, fish MC4Rs shared low identities with hMC4R in N-termini and ECL1s (Fig. 4.2). We speculated that evolutionarily dissimilar structure of N-terminal domain of maMC4R might be the reason for its high basal activity. Two inverse agonists, Ipsen 5i and ML00253764, were used to investigate their effects on basal activities of maMC4R. As expected, they were able to decrease the basal cAMP levels in cells transfected with hMC4R. The inverse agonistic effect of ML00253764 on maMC4R was also verified, further confirming constitutive activation of maMC4R. However, Ipsen 5i induced an approximate two-fold increase of constitutive activity on maMC4R rather than generating an inhibitory effect, showing its agonistic effect on maMC4R (Fig. 4.9). The different effects of Ipsen 5i on hMC4R and maMC4R might be due to the dissimilar structures of two receptors. It is interesting to note that Ipsen 5i and ML00253764 bound to allosteric site(s) (Fig. 4.8), indicating that they were also allosteric ligands for maMC4R.

The constitutive activity of fish MC4R is thought to be physiologically relevant. Mutations in cavefish *mc4r* leading to decreased constitutive activity and signaling efficiency of the receptor were proposed as the cause of elevated appetite, growth, and starvation resistance (Aspiras et al., 2015). Knock-down of *agrp* or *mrap2a* in zebrafish caused decreased growth by increasing the constitutive activity of MC4R (Sebag et al., 2013). Hence, in pisciculture, inhibition of the constitutive activity of MC4R might be a novel strategy for feed intake promotion and accelerated growth of the economically important fishes. The small molecule inverse agonists might be effective food additives promoting appetite and reducing energy expenditure of those species to achieve better

economic return. ML00253764, shown to be an inverse agonist for maMC4R in the present study, could be one small molecule with economic value for swamp eel farming. Further in vivo studies are needed to verify whether ML00253764 could potentially be added to swamp eel feed.

In summary, the cloned maMC4R was demonstrated to be evolutionarily conserved in piscine MC4Rs. We found that the expression of maMC4R was also highly expressed in gonad in addition to brain. The receptor was also found in various peripheral tissues, indicating its important roles in mediating various physiological processes in swamp eel. The pharmacological studies have demonstrated that the cloned maMC4R was a functional receptor with its unique pharmacological properties, providing us the foundation for future physiological studies.

Table 4.1 Primers used for cDNA cloning and qRT-PCR. *β-actin* was used as housekeeping gene.

Primer name	Primer sequence (5'-3')	Purpose
mc4r-Fw	AGCATGTTCTTTACCATGCT	*mc4r* fragment PCR
mc4r-Rv	TTGAAGTGTGACATGAAGCA	*mc4r* fragment PCR
mc4r-3RACE1	CTGTATGTCCACATGTTCCTG	*mc4r* 3'-RACE PCR
mc4r-3RACE2	ATGTTCCTGTTGGCACGCTT	*mc4r* 3'-RACE PCR
mc4r-5RACE1	GCCCAGCATACCACAAACAC	*mc4r* 5'-RACE PCR
mc4r-5RACE2	GAGGAGGATAGTGAGGGTGATG	*mc4r* 5'-RACE PCR
mc4r-w-Fw	CTCTCACGTTCCCTTTCACTGT	*mc4r* full-length PCR
mc4r-w-Rv	CTTGGCTGCGAAAAGCATAGAT	*mc4r* full-length PCR
β-actin-Fw	CTGGACTTCGAGCAGGAGAT	*β-actin* qRT-PCR
β-actin-Rv	ACCAAGGAAAGAAGGCTGGA	*β-actin* qRT-PCR
mc4r-RT-Fw	TCCTCACTCTGGGCATCATC	*mc4r* qRT-PCR
mc4r-RT-Rv	GGAGACACTGACCAGCATGT	*mc4r* qRT-PCR

Table 4.2 The ligand binding properties of hMC4R and maMC4R.

MC4R	B_{max}	NDP-MSH	α-MSH	β-MSH	ACTH (1-24)	THIQ	Ipsen 5i	ML00253764
		IC_{50} (nM)	IC_{50} (nM)	IC_{50} (nM)	IC_{50} (nM)	IC_{50} (nM)	IC_{50} (nM)	IC_{50} (nM)
hMC4R	100	30.07 ± 3.92	835.53 ± 101.64	703.33 ± 77.11	110.32 ± 30.98	159.12 ± 46.68	333.83 ± 70.29	513.17 ± 297.13
maMC4R	30.89 ± 1.38[a]	2.20 ± 0.19[a]	205.23 ± 19.32[a]	459.47 ± 66.26	33.07 ± 4.91[a]	N/A[b]	N/A[b]	N/A[b]

Results are expressed as the mean ± SEM of at least three independent experiments.

[a] Significantly different from the parameter of hMC4R, $P < 0.01$.

[b] Could not be determined.

Table 4.3 The signaling properties of hMC4R and maMC4R.

MC4R	Basal (%)	NDP-MSH		α-MSH		β-MSH		ACTH (1-24)		THIQ	
		EC_{50} (nM)	R_{max} (%)	EC_{50} (nM)	R_{max} (%)	EC_{50} (nM)	R_{max} (%)	EC_{50} (nM)	R_{max} (%)	EC_{50} (nM)	R_{max} (%)
hMC4R	100	0.34 ± 0.16	100	1.67 ± 0.53	100	1.75 ± 0.33	100	0.63 ± 0.10	100	3.88 ± 0.68	100
maMC4R	673.78 ± 104.13[b]	0.02 ± 0.01	87.56 ± 10.09	0.14 ± 0.02[a]	98.04 ± 14.07	0.24 ± 0.11[a]	137.45 ± 41.74	0.17 ± 0.03[a]	76.73 ± 7.81[a]	74.45 ± 28.99[a]	54.92 ± 13.71[a]

Results are expressed as the mean ± SEM of at least three independent experiments.

[a] Significantly different from the parameter of hMC4R, $P < 0.05$.

[b] Significantly different from the parameter of hMC4R, $P < 0.01$.

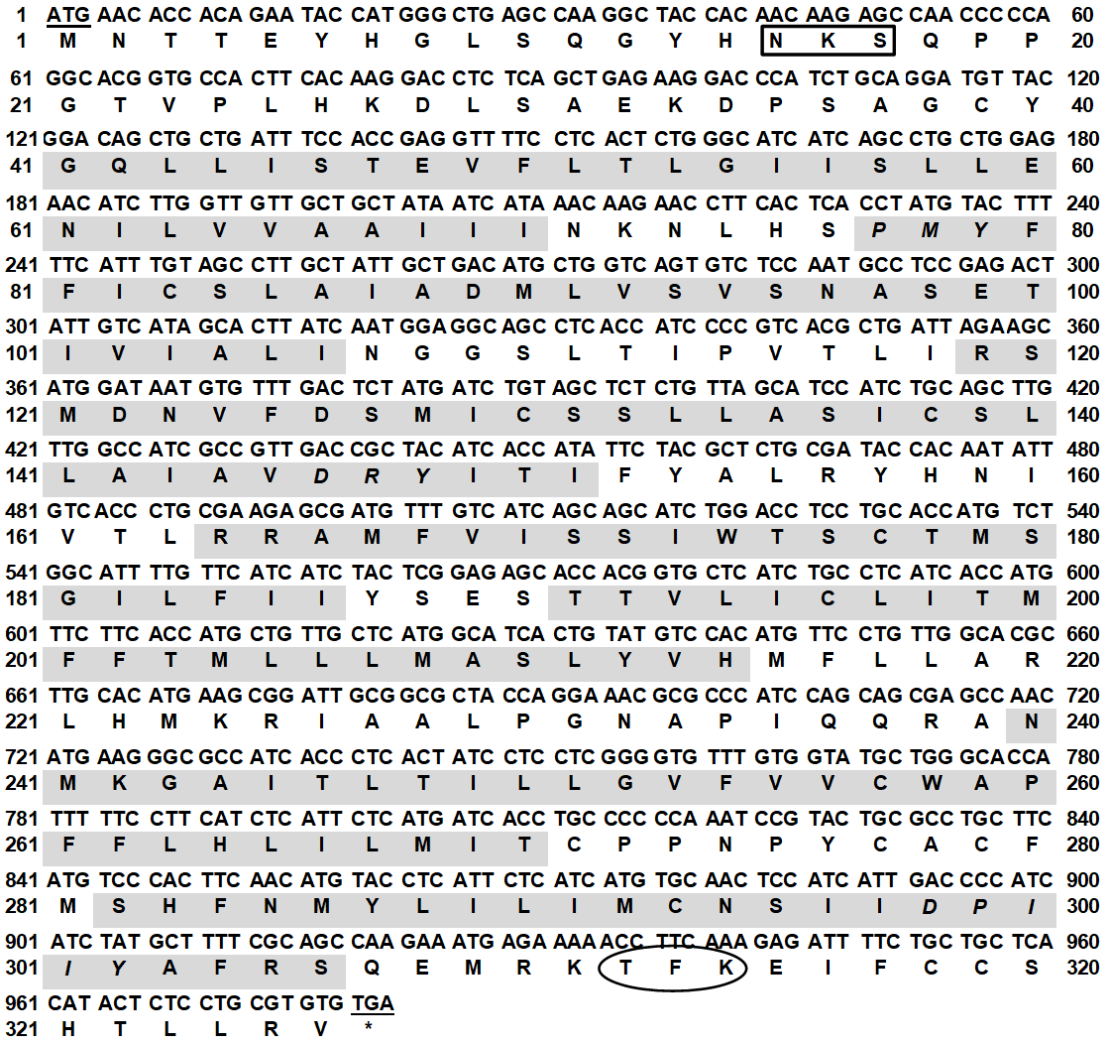

Fig. 4.1 Nucleotide and deduced amino acid sequence of maMC4R. Positions of nucleotide and amino acid sequences are indicated on both sides. Amino acids in shaded boxes indicate putative transmembrane domains. Open boxes frame tripeptide sequences with the consensus sequence for N-linked glycosylation sites. Oval frames enclose potential phosphorylation sites. PMY, DRYxxI, DPIIY (DPxxY) motifs are highlighted in italic. Underlines show initiation codon and stop codon. Asterisk (*) denotes stop codon

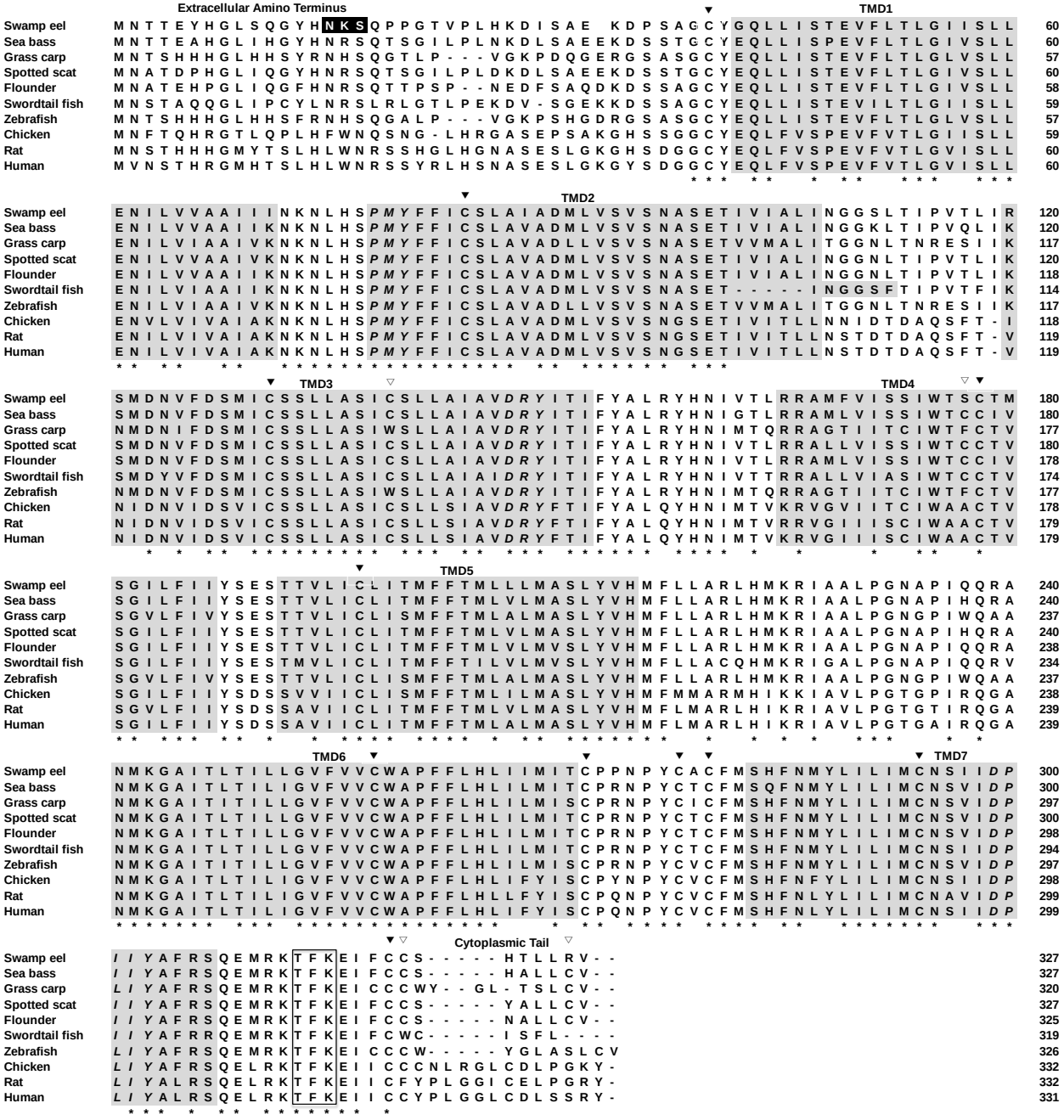

Fig. 4.2 Comparison of amino acid sequences between maMC4R and MC4Rs from other species. Labeled as follows: transmembrane domains in shaded boxes as TMD

1–7, amino- and carboxyl-termini as extracellular amino terminus and cytoplasmic tail, respectively. Fully conserved and conserved cysteine residues are indicated by arrowheads. Predicted phosphorylation sites are shown by open boxes. PMY, DRYxxI, DPIIY (NPXXY) motifs are highlighted in italic. Dark shadow shows *N*-linked glycosylation sites. Asterisk (*) indicates the identical amino acids.

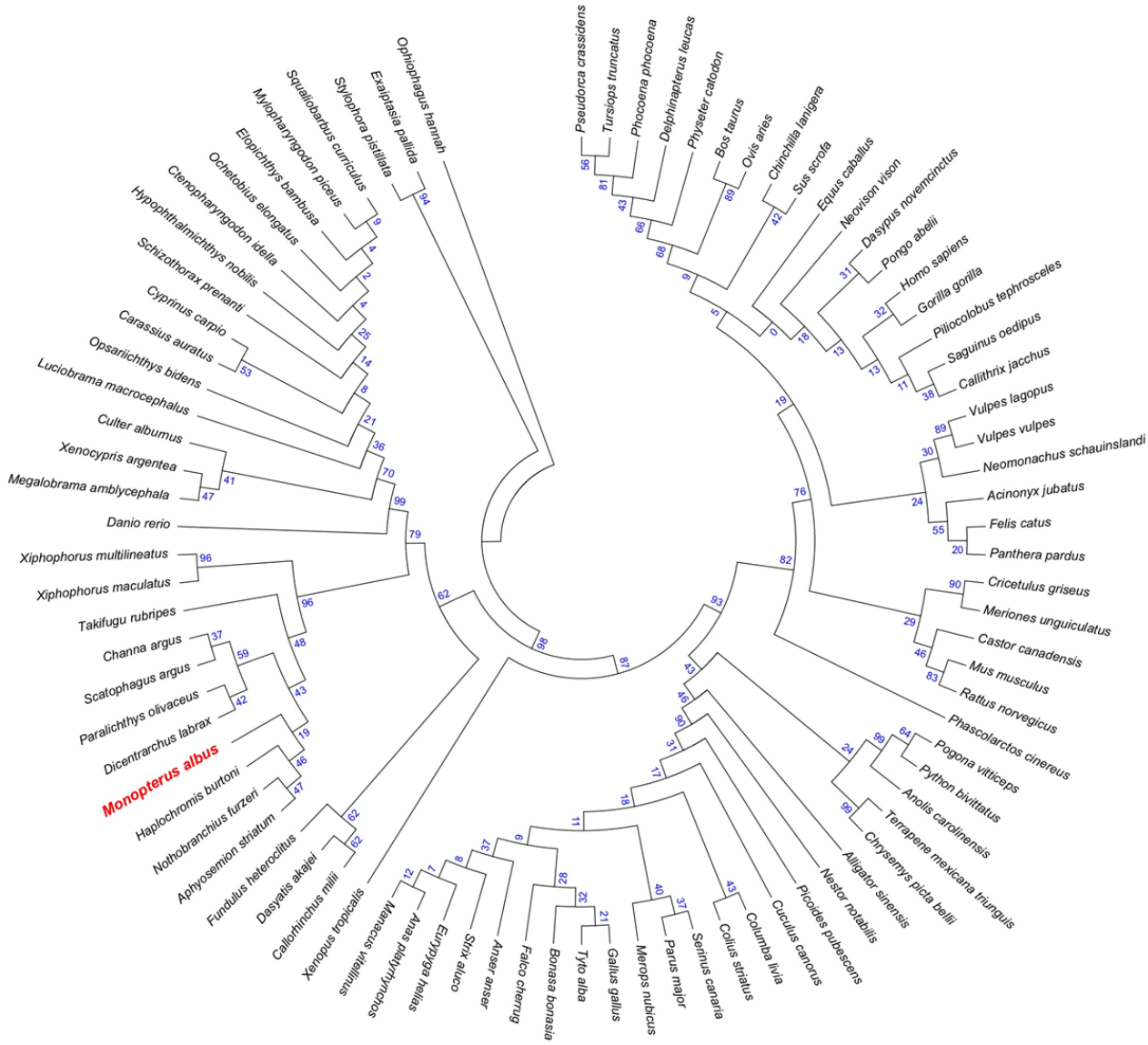

Fig. 4.3 Phylogenetic tree of MC4R proteins. The trees were constructed using the neighbor-joining (NJ) method. Numbers at nodes indicate the bootstrap value, as percentages, obtained for 1000 replicates. Dot shows maMC4R. MC4Rs: *Monopterus albus* (AVZ65970.1), *Castor canadensis* (XP_020009048.1), *Neovison vison* (AGT56096.1), *Aphyosemion striatum* (SBP15058.1), *Vulpes lagopus* (ACN55093.1), *Squaliobarbus curriculus* (ADV40875.1), *Tyto alba* (ATN96237.1), *Delphinapterus leucas*

(XP_022439973.1), *Hypophthalmichthys nobilis* (ADV40874.1), *Mylopharyngodon piceus* (ADV40871.1), *Tursiops truncates* (AKH66529.1), *Python bivittatus* (XP_007441304.1), *Haplochromis burtoni* (NP_001274332.1), *Merops nubicus* (XP_008934286.1), *Bos taurus* (NP_776535.1), *Pogona vitticeps* (XP_020642338.1), *Acinonyx jubatus* (XP_014940693.1), *Gallus gallus* (NP_001026685.1), *Alligator sinensis* (XP_006025279.1), *Serinus canaria* (XP_009092806.1), *Cyprinus carpio* (CBX89936.1), *Felis catus* (XP_019670932.2), *Anser anser* (ABF19809.1), *Picoides pubescens* (XP_009899122.1), *Callorhinchus milii* (XP_007893711.1), *Dicentrarchus labrax* (CBN82190.1), *Exaiptasia pallida* (KXJ23657.1), *Manacus vitellinus* (XP_008930852.1), *Carassius auratus* (CAD58853.1), *Ctenopharyngodon idella* (AOZ60534.1), *Parus major* (XP_018861381.1), *Anolis carolinensis* (XP_003226797.1), *Neomonachus schauinslandi* (XP_021542070.1), *Equus caballus* (XP_001489706.1), *Mus musculus* (NP_058673.2), *Homo sapiens* (NP_005903.2), *Paralichthys olivaceus* (ADP09415.1), *Nestor notabilis* (XP_010022838.1), *Ophiophagus hannah* (ETE68963.1), *Phascolarctos cinereus* (XP_020851420.1), *Panthera pardus* (XP_019319420.1), *Chinchilla lanigera* (AMO64347.1), *Luciobrama macrocephalus* (ADV40882.1), *Anas platyrhynchos* (XP_005016300.1), *Meriones unguiculatus* (XP_021482503.1), *Fundulus heteroclitus* (JAR81631.1), *Channa argus* (AMM02541.1), *Rattus norvegicus* (NP_037231.1), *Ochetobius elongatus* (ADV40881.1), *Opsariichthys bidens* (ADV40880.1), *Sus scrofa* (ABD28176.1), *Vulpes vulpes* (ACN55092.1), *Dasyatis akajei* (BAU98233.1), *Columba livia* (XP_021153678.1), *Falco cherrug* (XP_005434907.1), *Scatophagus argus* (AOQ25859.1), *Schizothorax prenanti* (AGF80338.1), *Ovis aries* (NP_001119842.1), *Xiphophorus maculatus* (AHC02881.1), *Colius striatus* (XP_010207099.1), *Physeter*

catodon (XP_007111342.1), *Stylophora pistillata* (PFX22344.1), *Pongo abelii* (XP_002828309.1), *Eurypyga helias* (XP_010150784.1), *Strix aluco* (ATN96239.1), *Terrapene mexicana triunguis* (XP_024059247.1), *Culter alburnus* (ADV40879.1), *Takifugu rubripes* (AAO65551.1), *Xenopus tropicalis* (XP_004915370.1), *Nothobranchius furzeri* (SBP43904.1), *Piliocolobus tephrosceles* (XP_023074139.1), *Gorilla gorilla* (ACO90013.1), *Chrysemys picta bellii* (XP_005286507.1), *Callithrix jacchus* (ABW94915.1), *Megalobrama amblycephala* (ADV40876.1), *Xiphophorus multilineatus* (ADO60283.1), *Elopichthys bambusa* (ADV40877.1), *Xenocypris argentea* (ADV40878.1), *Danio rerio* (AAO24745.1).

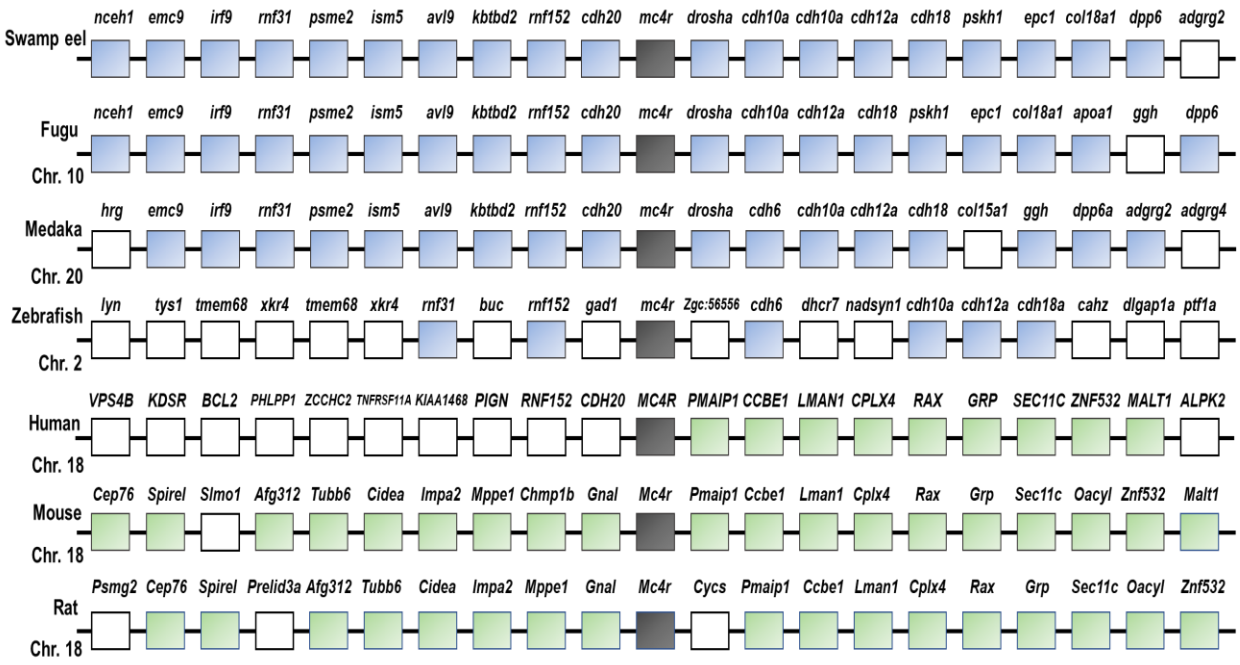

Fig. 4.4 Chromosomal synteny analyses of MC4Rs in representative species. The syntenic genes are displayed as boxes and linked by lines. *MC4R* genes are shown in grey boxes. The genes showing conserved synteny in fishes are indicated in blue boxes and those in mammals are shown in green boxes.

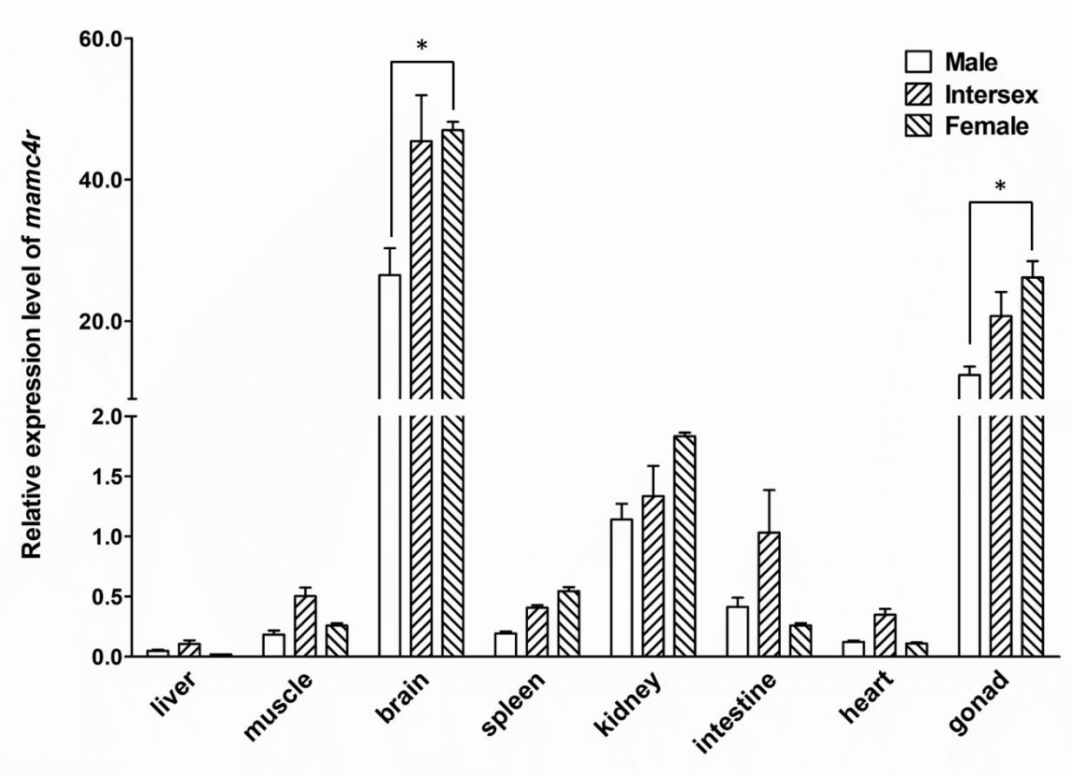

Fig. 4.5 Expression profiles of *mc4r* in various tissues of swamp eel. Tissue expression of ma*mc4r* mRNA was analyzed by qRT-PCR with a stable reference gene β-*actin*. The data were presented as means ± SEM (n = 6). Asterisk (*) indicates significant difference between male and female ($P < 0.05$).

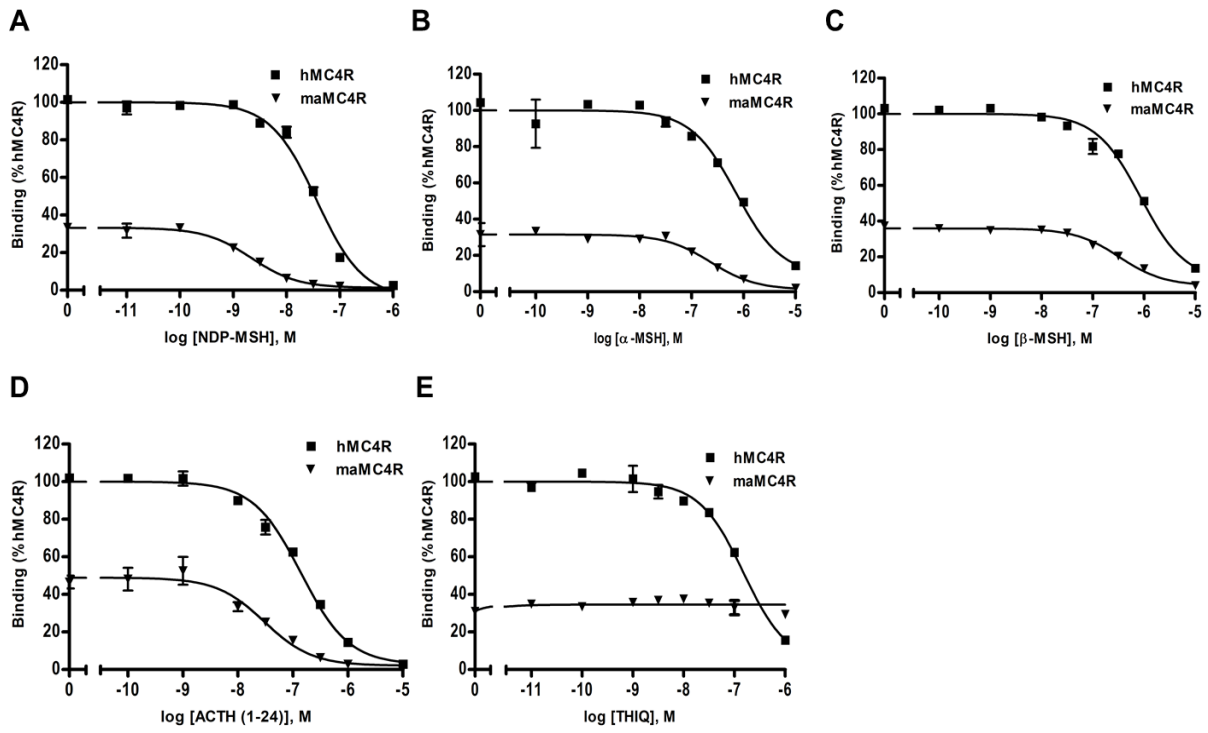

Fig. 4.6 Ligand binding properties of agonists to maMC4R. Different concentrations of unlabeled (A) NDP-MSH, (B) α-MSH, (C) β-MSH, (D) ACTH (1-24) or (E) THIQ was used to displace the binding of $^{[125]}$I-NDP-MSH. Data are expressed as % of hMC4R binding ± range from duplicate measurements within one experiment. The curves are representative of at least three independent experiments.

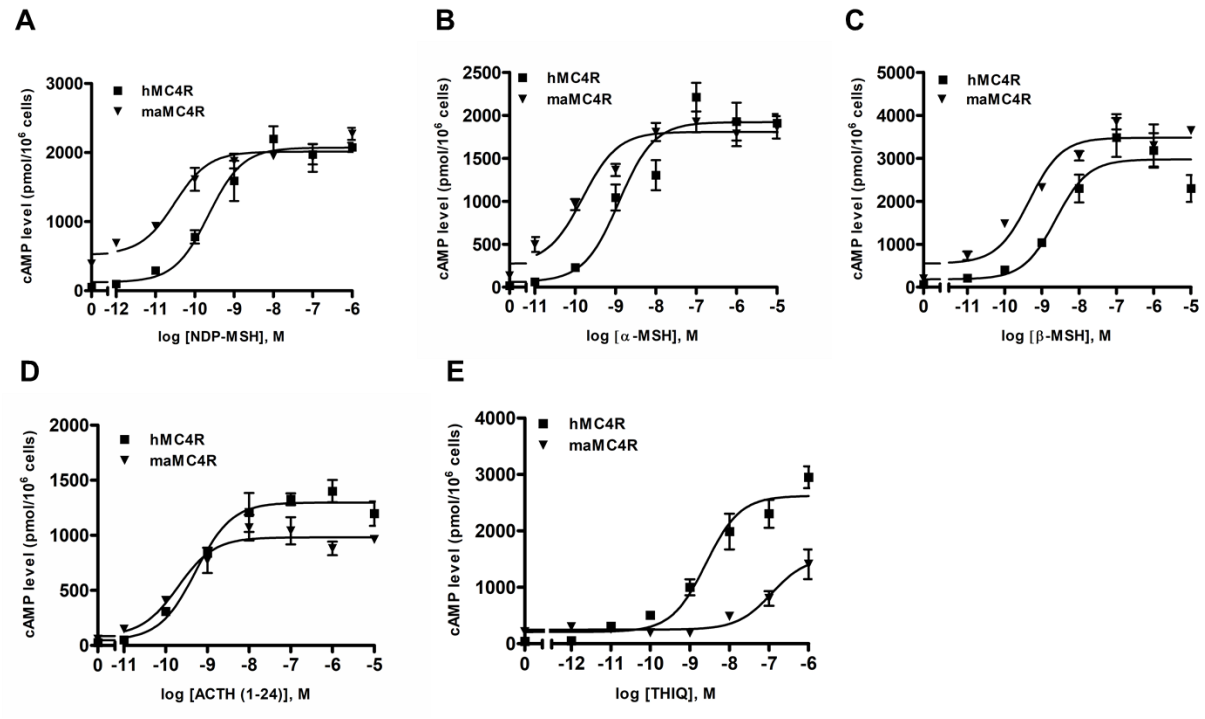

Fig. 4.7 Signaling properties of maMC4R. Different concentrations of (A) NDP-MSH, (B) α-MSH, (C) β-MSH, (D) ACTH (1-24) or (E) THIQ was used to stimulate HEK293T cell transfected with hMC4R and maMC4R. Intracellular cAMP levels were measured via RIA. Data are expressed as mean ± SEM from triplicate measurements within one experiment. The curves are representative of at least three independent experiments.

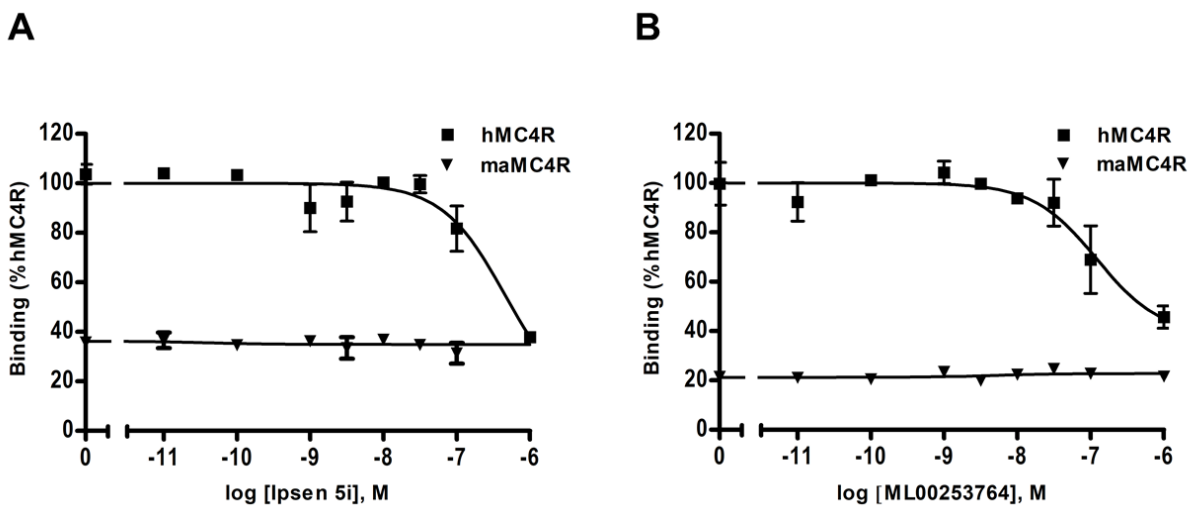

Fig. 4.8 Ligand binding properties of antagonists to maMC4R. Different concentrations of unlabeled (A) Ipsen 5i or (B) ML00253764 was used to displace the binding of ^{125}I-NDP-MSH. Data are expressed as % of hMC4R binding ± range from duplicates within one experiment. The curves are representative of at least three independent experiments.

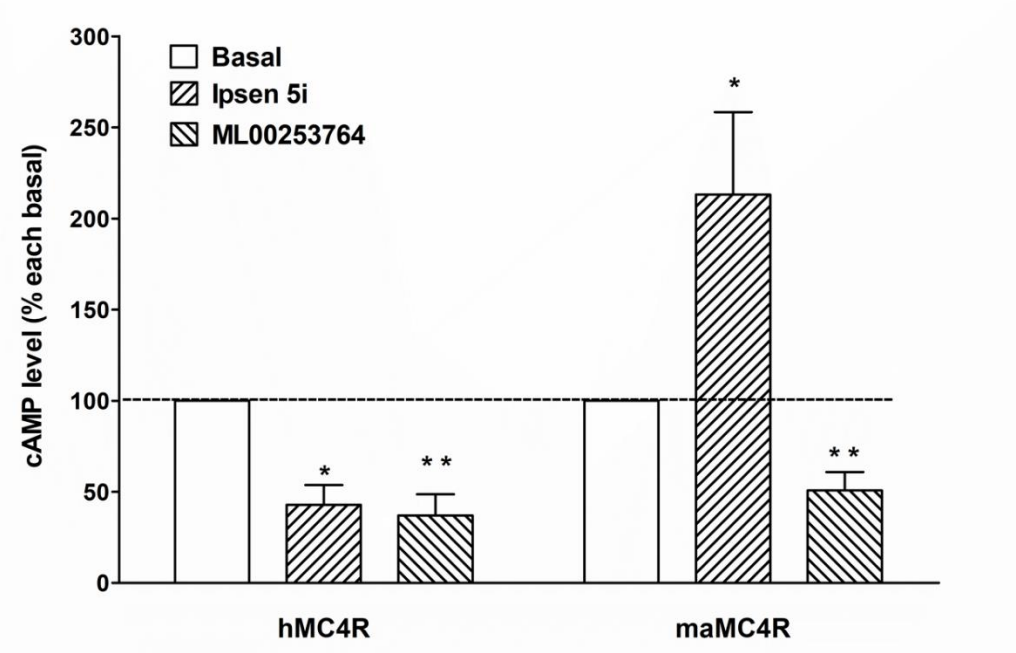

Fig. 4.9 Effects of the ligands on the basal activities of maMC4R. HEK293T cells transfected with hMC4R or maMC4R were treated without or with 1 μM Ipsen 5i or 1 μM ML00253764. The intracellular cAMP levels were measured via RIA. The data are mean ± SEM from three independent experiments. * indicates significant difference between vehicle and ligand treatment (*$P < 0.05$, **$P < 0.01$).

Conclusions

In conclusion, firstly, we have performed systematic functional study of DRYxxI motif and ICL2 of hMC4R. We have identified several residues important for receptor cell surface expression, receptor and ligand interaction, constitutive cAMP signaling, ligand-induced cAMP and ERK1/2 signaling pathways, as well as biased signaling between cAMP and ERK1/2 pathways. The investigation of structure-function relationship of hMC4R provides a better understanding towards the role of MC4R in obesity pathogenesis and will be valuable for structure-based drug design of molecules with the capacity to modulate MC4R activity as potential therapeutics.

Secondly, we functionally investigated MC3R in channel catfish. Five agonists, including α-MSH, β-MSH, NDP-MSH, ACTH (1-24), and D-Trp^8-γ-MSH, were used in the pharmacological studies. Our results showed that ipMC3R bound β-MSH with higher affinity and D-Trp^8-γ-MSH with lower affinity compared with hMC3R. All agonists could stimulate ipMC3R and increase intracellular cAMP production with sub-nanomolar potencies. The ERK1/2 activation could also be triggered by ipMC3R. The ipMC3R exhibited constitutive activities in both cAMP and ERK1/2 pathways, and AgRP served as an inverse agonist at ipMC3R, potently inhibiting the high basal cAMP level. Moreover, we showed that MRAP2 preferentially modulated ipMC3R in cAMP production rather than

ERK1/2 activation. Our study will assist further investigation of the physiological roles of the ipMC3R, especially in energy homeostasis, in channel catfish.

Finally, we cloned swamp eel *mc4r* and pharmacologically characterized maMC4R. The transcripts of ma*mc4r* were highly expressed in brain and gonads of swamp eel. Four agonists, α-MSH, β-MSH, NDP-MSH, and ACTH (1-24), could bind to maMC4R and induce intracellular cAMP production dose-dependently. Small molecule agonist THIQ allosterically bound to maMC4R and exerted its effect. Similar to other fish MC4Rs, maMC4R also exhibited significantly increased basal activity compared with that of hMC4R. The high basal activity of maMC4R could be decreased by inverse agonist ML00253764, suggesting that maMC4R was indeed constitutively active. The availability of maMC4R and its pharmacological characteristics will facilitate the investigation of its function in regulating diverse physiological processes in swamp eel.

References

Agosti, F., Gonzalez, S.C., Damonte, V.M., Tolosa, M.J., Di Siervi, N., Schioth, H.B., Davio, C., Perello, M. and Raingo, J., 2017. Melanocortin 4 receptor constitutive activity inhibits L-type voltage-gated calcium channels in neurons. Neuroscience 346, 102-112.

Angelova, K., Fanelli, F. and Puett, D., 2002. A model for constitutive lutropin receptor activation based on molecular simulation and engineered mutations in transmembrane helices 6 and 7. J Biol Chem 277, 32202-32213.

Asai, M., Ramachandrappa, S., Joachim, M., Shen, Y., Zhang, R., Nuthalapati, N., Ramanathan, V., Strochlic, D.E., Ferket, P., Linhart, K., Ho, C., Novoselova, T.V., Garg, S., Ridderstrale, M., Marcus, C., Hirschhorn, J.N., Keogh, J.M., O'Rahilly, S., Chan, L.F., Clark, A.J., Farooqi, I.S. and Majzoub, J.A., 2013. Loss of function of the melanocortin 2 receptor accessory protein 2 is associated with mammalian obesity. Science 341, 275-278.

Aspiras, A.C., Rohner, N., Martineau, B., Borowsky, R.L. and Tabin, C.J., 2015. Melanocortin 4 receptor mutations contribute to the adaptation of cavefish to nutrient-poor conditions. Proc Natl Acad Sci U S A 112, 9668-9673.

Bagnol, D., Lu, X.Y., Kaelin, C.B., Day, H.E., Ollmann, M., Gantz, I., Akil, H., Barsh, G.S. and Watson, S.J., 1999. Anatomy of an endogenous antagonist: relationship

between Agouti-related protein and proopiomelanocortin in brain. J Neurosci 19, RC26.

Ballesteros, J.A., Jensen, A.D., Liapakis, G., Rasmussen, S.G., Shi, L., Gether, U. and Javitch, J.A., 2001. Activation of the β_2-adrenergic receptor involves disruption of an ionic lock between the cytoplasmic ends of transmembrane segments 3 and 6. J Biol Chem 276, 29171-29177.

Ballesteros, J.A. and Weinstein, H., 1995. Integrated methods for the construction of three-dimensional models and computational probing of structure-function relations in G protein-coupled receptors. Methods Neurosci 25, 366-428.

Balthasar, N., Dalgaard, L.T., Lee, C.E., Yu, J., Funahashi, H., Williams, T., Ferreira, M., Tang, V., McGovern, R.A., Kenny, C.D., Christiansen, L.M., Edelstein, E., Choi, B., Boss, O., Aschkenasi, C., Zhang, C.Y., Mountjoy, K., Kishi, T., Elmquist, J.K. and Lowell, B.B., 2005. Divergence of melanocortin pathways in the control of food intake and energy expenditure. Cell 123, 493-505.

Begriche, K., Girardet, C., McDonald, P. and Butler, A.A., 2013. Melanocortin-3 receptors and metabolic homeostasis. Prog Mol Biol Transl Sci 114, 109-46.

Begriche, K., Marston, O.J., Rossi, J., Burke, L.K., McDonald, P., Heisler, L.K. and Butler, A.A., 2012. Melanocortin-3 receptors are involved in adaptation to restricted feeding. Genes Brain Behav 11, 291-302.

Bockaert, J. and Pin, J.P., 1999. Molecular tinkering of G protein-coupled receptors: an evolutionary success. EMBO J 18, 1723-1729.

Breit, A., Wolff, K., Kalwa, H., Jarry, H., Buch, T. and Gudermann, T., 2006. The natural inverse agonist agouti-related protein induces arrestin-mediated endocytosis of melanocortin-3 and -4 receptors. J Biol Chem 281, 37447-37456.

Büch, T.R., Heling, D., Damm, E., Gudermann, T. and Breit, A., 2009. Pertussis toxin-sensitive signaling of melanocortin-4 receptors in hypothalamic GT1-7 cells defines agouti-related protein as a biased agonist. J Biol Chem 284, 26411-26420.

Butler, A.A., Kesterson, R.A., Khong, K., Cullen, M.J., Pelleymounter, M.A., Dekoning, J., Baetscher, M. and Cone, R.D., 2000. A unique metabolic syndrome causes obesity in the melanocortin-3 receptor-deficient mouse. Endocrinology 141, 3518-3521.

Cerda-Reverter, J.M., Ringholm, A., Schioth, H.B. and Peter, R.E., 2003a. Molecular cloning, pharmacological characterization, and brain mapping of the melanocortin 4 receptor in the goldfish: involvement in the control of food intake. Endocrinology 144, 2336-2349.

Cerda-Reverter, J.M., Schioth, H.B. and Peter, R.E., 2003b. The central melanocortin system regulates food intake in goldfish. Regul Pept 115, 101-113.

Chai, B., Li, J.Y., Zhang, W., Ammori, J.B. and Mulholland, M.W., 2007. Melanocortin-3 receptor activates MAP kinase via PI3 kinase. Regul Pept 139, 115-121.

Chai, B., Li, J.Y., Zhang, W., Newman, E., Ammori, J. and Mulholland, M.W., 2006. Melanocortin-4 receptor-mediated inhibition of apoptosis in immortalized hypothalamic neurons via mitogen-activated protein kinase. Peptides 27, 2846-2857.

Chai, B., Li, J.Y., Zhang, W., Wang, H. and Mulholland, M.W., 2009. Melanocortin-4 receptor activation inhibits c-Jun N-terminal kinase activity and promotes insulin signaling. Peptides 30, 1098-1104.

Chai, B.X., Neubig, R.R., Millhauser, G.L., Thompson, D.A., Jackson, P.J., Barsh, G.S., Dickinson, C.J., Li, J.Y., Lai, Y.M. and Gantz, I., 2003. Inverse agonist activity of agouti and agouti-related protein. Peptides 24, 603-609.

Chaly, A.L., Srisai, D., Gardner, E.E. and Sebag, J.A., 2016. The Melanocortin Receptor Accessory Protein 2 promotes food intake through inhibition of the Prokineticin Receptor-1. Elife 5, e12397.

Chan, L.F., Webb, T.R., Chung, T.T., Meimaridou, E., Cooray, S.N., Guasti, L., Chapple, J.P., Egertova, M., Elphick, M.R., Cheetham, M.E., Metherell, L.A. and Clark, A.J., 2009. MRAP and MRAP2 are bidirectional regulators of the melanocortin receptor family. Proc Natl Acad Sci U S A 106, 6146-6151.

Chen, A.S., Marsh, D.J., Trumbauer, M.E., Frazier, E.G., Guan, X.M., Yu, H., Rosenblum, C.I., Vongs, A., Feng, Y., Cao, L., Metzger, J.M., Strack, A.M., Camacho, R.E., Mellin, T.N., Nunes, C.N., Min, W., Fisher, J., Gopal-Truter, S., MacIntyre, D.E., Chen, H.Y. and Van der Ploeg, L.H., 2000. Inactivation of the mouse melanocortin-3 receptor results in increased fat mass and reduced lean body mass. Nat Genet 26, 97-102.

Chen, C. and Okayama, H., 1987. High-efficiency transformation of mammalian cells by plasmid DNA. Mol Cell Biol 7, 2745-2752.

Chen, M., Berger, A., Kablan, A., Zhang, J., Gavrilova, O. and Weinstein, L.S., 2012. Gsα deficiency in the paraventricular nucleus of the hypothalamus partially contributes to obesity associated with Gsα mutations. Endocrinology 153, 4256-65.

Chen, M., Shrestha, Y.B., Podyma, B., Cui, Z., Naglieri, B., Sun, H., Ho, T., Wilson, E.A., Li, Y.Q., Gavrilova, O. and Weinstein, L.S., 2017. Gsα deficiency in the dorsomedial hypothalamus underlies obesity associated with Gsα mutations. J Clin Invest 127, 500-510.

Chen, M., Wang, J., Dickerson, K.E., Kelleher, J., Xie, T., Gupta, D., Lai, E.W., Pacak, K., Gavrilova, O. and Weinstein, L.S., 2009. Central nervous system imprinting of the G protein G_sα and its role in metabolic regulation. Cell Metab 9, 548-55.

Chen, W., Kelly, M.A., Opitz-Araya, X., Thomas, R.E., Low, M.J. and Cone, R.D., 1997. Exocrine gland dysfunction in MC5-R-deficient mice: evidence for coordinated regulation of exocrine gland function by melanocortin peptides. Cell 91, 789-798.

Cheng, H., Guo, Y., Yu, Q. and Zhou, R., 2003. The rice field eel as a model system for vertebrate sexual development. Cytogenet Genome Res 101, 274-277.

Cheung, C.C., Clifton, D.K. and Steiner, R.A., 1997. Proopiomelanocortin neurons are direct targets for leptin in the hypothalamus. Endocrinology 138, 4489-4492.

Chhajlani, V., 1996. Distribution of cDNA for melanocortin receptor subtypes in human tissues. Biochem Mol Biol Int 38, 73-80.

Chung, T.T.L.L., Chan, L.F., Metherell, L.A. and Clark, A.J.L., 2010. Phenotypic characteristics of familial glucocorticoid deficiency (FGD) type 1 and 2. Clin Endocrinol 72, 589-594.

Cone, R.D., 2005. Anatomy and regulation of the central melanocortin system. Nat Neurosci 8, 571-578.

Cone, R.D., 2006. Studies on the physiological functions of the melanocortin system. Endocr Rev 27, 736-749.

Cowley, M.A., 2003. Hypothalamic melanocortin neurons integrate signals of energy state. Eur J Pharmacol 480, 3-11.

Cowley, M.A., Smart, J.L., Rubinstein, M., Cerdan, M.G., Diano, S., Horvath, T.L., Cone, R.D. and Low, M.J., 2001. Leptin activates anorexigenic POMC neurons through a neural network in the arcuate nucleus. Nature 411, 480-484.

Damm, E., Buech, T.R., Gudermann, T. and Breit, A., 2012. Melanocortin-induced PKA activation inhibits AMPK activity via ERK-1/2 and LKB-1 in hypothalamic GT1-7 cells. Mol Endocrinol 26, 643-654.

Daniels, D., Patten, C.S., Roth, J.D., Yee, D.K. and Fluharty, S.J., 2003. Melanocortin receptor signaling through mitogen-activated protein kinase in vitro and in rat hypothalamus. Brain Res 986, 1-11.

Dascal, N., 2001. Ion-channel regulation by G proteins. Trends Endocrinol Metab 12, 391-8.

Demidowich, A.P., Jun, J.Y. and Yanovski, J.A., 2017. Polymorphisms and mutations in the melanocortin-3 receptor and their relation to human obesity. Biochim Biophys Acta 1863, 2468-2476.

DeWire, S.M., Ahn, S., Lefkowitz, R.J. and Shenoy, S.K., 2007. β-Arrestins and cell signaling. Annu Rev Physiol 69, 483-510.

do Carmo, J.M., da Silva, A.A., Rushing, J.S., Pace, B. and Hall, J.E., 2013. Differential control of metabolic and cardiovascular functions by melanocortin-4 receptors in proopiomelanocortin neurons. Am J Physiol Regul Integr Comp Physiol 305, R359-68.

Dores, R.M. and Lecaude, S., 2005. Trends in the evolution of the proopiomelanocortin gene. Gen Comp Endocrinol 142, 81-93.

Erlenbach, I., Kostenis, E., Schmidt, C., Serradeil-Le Gal, C., Raufaste, D., Dumont, M.E., Pausch, M.H. and Wess, J., 2001. Single amino acid substitutions and deletions that alter the G protein coupling properties of the V2 vasopressin receptor identified in yeast by receptor random mutagenesis. J Biol Chem 276, 29382-29392.

Fan, Z.C., Sartin, J.L. and Tao, Y.X., 2008. Molecular cloning and pharmacological characterization of porcine melanocortin-3 receptor. J Endocrinol 196, 139-148.

Fan, Z.C. and Tao, Y.X., 2009. Functional characterization and pharmacological rescue of melanocortin-4 receptor mutations identified from obese patients. J Cell Mol Med 13, 3268-3282.

Farooqi, I.S., Keogh, J.M., Yeo, G.S., Lank, E.J., Cheetham, T. and O'Rahilly, S., 2003. Clinical spectrum of obesity and mutations in the melanocortin 4 receptor gene. N Engl J Med 348, 1085-1095.

Fong, T.M., Mao, C., MacNeil, T., Kalyani, R., Smith, T., Weinberg, D., Tota, M.R. and Van der Ploeg, L.H., 1997. ART (protein product of agouti-related transcript) as an antagonist of MC-3 and MC-4 receptors. Biochem Biophys Res Commun 237, 629-631.

Gantz, I., Konda, Y., Tashiro, T., Shimoto, Y., Miwa, H., Munzert, G., Watson, S.J., DelValle, J. and Yamada, T., 1993a. Molecular cloning of a novel melanocortin receptor. J Biol Chem 268, 8246-8250.

Gantz, I., Miwa, H., Konda, Y., Shimoto, Y., Tashiro, T., Watson, S.J., DelValle, J. and Yamada, T., 1993b. Molecular cloning, expression, and gene localization of a fourth melanocortin receptor. J Biol Chem 268, 15174-15179.

Getting, S.J., Christian, H.C., Lam, C.W., Gavins, F.N., Flower, R.J., Schioth, H.B. and Perretti, M., 2003. Redundancy of a functional melanocortin 1 receptor in the anti-inflammatory actions of melanocortin peptides: studies in the recessive yellow (e/e) mouse suggest an important role for melanocortin 3 receptor. J Immunol 170, 3323-3330.

Getting, S.J., Riffo-Vasquez, Y., Pitchford, S., Kaneva, M., Grieco, P., Page, C.P., Perretti, M. and Spina, D., 2008. A role for MC3R in modulating lung inflammation. Pulm Pharmacol Ther 21, 866-873.

Ghamari-Langroudi, M., Cakir, I., Lippert, R.N., Sweeney, P., Litt, M.J., Ellacott, K.L.J. and Cone, R.D., 2018. Regulation of energy rheostasis by the melanocortin-3 receptor. Sci Adv 4, eaat0866.

Ghamari-Langroudi, M., Digby, G.J., Sebag, J.A., Millhauser, G.L., Palomino, R., Matthews, R., Gillyard, T., Panaro, B.L., Tough, I.R., Cox, H.M., Denton, J.S. and Cone, R.D., 2015. G-protein-independent coupling of MC4R to Kir7.1 in hypothalamic neurons. Nature 520, 94-98.

Girardet, C. and Butler, A.A., 2014. Neural melanocortin receptors in obesity and related metabolic disorders. Biochim Biophys Acta 1842, 482-494.

Greasley, P.J., Fanelli, F., Rossier, O., Abuin, L. and Cotecchia, S., 2002. Mutagenesis and modelling of the a_{1b}-adrenergic receptor highlight the role of the helix 3/helix 6 interface in receptor activation. Mol Pharmacol 61, 1025-1032.

Grieco, P., Balse, P.M., Weinberg, D., MacNeil, T. and Hruby, V.J., 2000. D-Amino acid scan of γ-melanocyte-stimulating hormone: importance of Trp^8 on human MC3 receptor selectivity. J Med Chem 43, 4998-5002.

Guan, R.Z., Zhou, L.H., Cui, G.H. and Feng, X.H., 1996. Studies on the artificial propagation of Monopterus albus (Zuiew). Aquac Res 27, 587-596.

Guh, D.P., Zhang, W., Bansback, N., Amarsi, Z., Birmingham, C.L. and Anis, A.H., 2009. The incidence of co-morbidities related to obesity and overweight: a systematic review and meta-analysis. BMC Public Health 9, 88.

Hagan, M.M., Rushing, P.A., Pritchard, L.M., Schwartz, M.W., Strack, A.M., Van Der Ploeg, L.H., Woods, S.C. and Seeley, R.J., 2000. Long-term orexigenic effects of AgRP-(83---132) involve mechanisms other than melanocortin receptor blockade. Am J Physiol Regul Integr Comp Physiol 279, R47-R52.

Haitina, T., Klovins, J., Andersson, J., Fredriksson, R., Lagerstrom, M.C., Larhammar, D., Larson, E.T. and Schioth, H.B., 2004. Cloning, tissue distribution, pharmacology and three-dimensional modelling of melanocortin receptors 4 and 5 in rainbow trout suggest close evolutionary relationship of these subtypes. Biochem J 380, 475-486.

Haskell-Luevano, C. and Monck, E.K., 2001. Agouti-related protein functions as an inverse agonist at a constitutively active brain melanocortin-4 receptor. Regul Pept 99, 1-7.

He, S. and Tao, Y.X., 2014. Defect in MAPK signaling as a cause for monogenic obesity caused by inactivating mutations in the melanocortin-4 receptor gene. Int J Biol Sci 10, 1128-1137.

Hill, J.W., Williams, K.W., Ye, C., Luo, J., Balthasar, N., Coppari, R., Cowley, M.A., Cantley, L.C., Lowell, B.B. and Elmquist, J.K., 2008. Acute effects of leptin require PI3K signaling in hypothalamic proopiomelanocortin neurons in mice. J Clin Invest 118, 1796-805.

Hinney, A., Bettecken, T., Tarnow, P., Brumm, H., Reichwald, K., Lichtner, P., Scherag, A., Nguyen, T.T., Schlumberger, P., Rief, W., Vollmert, C., Illig, T., Wichmann, H.E., Schafer, H., Platzer, M., Biebermann, H., Meitinger, T. and Hebebrand, J., 2006. Prevalence, spectrum, and functional characterization of melanocortin-4 receptor gene mutations in a representative population-based sample and obese adults from Germany. J Clin Endocrinol Metab 91, 1761-1769.

Hinney, A., Hohmann, S., Geller, F., Vogel, C., Hess, C., Wermter, A.K., Brokamp, B., Goldschmidt, H., Siegfried, W., Remschmidt, H., Schafer, H., Gudermann, T. and Hebebrand, J., 2003. Melanocortin-4 receptor gene: case-control study and transmission disequilibrium test confirm that functionally relevant mutations are compatible with a major gene effect for extreme obesity. J Clin Endocrinol Metab 88, 4258-4267.

Hinney, A., Schmidt, A., Nottebom, K., Heibult, O., Becker, I., Ziegler, A., Gerber, G., Sina, M., Gorg, T., Mayer, H., Siegfried, W., Fichter, M., Remschmidt, H. and Hebebrand, J., 1999. Several mutations in the melanocortin-4 receptor gene including a

nonsense and a frameshift mutation associated with dominantly inherited obesity in humans. J Clin Endocrinol Metab 84, 1483-1486.

Hinney, A., Volckmar, A.L. and Knoll, N., 2013. Melanocortin-4 receptor in energy homeostasis and obesity pathogenesis. Prog Mol Biol Transl Sci 114, 147-191.

Hirata, F., Strittmatter, W.J. and Axelrod, J., 1979. beta-Adrenergic receptor agonists increase phospholipid methylation, membrane fluidity, and beta-adrenergic receptor-adenylate cyclase coupling. Proc Natl Acad Sci U S A 76, 368-372.

Huang, H. and Tao, Y.X., 2012. Pleiotropic functions of the transmembrane domain 6 of human melanocortin-4 receptor. J Mol Endocrinol 49, 237-248.

Huang, H. and Tao, Y.X., 2014. Functions of the DRY motif and intracellular loop 2 of human melanocortin 3 receptor. J Mol Endocrinol 53, 319-330.

Huszar, D., Lynch, C.A., Fairchild-Huntress, V., Dunmore, J.H., Fang, Q., Berkemeier, L.R., Gu, W., Kesterson, R.A., Boston, B.A., Cone, R.D., Smith, F.J., Campfield, L.A., Burn, P. and Lee, F., 1997. Targeted disruption of the melanocortin-4 receptor results in obesity in mice. Cell 88, 131-141.

Jegou, S., Boutelet, I. and Vaudry, H., 2000. Melanocortin-3 receptor mRNA expression in pro-opiomelanocortin neurones of the rat arcuate nucleus. J Neuroendocrinol 12, 501-505.

Jiang, D.N., Li, J.T., Tao, Y.X., Chen, H.P., Deng, S.P., Zhu, C.H. and Li, G.L., 2017. Effects of melanocortin-4 receptor agonists and antagonists on expression of genes related to reproduction in spotted scat, *Scatophagus argus*. J Comp Physiol B 187, 603-612.

Johnson, G.L. and Lapadat, R., 2002. Mitogen-activated protein kinase pathways mediated by ERK, JNK, and p38 protein kinases. Science 298, 1911-1912.

Karsi, A., Waldbieser, G.C., Small, B.C., Liu, Z. and Wolters, W.R., 2004. Molecular cloning of proopiomelanocortin cDNA and multi-tissue mRNA expression in channel catfish. Gen Comp Endocrinol 137, 312-321.

Kay, E.I., Botha, R., Montgomery, J.M. and Mountjoy, K.G., 2013. hMRAPa increases αMSH-induced hMC1R and hMC3R functional coupling and hMC4R constitutive activity. J Mol Endocrinol 50, 203-215.

Khong, K., Kurtz, S.E., Sykes, R.L. and Cone, R.D., 2001. Expression of functional melanocortin-4 receptor in the hypothalamic GT1-1 cell line. Neuroendocrinology 74, 193-201.

Klovins, J., Haitina, T., Fridmanis, D., Kilianova, Z., Kapa, I., Fredriksson, R., Gallo-Payet, N. and Schioth, H.B., 2004a. The melanocortin system in Fugu: determination of POMC/AGRP/MCR gene repertoire and synteny, as well as pharmacology and anatomical distribution of the MCRs. Mol Biol Evol 21, 563-579.

Klovins, J., Haitina, T., Ringholm, A., Lowgren, M., Fridmanis, D., Slaidina, M., Stier, S. and Schioth, H.B., 2004b. Cloning of two melanocortin (MC) receptors in spiny dogfish: MC3 receptor in cartilaginous fish shows high affinity to ACTH-derived peptides while it has lower preference to γ-MSH. Eur J Biochem 271, 4320-4331.

Kobayashi, Y., Tsuchiya, K., Yamanome, T., Schioth, H.B., Kawauchi, H. and Takahashi, A., 2008. Food deprivation increases the expression of melanocortin-4 receptor in the liver of barfin flounder, *Verasper moseri*. Gen Comp Endocrinol 155, 280-287.

Konda, Y., Gantz, I., DelValle, J., Shimoto, Y., Miwa, H. and Yamada, T., 1994. Interaction of dual intracellular signaling pathways activated by the melanocortin-3 receptor. J Biol Chem 269, 13162-13166.

Konner, A.C., Janoschek, R., Plum, L., Jordan, S.D., Rother, E., Ma, X., Xu, C., Enriori, P., Hampel, B., Barsh, G.S., Kahn, C.R., Cowley, M.A., Ashcroft, F.M. and Bruning, J.C., 2007. Insulin action in AgRP-expressing neurons is required for suppression of hepatic glucose production. Cell Metab 5, 438-449.

Krashes, M.J., Lowell, B.B. and Garfield, A.S., 2016. Melanocortin-4 receptor-regulated energy homeostasis. Nat Neurosci 19, 206-19.

Kumar, S., Stecher, G., Li, M., Knyaz, C. and Tamura, K., 2018. MEGA X: Molecular Evolutionary Genetics Analysis across Computing Platforms. Mol Biol Evol 35, 1547-1549.

Kumar, S., Stecher, G. and Tamura, K., 2016. MEGA7: molecular evolutionary genetics analysis version 7.0 for bigger datasets. Mol Biol Evol 33, 1870-1874.

Lampert, K.P., Schmidt, C., Fischer, P., Volff, J.N., Hoffmann, C., Muck, J., Lohse, M.J., Ryan, M.J. and Schartl, M., 2010. Determination of onset of sexual maturation and mating behavior by melanocortin receptor 4 polymorphisms. Curr Biol 20, 1729-1734.

Li, J.T., Yang, Z., Chen, H.P., Zhu, C.H., Deng, S.P., Li, G.L. and Tao, Y.X., 2016a. Molecular cloning, tissue distribution, and pharmacological characterization of melanocortin-4 receptor in spotted scat, *Scatophagus argus*. Gen Comp Endocrinol 230-231, 143 -152.

Li, L., Yang, Z., Zhang, Y.P., He, S., Liang, X.F. and Tao, Y.X., 2017. Molecular cloning, tissue distribution, and pharmacological characterization of melanocortin-4 receptor in grass carp (*Ctenopharyngodon idella*). Domest Anim Endocrinol 59, 140-151.

Li, Y.Q., Shrestha, Y., Pandey, M., Chen, M., Kablan, A., Gavrilova, O., Offermanns, S. and Weinstein, L.S., 2016b. $G_{q/11}\alpha$ and $G_s\alpha$ mediate distinct physiological responses to central melanocortins. J Clin Invest 126, 40-9.

Liem, K.F., 1963. Sex reversal as a natural process in the synbranchiform fish Monopterus albus. Copeia, 303-312.

Liu, C.K., 1944. Rudimentary hermaphroditism in the symbranchoid eel, *Monopterus javanensis*. Sinensia 15, 1-8.

Liu, Z., Liu, S., Yao, J., Bao, L., Zhang, J., Li, Y., Jiang, C., Sun, L., Wang, R. and Zhang, Y., 2016. The channel catfish genome sequence provides insights into the evolution of scale formation in teleosts. Nat Commun 7, 11757.

Livak, K.J. and Schmittgen, T.D., 2001. Analysis of relative gene expression data using real-time quantitative PCR and the $2^{-\Delta\Delta CT}$ method. Methods 25, 402-408.

Lo Nostro, F., Grier, H., Andreone, L. and Guerrero, G.A., 2003. Involvement of the gonadal germinal epithelium during sex reversal and seasonal testicular cycling in the protogynous swamp eel, *Synbranchus marmoratus* Bloch 1795 (Teleostei, Synbranchidae). Journal of Morphology 257, 107-126.

Logan, D.W., Bryson-Richardson, R.J., Pagan, K.E., Taylor, M.S., Currie, P.D. and Jackson, I.J., 2003. The structure and evolution of the melanocortin and MCH receptors in fish and mammals. Genomics 81, 184-91.

Lu, Z.L., Gallagher, R., Sellar, R., Coetsee, M. and Millar, R.P., 2005. Mutations remote from the human gonadotropin-releasing hormone (GnRH) receptor-binding sites specifically increase binding affinity for GnRH II but not GnRH I: evidence for ligand-selective, receptor-active conformations. J Biol Chem 280, 29796-29803.

Magenis, R.E., Smith, L., Nadeau, J.H., Johnson, K.R., Mountjoy, K.G. and Cone, R.D., 1994. Mapping of the ACTH, MSH, and neural (MC3 and MC4) melanocortin receptors in the mouse and human. Mamm Genome 5, 503-508.

Marsh, D.J., Hollopeter, G., Huszar, D., Laufer, R., Yagaloff, K.A., Fisher, S.L., Burn, P. and Palmiter, R.D., 1999. Response of melanocortin-4 receptor-deficient mice to anorectic and orexigenic peptides. Nat Genet 21, 119-122.

Metherell, L.A., Chapple, J.P., Cooray, S., David, A., Becker, C., Ruschendorf, F., Naville, D., Begeot, M., Khoo, B., Nurnberg, P., Huebner, A., Cheetham, M.E. and Clark, A.J., 2005. Mutations in MRAP, encoding a new interacting partner of the ACTH receptor, cause familial glucocorticoid deficiency type 2. Nat Genet 37, 166-70.

Minokoshi, Y., Alquier, T., Furukawa, N., Kim, Y.B., Lee, A., Xue, B., Mu, J., Foufelle, F., Ferre, P., Birnbaum, M.J., Stuck, B.J. and Kahn, B.B., 2004. AMP-kinase regulates food intake by responding to hormonal and nutrient signals in the hypothalamus. Nature 428, 569-74.

Miura, S.I., Zhang, J. and Karnik, S.S., 2000. Angiotensin II type 1 receptor-function affected by mutations in cytoplasmic loop CD. FEBS Lett 470, 331-335.

Mo, X.L. and Tao, Y.X., 2013. Activation of MAPK by inverse agonists in six naturally occurring constitutively active mutant human melanocortin-4 receptors. Biochim Biophys Acta 1832, 1939-1948.

Mo, X.L., Yang, R. and Tao, Y.X., 2012. Functions of transmembrane domain 3 of human melanocortin-4 receptor. J Mol Endocrinol 49, 221-235.

Montero-Melendez, T., Gobbetti, T., Cooray, S.N., Jonassen, T.E. and Perretti, M., 2015. Biased agonism as a novel strategy to harness the proresolving properties of melanocortin receptors without eliciting melanogenic effects. J Immunol 194, 3381-3388.

Mountjoy, K.G., Jenny Wu, C.S., Dumont, L.M. and Wild, J.M., 2003. Melanocortin-4 receptor messenger ribonucleic acid expression in rat cardiorespiratory, musculoskeletal, and integumentary systems. Endocrinology 144, 5488-5496.

Mountjoy, K.G., Kong, P.L., Taylor, J.A., Willard, D.H. and Wilkison, W.O., 2001. Melanocortin receptor-mediated mobilization of intracellular free calcium in HEK293 cells. Physiol Genomics 5, 11-19.

Mountjoy, K.G., Mortrud, M.T., Low, M.J., Simerly, R.B. and Cone, R.D., 1994. Localization of the melanocortin-4 receptor (MC4-R) in neuroendocrine and autonomic control circuits in the brain. Mol Endocrinol 8, 1298-1308.

Mountjoy, K.G., Robbins, L.S., Mortrud, M.T. and Cone, R.D., 1992. The cloning of a family of genes that encode the melanocortin receptors. Science 257, 1248-1251.

Newman, E.A., Chai, B.X., Zhang, W., Li, J.Y., Ammori, J.B. and Mulholland, M.W., 2006. Activation of the melanocortin-4 receptor mobilizes intracellular free calcium in immortalized hypothalamic neurons. J Surg Res 132, 201-207.

Ni, X.P., Butler, A.A., Cone, R.D. and Humphreys, M.H., 2006. Central receptors mediating the cardiovascular actions of melanocyte stimulating hormones. J Hypertens 24, 2239-2246.

Nickolls, S.A., Fleck, B., Hoare, S.R. and Maki, R.A., 2005. Functional selectivity of melanocortin 4 receptor peptide and nonpeptide agonists: evidence for ligand-specific conformational states. J Pharmacol Exp Ther 313, 1281-1288.

Nijenhuis, W.A., Oosterom, J. and Adan, R.A., 2001. AgRP(83-132) acts as an inverse agonist on the human melanocortin-4 receptor. Mol Endocrinol 15, 164-171.

Nishi, S., Nakabayashi, K., Kobilka, B. and Hsueh, A.J., 2002. The ectodomain of the luteinizing hormone receptor interacts with exoloop 2 to constrain the transmembrane region. Studies using chimeric human and fly receptors. J Biol Chem 277, 3958-3964.

Novoselova, T.V., Larder, R., Rimmington, D., Lelliott, C., Wynn, E.H., Gorrigan, R.J., Tate, P.H., Guasti, L., O'Rahilly, S. and Clark, A.J.L., 2016. Loss of Mrap2 is associated with Sim1 deficiency and increased circulating cholesterol. J Endocrinol 230, 13-26.

Nyan, D.C., Anbazhagan, R., Hughes-Darden, C.A. and Wachira, S.J., 2008. Endosomal colocalization of melanocortin-3 receptor and β-arrestins in CAD cells with altered modification of AKT/PKB. Neuropeptides 42, 355-366.

O'rahilly, S., Farooqi, I.S., Yeo, G.S.H. and Challis, B.G., 2003. Minireview: Human Obesity—Lessons from Monogenic Disorders. Endocrinology 144, 3757-3764.

Ollmann, M.M., Wilson, B.D., Yang, Y.K., Kerns, J.A., Chen, Y., Gantz, I. and Barsh, G.S., 1997. Antagonism of central melanocortin receptors in vitro and in vivo by agouti-related protein. Science 278, 135-138.

Paavola, K.J., Stephenson, J.R., Ritter, S.L., Alter, S.P. and Hall, R.A., 2011. The N terminus of the adhesion G protein-coupled receptor GPR56 controls receptor signaling activity. J Biol Chem 286, 28914-28921.

Palczewski, K., Kumasaka, T., Hori, T., Behnke, C.A., Motoshima, H., Fox, B.A., Le Trong, I., Teller, D.C., Okada, T., Stenkamp, R.E., Yamamoto, M. and Miyano, M., 2000. Crystal structure of rhodopsin: A G protein-coupled receptor. Science 289, 739-745.

Park, J., Sharma, N. and Cutting, G.R., 2014. Melanocortin 3 receptor has a 5' exon that directs translation of apically localized protein from the second in-frame ATG. Mol Endocrinol 28, 1547-1557.

Parton, L.E., Ye, C.P., Coppari, R., Enriori, P.J., Choi, B., Zhang, C.Y., Xu, C., Vianna, C.R., Balthasar, N., Lee, C.E., Elmquist, J.K., Cowley, M.A. and Lowell, B.B., 2007. Glucose sensing by POMC neurons regulates glucose homeostasis and is impaired in obesity. Nature 449, 228-232.

Patel, H.B., Montero-Melendez, T., Greco, K.V. and Perretti, M., 2011. Melanocortin receptors as novel effectors of macrophage responses in inflammation. Front Immunol 2, 41.

Peterson, B.C., Waldbieser, G.C., Riley Jr, L.G., Upton, K.R., Kobayashi, Y. and Small, B.C., 2012. Pre-and postprandial changes in orexigenic and anorexigenic factors in channel catfish (Ictalurus punctatus). Gen Comp Endocrinol 176, 231-239.

Poitout, L., Brault, V., Sackur, C., Bernetiere, S., Camara, J., Plas, P. and Roubert, P., 2007. Identification of a novel series of benzimidazoles as potent and selective

antagonists of the human melanocortin-4 receptor. Bioorg Med Chem Lett 17, 4464-4470.

Pritchard, L.E., Turnbull, A.V. and White, A., 2002. Pro-opiomelanocortin processing in the hypothalamus: impact on melanocortin signalling and obesity. J Endocrinol 172, 411-21.

Raman, D., Osawa, S. and Weiss, E.R., 1999. Binding of arrestin to cytoplasmic loop mutants of bovine rhodopsin. Biochemistry 38, 5117-5123.

Rasmussen, S.G., Choi, H.J., Fung, J.J., Pardon, E., Casarosa, P., Chae, P.S., Devree, B.T., Rosenbaum, D.M., Thian, F.S., Kobilka, T.S., Schnapp, A., Konetzki, I., Sunahara, R.K., Gellman, S.H., Pautsch, A., Steyaert, J., Weis, W.I. and Kobilka, B.K., 2011. Structure of a nanobody-stabilized active state of the β_2 adrenoceptor. Nature 469, 175-180.

Ravaglia, M.A., Nostro, F.L.L., Maggese, M.C., Guerrero, G.A. and Somoza, G.M., 1997. Characterization of molecular variants of GnRH, induction of spermiation and sex reversal using salmon GnRH-A and domperidone in the protogynous diandric fish, *Synbranchus marmoratus* Bloch, (Teleostei, Synbranchidae). Fish Physiol Biochem 16, 425.

Renquist, B.J., Zhang, C., Williams, S.Y. and Cone, R.D., 2013. Development of an assay for high-throughput energy expenditure monitoring in the zebrafish. Zebrafish 10, 343-352.

Ringholm, A., Klovins, J., Fredriksson, R., Poliakova, N., Larson, E.T., Kukkonen, J.P., Larhammar, D. and Schioth, H.B., 2003. Presence of melanocortin (MC4) receptor

in spiny dogfish suggests an ancient vertebrate origin of central melanocortin system. Eur J Biochem 270, 213-221.

Roa, J. and Herbison, A.E., 2012. Direct regulation of GnRH neuron excitability by arcuate nucleus POMC and NPY neuron neuropeptides in female mice. Endocrinology 153, 5587-5599.

Rodrigues, A.R., Almeida, H. and Gouveia, A.M., 2012. Melanocortin 5 receptor signaling and internalization: role of MAPK/ERK pathway and β-arrestins 1/2. Mol Cell Endocrinol 361, 69-79.

Roselli-Rehfuss, L., Mountjoy, K.G., Robbins, L.S., Mortrud, M.T., Low, M.J., Tatro, J.B., Entwistle, M.L., Simerly, R.B. and Cone, R.D., 1993. Identification of a receptor for g melanotropin and other proopiomelanocortin peptides in the hypothalamus and limbic system. Proc Natl Acad Sci U S A 90, 8856-8860.

Rosenbaum, D.M., Rasmussen, S.G. and Kobilka, B.K., 2009. The structure and function of G-protein-coupled receptors. Nature 459, 356-363.

Rossi, J., Balthasar, N., Olson, D., Scott, M., Berglund, E., Lee, C.E., Choi, M.J., Lauzon, D., Lowell, B.B. and Elmquist, J.K., 2011. Melanocortin-4 receptors expressed by cholinergic neurons regulate energy balance and glucose homeostasis. Cell Metab 13, 195-204.

Rouault, A.A.J., Srinivasan, D.K., Yin, T.C., Lee, A.A. and Sebag, J.A., 2017. Melanocortin receptor accessory proteins (MRAPs): Functions in the melanocortin system and beyond. Biochim Biophys Acta 1863, 2462-2467.

Rovati, G.E., Capra, V. and Neubig, R.R., 2007. The highly conserved DRY motif of class A G protein-coupled receptors: beyond the ground state. Mol Pharmacol 71, 959-964.

Saitou, N. and Nei, M., 1987. The neighbor-joining method: a new method for reconstructing phylogenetic trees. Mol Biol Evol 4, 406-425.

Sanchez, E., Rubio, V.C., Thompson, D., Metz, J., Flik, G., Millhauser, G.L. and Cerda-Reverter, J.M., 2009. Phosphodiesterase inhibitor-dependent inverse agonism of agouti-related protein on melanocortin 4 receptor in sea bass (*Dicentrarchus labrax*). Am J Physiol Regul Integr Comp Physiol 296, R1293-R1306.

Sawyer, T.K., Sanfilippo, P.J., Hruby, V.J., Engel, M.H., Heward, C.B., Burnett, J.B. and Hadley, M.E., 1980. 4-Norleucine, 7-D-phenylalanine-a-melanocyte-stimulating hormone: a highly potent a-melanotropin with ultralong biological activity. Proc Natl Acad Sci U S A 77, 5754-5758.

Scheerer, P., Park, J.H., Hildebrand, P.W., Kim, Y.J., Krauss, N., Choe, H.W., Hofmann, K.P. and Ernst, O.P., 2008. Crystal structure of opsin in its G-protein-interacting conformation. Nature 455, 497-502.

Schjolden, J., Schioth, H.B., Larhammar, D., Winberg, S. and Larson, E.T., 2009. Melanocortin peptides affect the motivation to feed in rainbow trout (*Oncorhynchus mykiss*). Gen Comp Endocrinol 160, 134-138.

Schonnop, L., Kleinau, G., Herrfurth, N., Volckmar, A.L., Cetindag, C., Müller, A., Peters, T., Herpertz, S., Antel, J. and Hebebrand, J., 2016. Decreased melanocortin-4 receptor function conferred by an infrequent variant at the human melanocortin receptor accessory protein 2 gene. Obesity 24, 1976-1982.

Schroeter, J.C., Fenn, C.M. and Small, B.C., 2015. Elucidating the roles of gut neuropeptides on channel catfish feed intake, glycemia, and hypothalamic NPY and POMC expression. Comp Biochem Physiol A Mol Integr Physiol 188, 168-174.

Sebag, J.A., Zhang, C., Hinkle, P.M., Bradshaw, A.M. and Cone, R.D., 2013. Developmental control of the melanocortin-4 receptor by MRAP2 proteins in zebrafish. Science 341, 278-281.

Sebhat, I.K., Martin, W.J., Ye, Z., Barakat, K., Mosley, R.T., Johnston, D.B., Bakshi, R., Palucki, B., Weinberg, D.H., MacNeil, T., Kalyani, R.N., Tang, R., Stearns, R.A., Miller, R.R., Tamvakopoulos, C., Strack, A.M., McGowan, E., Cashen, D.E., Drisko, J.E., Hom, G.J., Howard, A.D., MacIntyre, D.E., van der Ploeg, L.H., Patchett, A.A. and Nargund, R.P., 2002. Design and pharmacology of N-[(3R)-1,2,3,4-tetrahydroisoquinolinium- 3-ylcarbonyl]-(1R)-1-(4-chlorobenzyl)- 2-[4-cyclohexyl-4-(1H-1,2,4-triazol- 1-ylmethyl)piperidin-1-yl]-2-oxoethylamine (1), a potent, selective, melanocortin subtype-4 receptor agonist. J Med Chem 45, 4589-4593.

Selz, Y., Braasch, I., Hoffmann, C., Schmidt, C., Schultheis, C., Schartl, M. and Volff, J.N., 2007. Evolution of melanocortin receptors in teleost fish: the melanocortin type 1 receptor. Gene 401, 114-122.

Sheng, Y., Chen, B., Zhang, L., Luo, M., Cheng, H. and Zhou, R., 2014. Identification of Dmrt genes and their up-regulation during gonad transformation in the swamp eel (*Monopterus albus*). Mol Biol Rep 41, 1237-1245.

Shinyama, H., Masuzaki, H., Fang, H. and Flier, J.S., 2003. Regulation of melanocortin-4 receptor signaling: agonist-mediated desensitization and internalization. Endocrinology 144, 1301-1314.

Siljee, J.E., Unmehopa, U.A., Kalsbeek, A., Swaab, D.F., Fliers, E. and Alkemade, A., 2013. Melanocortin 4 receptor distribution in the human hypothalamus. Eur J Endocrinol 168, 361-369.

Smith, A.I. and Funder, J.W., 1988. Proopiomelanocortin processing in the pituitary, central nervous system, and peripheral tissues. Endocr Rev 9, 159-179.

Smith, C.C., Harris, R.M., Lampert, K.P., Schartl, M., Hofmann, H.A. and Ryan, M.J., 2015. Copy number variation in the melanocortin 4 receptor gene and alternative reproductive tactics the swordtail *Xiphophorus multilineatus*. Environmental Biology of Fishes 98, 23-33.

Song, Y. and Cone, R.D., 2007. Creation of a genetic model of obesity in a teleost. FASEB J 21, 2042-2049.

Srinivasan, S., Lubrano-Berthelier, C., Govaerts, C., Picard, F., Santiago, P., Conklin, B.R. and Vaisse, C., 2004. Constitutive activity of the melanocortin-4 receptor is maintained by its N-terminal domain and plays a role in energy homeostasis in humans. J Clin Invest 114, 1158-1164.

Srisai, D., Yin, T.C., Lee, A.A., Rouault, A.A.J., Pearson, N.A., Grobe, J.L. and Sebag, J.A., 2017. MRAP2 regulates ghrelin receptor signaling and hunger sensing. Nat Commun 8, 713.

Ste Marie, L., Miura, G.I., Marsh, D.J., Yagaloff, K. and Palmiter, R.D., 2000. A metabolic defect promotes obesity in mice lacking melanocortin-4 receptors. Proc Natl Acad Sci U S A 97, 12339-12344.

Steiner, A.L., Kipnis, D.M., Utiger, R. and Parker, C., 1969. Radioimmunoassay for the measurement of adenosine 3',5'-cyclic phosphate. Proc Natl Acad Sci U S A 64, 367-373.

Strickland, S. and Loeb, J.N., 1981. Obligatory separation of hormone binding and biological response curves in systems dependent upon secondary mediators of hormone action. Proc Natl Acad Sci U S A 78, 1366-1370.

Sutton, G.M., Begriche, K., Kumar, K.G., Gimble, J.M., Perez-Tilve, D., Nogueiras, R., McMillan, R.P., Hulver, M.W., Tschop, M.H. and Butler, A.A., 2010. Central nervous system melanocortin-3 receptors are required for synchronizing metabolism during entrainment to restricted feeding during the light cycle. FASEB J 24, 862-872.

Sutton, G.M., Duos, B., Patterson, L.M. and Berthoud, H.R., 2005. Melanocortinergic modulation of cholecystokinin-induced suppression of feeding through extracellular signal-regulated kinase signaling in rat solitary nucleus. Endocrinology 146, 3739-47.

Sutton, G.M., Trevaskis, J.L., Hulver, M.W., McMillan, R.P., Markward, N.J., Babin, M.J., Meyer, E.A. and Butler, A.A., 2006. Diet-genotype interactions in the development of the obese, insulin-resistant phenotype of C57BL/6J mice lacking melanocortin-3 or -4 receptors. Endocrinology 147, 2183-2196.

Takahashi, A., Davis, P., Reinick, C., Mizusawa, K., Sakamoto, T. and Dores, R.M., 2016. Characterization of melanocortin receptors from stingray Dasyatis akajei, a cartilaginous fish. Gen Comp Endocrinol 232, 115-24.

Tao, Y.X., 2005. Molecular mechanisms of the neural melanocortin receptor dysfunction in severe early onset obesity. Mol Cell Endocrinol 239, 1-14.

Tao, Y.X., 2007. Functional characterization of novel melanocortin-3 receptor mutations identified from obese subjects. Biochim Biophys Acta 1772, 1167-1174.

Tao, Y.X., 2008. Constitutive activation of G protein-coupled receptors and diseases: Insights into mechanism of activation and therapeutics. Pharmacol Ther 120, 129-148.

Tao, Y.X., 2009. Mutations in melanocortin-4 receptor and human obesity. Prog Mol Biol Transl Sci 88, 173-204.

Tao, Y.X., 2010a. The melanocortin-4 receptor: Physiology, pharmacology, and pathophysiology. Endocr Rev 31, 506-543.

Tao, Y.X., 2010b. Mutations in the melanocortin-3 receptor (MC3R) gene: Impact on human obesity or adiposity. Curr Opin Investig Drugs 11, 1092-1096.

Tao, Y.X., 2014. Constitutive activity in melanocortin-4 receptor: biased signaling of inverse agonists. Adv Pharmacol 70, 135-154.

Tao, Y.X., 2017. Melanocortin receptors. Biochim Biophys Acta 1863, 2411-2413.

Tao, Y.X. and Huang, H., 2014. Ipsen 5i is a novel potent pharmacoperone for intracellularly retained melanocortin-4 receptor mutants. Front Endocrinol (Lausanne) 5, 131.

Tao, Y.X., Huang, H., Wang, Z.Q., Yang, F., Williams, J.N. and Nikiforovich, G.V., 2010. Constitutive activity of neural melanocortin receptors. Methods Enzymol 484, 267-279.

Tao, Y.X., Lin, H.R., Van Der Kraak, G. and Peter, R.E., 1993. Hormonal induction of precocious sex reversal in ricefield eel, *Monopterus albus*. Aquaculture 118, 131-140.

Tao, Y.X. and Segaloff, D.L., 2003. Functional characterization of melanocortin-4 receptor mutations associated with childhood obesity. Endocrinology 144, 4544-4551.

Tao, Y.X. and Segaloff, D.L., 2004. Functional characterization of melanocortin-3 receptor variants identify a loss-of-function mutation involving an amino acid critical for G protein-coupled receptor activation. J Clin Endocrinol Metab 89, 3936-3942.

Tao, Y.X. and Segaloff, D.L., 2005. Functional analyses of melanocortin-4 receptor mutations identified from patients with binge eating disorder and nonobese or obese subjects. J Clin Endocrinol Metab 90, 5632-5638.

Tarnow, P., Rediger, A., Schulz, A., Gruters, A. and Biebermann, H., 2012. Identification of the translation start site of the human melanocortin 3 receptor. Obes Facts 5, 45-51.

Timossi, C., Maldonado, D., Vizcaíno, A., Lindau-Shepard, B., Conn, P.M. and Ulloa-Aguirre, A., 2002. Structural determinants in the second intracellular loop of the human follicle-stimulating hormone receptor are involved in Gs protein activation. Mol Cell Endocrinol 189, 157-168.

Tolle, V. and Low, M.J., 2008. In vivo evidence for inverse agonism of Agouti-related peptide in the central nervous system of proopiomelanocortin-deficient mice. Diabetes 57, 86-94.

Vaisse, C., Clement, K., Durand, E., Hercberg, S., Guy-Grand, B. and Froguel, P., 2000. Melanocortin-4 receptor mutations are a frequent and heterogeneous cause of morbid obesity. J Clin Invest 106, 253-262.

Vaisse, C., Clement, K., Guy-Grand, B. and Froguel, P., 1998. A frameshift mutation in human MC4R is associated with a dominant form of obesity. Nat Genet 20, 113-114.

Valli-Jaakola, K., Lipsanen-Nyman, M., Oksanen, L., Hollenberg, A.N., Kontula, K., Bjorbaek, C. and Schalin-Jantti, C., 2004. Identification and characterization of melanocortin-4 receptor gene mutations in morbidly obese Finnish children and adults. J Clin Endocrinol Metab 89, 940-945.

Valverde, P., Healy, E., Jackson, I., Rees, J.L. and Thody, A.J., 1995. Variants of the melanocyte-stimulating hormone receptor gene are associated with red hair and fair skin in humans. Nat Genet 11, 328-330.

van den Top, M., Lee, K., Whyment, A.D., Blanks, A.M. and Spanswick, D., 2004. Orexigen-sensitive NPY/AgRP pacemaker neurons in the hypothalamic arcuate nucleus. Nat Neurosci 7, 493-494.

Vogel, R., Mahalingam, M., Lüdeke, S., Huber, T., Siebert, F. and Sakmar, T.P., 2008. Functional role of the “ionic lock”—an interhelical hydrogen-bond network in family A heptahelical receptors. J Mol Biol 380, 648-655.

Volff, J.N., Selz, Y., Hoffmann, C., Froschauer, A., Schultheis, C., Schmidt, C., Zhou, Q., Bernhardt, W., Hanel, R., Bohne, A., Brunet, F., Segurens, B., Couloux, A., Bernard-Samain, S., Barbe, V., Ozouf-Costaz, C., Galiana, D., Lohse, M.J. and Schartl, M., 2013. Gene amplification and functional diversification of melanocortin

4 receptor at an extremely polymorphic locus controlling sexual maturation in the platyfish. Genetics 195, 1337-52.

Volkoff, H., 2016. The neuroendocrine regulation of food intake in fish: a review of current knowledge. Front Neurosci 10, 540.

Vongs, A., Lynn, N.M. and Rosenblum, C.I., 2004. Activation of MAP kinase by MC4-R through PI3 kinase. Regul Pept 120, 113-118.

Vos, T.J., Caracoti, A., Che, J.L., Dai, M., Farrer, C.A., Forsyth, N.E., Drabic, S.V., Horlick, R.A., Lamppu, D., Yowe, D.L., Balani, S., Li, P., Zeng, H., Joseph, I.B., Rodriguez, L.E., Maguire, M.P., Patane, M.A. and Claiborne, C.F., 2004. Identification of 2-[2-[2-(5-bromo-2- methoxyphenyl)-ethyl]-3-fluorophenyl]-4,5-dihydro-1H-imidazole (ML00253764), a small molecule melanocortin 4 receptor antagonist that effectively reduces tumor-induced weight loss in a mouse model. J Med Chem 47, 1602-1604.

Wachira, S.J., Hughes-Darden, C.A., Taylor, C.V., Ochillo, R. and Robinson, T.J., 2003. Evidence for the interaction of protein kinase C and melanocortin 3-receptor signaling pathways. Neuropeptides 37, 201-10.

Wacker, J.L., Feller, D.B., Tang, X.B., Defino, M.C., Namkung, Y., Lyssand, J.S., Mhyre, A.J., Tan, X., Jensen, J.B. and Hague, C., 2008. Disease-causing mutation in GPR54 reveals the importance of the second intracellular loop for class A G-protein-coupled receptor function. J Biol Chem 283, 31068-31078.

Wang, S.X., Fan, Z.C. and Tao, Y.X., 2008. Functions of acidic transmembrane residues in human melanocortin-3 receptor binding and activation. Biochem Pharmacol 76, 520-530.

Wang, Z.Q. and Tao, Y.X., 2011. Functional studies on twenty novel naturally occurring melanocortin-4 receptor mutations. Biochim Biophys Acta 1812, 1190-1199.

Watanobe, H., Schioth, H.B., Wikberg, J.E. and Suda, T., 1999. The melanocortin 4 receptor mediates leptin stimulation of luteinizing hormone and prolactin surges in steroid-primed ovariectomized rats. Biochem Biophys Res Commun 257, 860-864.

Wei, R., Yuan, D., Zhou, C., Wang, T., Lin, F., Chen, H., Wu, H., Xin, Z., Yang, S., Chen, D., Wang, Y., Liu, J., Gao, Y. and Li, Z., 2013. Cloning, distribution and effects of fasting status of melanocortin 4 receptor (MC4R) in *Schizothorax prenanti*. Gene 532, 100-107.

Wu, Q., Howell, M.P. and Palmiter, R.D., 2008. Ablation of neurons expressing agouti-related protein activates fos and gliosis in postsynaptic target regions. J Neurosci 28, 9218-26.

Xiang, Z., Litherland, S.A., Sorensen, N.B., Proneth, B., Wood, M.S., Shaw, A.M., Millard, W.J. and Haskell-Luevano, C., 2006. Pharmacological characterization of 40 human melanocortin-4 receptor polymorphisms with the endogenous proopiomelanocortin-derived agonists and the agouti-related protein (AGRP) antagonist. Biochemistry 45, 7277-7288.

Xu, Y., Jones, J.E., Kohno, D., Williams, K.W., Lee, C.E., Choi, M.J., Anderson, J.G., Heisler, L.K., Zigman, J.M., Lowell, B.B. and Elmquist, J.K., 2008. 5-HT_{2C}Rs expressed by pro-opiomelanocortin neurons regulate energy homeostasis. Neuron 60, 582-589.

Yang, F., Huang, H. and Tao, Y.X., 2015a. Biased signaling in naturally occurring mutations in human melanocortin-3 receptor gene. Int J Biol Sci 11, 423-433.

Yang, L.K. and Tao, Y.X., 2017. Biased signaling at neural melanocortin receptors in regulation of energy homeostasis. Biochim Biophys Acta 1863, 2486-2495.

Yang, Z., Huang, Z.L. and Tao, Y.X., 2015b. Functions of DPLIY motif and helix 8 of human melanocortin-3 receptor. J Mol Endocrinol 55, 107-17.

Yang, Z. and Tao, Y.X., 2016a. Biased signaling initiated by agouti-related peptide through human melanocortin-3 and -4 receptors. Biochim Biophys Acta Mol Basis Dis 1862, 1485-1494.

Yang, Z. and Tao, Y.X., 2016b. Mutations in melanocortin-3 receptor gene and human obesity. Prog Mol Biol Transl Sci 140, 97-129.

Yao, X., Parnot, C., Deupi, X., Ratnala, V.R.P., Swaminath, G., Farrens, D. and Kobilka, B., 2006. Coupling ligand structure to specific conformational switches in the β_2-adrenoceptor. Nat Chem Biol 2, 417.

Yeo, G.S., Farooqi, I.S., Aminian, S., Halsall, D.J., Stanhope, R.G. and O'Rahilly, S., 1998. A frameshift mutation in MC4R associated with dominantly inherited human obesity. Nat Genet 20, 111-112.

Yi, T.L., Yang, L.K., Ruan, G.L., Yang, D.Q. and Tao, Y.X., 2018. Melanocortin-4 receptor in swamp eel (*Monopterus albus*): Cloning, tissue distribution, and pharmacology. Gene 678, 79-89.

Zhang, H.J., Xie, H.J., Wang, W., Wang, Z.Q. and Tao, Y.X., 2019. Pharmacology of the giant panda (*Ailuropoda melanoleuca*) melanocortin-3 receptor. Gen Comp Endocrinol 277, 73-81.

Zhang, J., Li, X., Zhou, Y., Cui, L., Li, J., Wu, C., Wan, Y., Li, J. and Wang, Y., 2017. The interaction of MC3R and MC4R with MRAP2, ACTH, α-MSH and AgRP in chickens. J Endocrinol, JOE-17-0131.

Zhang, M., Mizrachi, D., Fanelli, F. and Segaloff, D.L., 2005a. The formation of a salt bridge between helices 3 and 6 is responsible for the constitutive activity and lack of hormone responsiveness of the naturally occurring L457R mutation of the human lutropin receptor. J Biol Chem 280, 26169-26176.

Zhang, M., Tong, K.P., Fremont, V., Chen, J., Narayan, P., Puett, D., Weintraub, B.D. and Szkudlinski, M.W., 2000. The extracellular domain suppresses constitutive activity of the transmembrane domain of the human TSH receptor: implications for hormone-receptor interaction and antagonist design. Endocrinology 141, 3514-3517.

Zhang, Y., Kilroy, G.E., Henagan, T.M., Prpic-Uhing, V., Richards, W.G., Bannon, A.W., Mynatt, R.L. and Gettys, T.W., 2005b. Targeted deletion of melanocortin receptor subtypes 3 and 4, but not CART, alters nutrient partitioning and compromises behavioral and metabolic responses to leptin. FASEB J 19, 1482-1491.

Zhou, F., Zhao, W., Zuo, Z., Sheng, Y., Zhou, X., Hou, Y., Cheng, H. and Zhou, R., 2010. Characterization of androgen receptor structure and nucleocytoplasmic shuttling of the rice field eel. J Biol Chem 285, 37030-37040.

Zhou, R., Cheng, H. and Tiersch, T.R., 2002. Differential genome duplication and fish diversity. Rev Fish Biol Fish 11, 331-337.